transnationale
UNIVERSITEIT LIMBURG

School voor Levenswetenschappen

Midgut Electrophysiology of *Orchesella cincta* (L.) Templeton 1835

Proefschrift voorgelegd tot het behalen van de graad van
Doctor in de Biomedische Wetenschappen,
te verdedigen door

Georg KLEIN

Promotor : Prof. Dr. E. Van Kerkhove

2003

Errata

Some errors crept into my thesis during the production process. Please consult the list below for corrections.

- "Members of the Jury" line 9; for "Institelling" read "Instelling"
- page 7, footnote; shoul be at the bottom of page 6
- page 15, Figure 1.3:

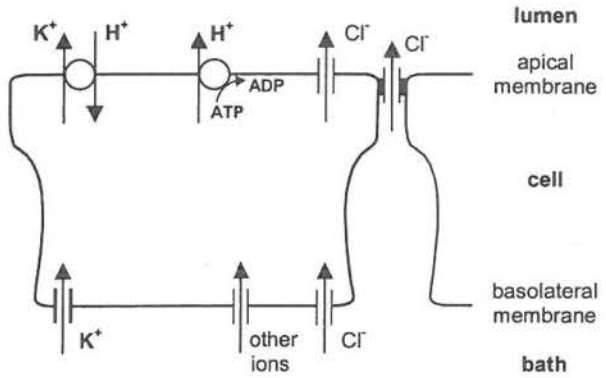

- page 17, Figure 1.4A:

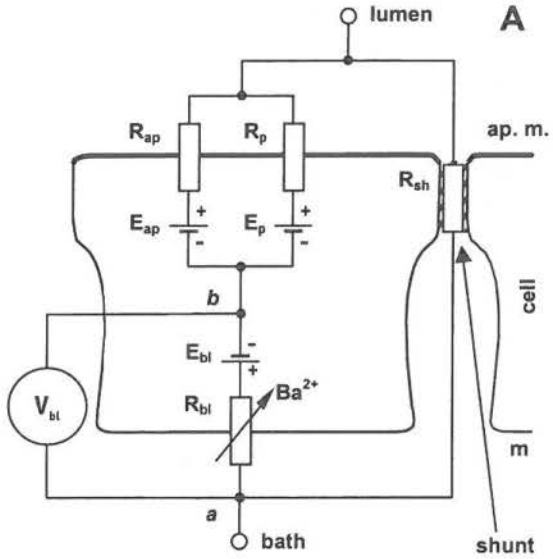

- page 127, line 2; for "... the length constant ." read "... the length constant (λ) ."
- page 132, bottom line; for "... expression for and the expression for R_{te} ..." read "... expression for λ and the expression for R_{te} ..."
- page 151, middle of the page; for "..., zij hebben mij met hun commentaren ..." read"..., zij hebben met hun commentaren ..."

U

t transnationale
UNIVERSITEIT LIMBURG

L

School voor Levenswetenschappen

Midgut Electrophysiology of *Orchesella cincta* (L.) Templeton 1835

Proefschrift voorgelegd tot het behalen van de graad van
Doctor in de Biomedische Wetenschappen,
te verdedigen door

Georg KLEIN

Promotor : Prof. Dr. E. Van Kerkhove

2003

LIMBURGS UNIVERSITAIR CENTRUM
PARTNER IN DE UNIVERSITEIT LIMBURG

According to the guidelines of the Limburgs Universitair Centrum,
a copy of this publication
has been filed in the Royal Library Albert I, Brussels, as publication
D/2003/2451/58

Members of the jury

Prof. Dr. Roland Valcke,	Limburgs Universitair Centrum, Diepenbeek, BELGIUM	chairman
Prof. Dr. E. Van Kerkhove,	Limburgs Universitair Centrum, Diepenbeek, BELGIUM	promotor
Prof. Dr. M. Ameloot,	Limburgs Universitair Centrum, Diepenbeek, BELGIUM	
Prof. Dr. J. Kleinjans,	Universiteit Maastricht, Maastricht, THE NETHERLANDS	
Prof. Dr. P. Steels,	Limburgs Universitair Centrum, Diepenbeek, BELGIUM	
Prof. Dr. R.J. Unwin,	Royal Free & University College London, London, UNITED KINGDOM	
Dr. A. Cuypers	Limburgs Universitair Centrum, Diepenbeek, BELGIUM	
Dr. R. Weltens	Vlaamse Instituelling voor Technologisch Onderzoek, Mol, BELGIUM	

List of Abbreviations and Symbols

ρ	Volume resistivity
$\Delta V_{te}(0)$; ΔV_{te}^{0}	Transepithelial voltage deflection at the perfusion end of the tubule
$\Delta V_{te}(L)$; ΔV_{te}^{L}	Transepithelial voltage deflection at the collection end of the tubule
ADP	Adenosine diphosphate
ATP	Adenosine triphosphate
C	Concentration
C_b	Background concentration
g	Conductivity, inverse of resistance
i_{core}	Axial current
i_m	Transmural current
i_{res}, i_{cap}	Resistive, capacitive current
L	Length of the tubule
PIPES	Piperazine-N,N'-bis(2-ethanosulfonic acid), a buffer
r	Radius of the tubule
R_{core}	Specific core resistance of the luminal fluid
R_{input}	Input resistance
R_{leak}	Insulation / leakage resistance at both ends of the tubule
R_m^x	Specific transmural resistance of the tubule wall per

R_{te}	Specific transepithelial resistance:
S	Slope of an ion-selective electrode
SEM	Standard error of the mean
SERIS	Self-referenceing ion-selective (probe, electrode)
V_{ap}	Apical cell membrane potential difference
V_{bl}	Basolateral cell membrane potential difference
V_{te}	Spontaneous transepithelial voltage difference
x	Distance away from the perfusion end, distance
ΔI_0	Amplitude of current pulse at the perfusion end of the tubule
λ	Length constant

List of Figures

List of Tables

Contents

1 General Introduction

1.1 THE EXPERIMENTAL ANIMAL

1.1.1 Taxonomic Position of *Orchesella cincta*

Orchesella cincta is a terrestrial arthropod[1] of the Northern Hemisphere. It belongs to the systematic group of the Collembola (springtails) comprising at least 6500 different extant species (Hopkin, 1997). Collembola share many morphological traits with the systematic group of the Protura (e.g. bark-lice) and the Euinsecta (insects *sensu strictu*). Modern taxonomy is based on phylogenetic principles: one particular systematic group should only contain those species, which have one single common ancestor. The system should reflect the evolutionary pathways. The phylogeny of these three groups however is far from clear. Some authors take them together in one group called the Insecta or the Hexapoda, assuming that they all have one ancestor in common (Kristensen, 1991; Kukalová-Peck, 1987; Kukalová-Peck, 1991). While others claim that they have different ancestors within the group of the Arthropoda, i.e. that the Collembola branch off the evolutionary line leading to the Euinsecta (Nardi et al. 2003; Friedrich & Trautz, 1995). The systematic relationships between the different arthropod groups is still an issue of debate (Hopkin, 1997). For the purpose of this work, *Orchesella cincta* is regarded as an insect. The results of our research were compared with data from other insect species. With the Collembola ranked as a Class, the relations of *O. cincta* can be categorized as follows (Hopkin, 1997):

Order: Arthropleona

Superfamily: Entomobryoidea

Family: Entomobryidae

Subfamily: Orchesellinae.

1.1.2 General Morphological Characteristics of the Collembola

The most characteristic trait of the Collembola, that separates them from the other insects, is the ventral tube (Fig. 1.1, vt), a sticky appendage of the 1st abdominal segment. The name Collembola was derived from the Greek hè kolla: the glue and hó èmbolos, the piston, the plug (Lubbock, 1873). Springtails do not possess Malpighian tubules, which are the organs of salt and water homeostasis in most insects (Euinsecta). Instead, the paired labial nephridia together with the epithelium of the eversible sacs of the ventral tube serve as the

organs of fluid and ion homeostasis (Sedlag, 1952; Eisenbeis & Wichard, 1975a,b). The most striking collembolan trait however is the spring-like jumping mechanism (hence the name springtails), which allows the animals to escape from predators. It consists of two ventral appendages, the tenaculum and the furca (Fig. 1.1, fu) at the 3rd and the 4th abdominal segment respectively. Another peculiarity of the Collembola is the most posterior part of their legs. Where the legs of the other insects have articulations between the tibia and at least one tarsus, the collembolan leg has a tibiotarsus (Fig. 1.1, mthl) instead. Where the other insects have up to 11 (true) segments, the Collembola have only 6. The mouthparts develop within the head capsule, the eye usually consists of up to eight separate single ommatidia (Fig. 1.1, om). Unlike other insects, the Collembola molt regularly throughout their adult live, they do not have obviously distinct larval and adult stadia.

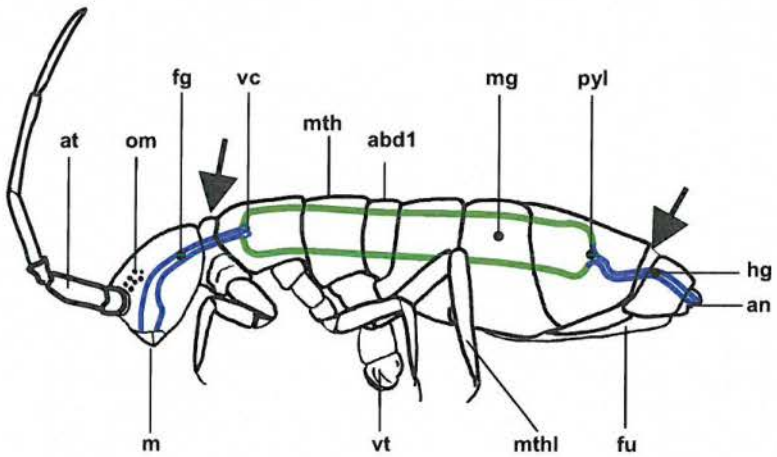

Fig. 1.1 *Orchesella cincta*: lateral view, habitus and alimentary canal. abd1: 1st abdominal segment, **an**: anus, **at**: antennae, **fg**: foregut, **fu**: furca (inserts at the 4th (!) abdominal segment, bent ventrally, extends to the metathorax), **hg**: hindgut, **m**: mouth (internal mouthparts within the head capsule), **mg**: midgut, **mth:** metathorax, **mthl**: metathoracal leg (line points to the tibiotarsus), **om**: ommatidia (single eyes), **pyl**: pylorus or pyloric region, **vc**: valvula cardiaca (cardiac valve), **vt**: ventral tube with everted tube vesicle arrows: sites where the animals were cut (see materials and methods section of chapter IA)

[1] Arthropoda: segmented invertebrate animals with joined appendages (antennae, mouthparts and legs)

1.1.3 Collembolan Midgut Morphology

The alimentary canal is a straight tube without infoldings, appendages or diverticula. It consists of the buccal cavity, the foregut, the midgut and the hindgut. The buccal cavity, the foregut and the hindgut are of ectodermal origin. They are therefore lined with a cuticle. The midgut, which is of entodermal origin, has no cuticle. The luminal side of the midgut epithelial cells is not in contact with the food bolus, a peritrophic matrix separates the food from the midgut epithelium. The peritrophic matrix is secreted at the very entrance of the midgut by a belt of cells in the cardiac valve (Hopkin, 1997), that can close the midgut at the oral side (Fig. 1.1, vc). At the hemolymph side the midgut is surrounded by an orderly latticework of circular and longitudinal muscles, which mix the food and drive it into the hindgut. A pyloric region (Fig. 1.1, pyl) connects the midgut with the hindgut where a sphincter muscle can shut the midgut at the aboral side. This region is sometimes the *valvula pylorica* (pyloric valve).

1.1.4 Collembolan Midgut Epithelium

As all invertebrate epithelia the collembolan midgut epithelium is single-layered. It is attached to a basement membrane. It consists of only one cell type, without any obvious differentiation along the midgut (Dallai, 1966, Hopkin, 1997). The cells are joined by smooth septate junctions (Lane, 1981), which are the occluding junctions of insects separating the basolateral from the apical cell membrane domain.

The epithelium possesses the characteristic properties of a digestive and transporting epithelium. The cells of the midgut epithelium bear microvilli at the luminal (apical) side. On the hemolymph (basolateral) side the cell membranes form a basal labyrinth. The cells have single but polyploid nuclei, a rough endoplasmatic reticulum, Golgi bodies and numerous mitochondria (Dallai, 1966, Humbert, 1979). The epithelium secretes digestive enzymes (Ferard & Poinsot-Balaguer, 1989) into the lumen. In the oral part the luminal pH is slightly acidic, whereas it is slightly alkaline in the aboral part. This probably optimizes the activity of different enzymes in different parts of the midgut (Humbert, 1974). The epithelium eventually absorbs the digested compounds from the luminal fluid (Eisenbeis & Meyer, 1986).

Besides digestion, the midgut serves as a site of storage-excretion. Between two molts the midgut cells accumulate waste in excretory vacuoles. They contain uric acid as

well as mineral concretions consisting of calcium phosphate and metals such as lead, cadmium, iron and zinc (Humbert, 1977; Humbert, 1978; Van Straalen et al., 1987; Pawert et al., 1996). Towards the following molt the epithelium degenerates. Regenerative cells on the basement membrane renew it from the basolateral side. During this phase between the molts the epithelium is double-layered. The degenerated epithelium is shed into the lumen right before a molt (Jura, 1958, Humbert, 1979, Joosse, 1981). After a molt the degenerated epithelium along with the waste is discharged as "gut pellet".

1.1.5 Habitat, Abundance and Ecological Importance

The cuticle of most springtails does not protect them from desiccation. Most springtails therefore appear in (micro-) habitats with high humidity (> 90% relative humidity) as in the soil or in the leaf litter layer of forests (Kaestner, 1973, Hopkin, 1997), where they usually occur in high densities. On 1 m^2 down to 0.3 m depth between $50 \cdot 10^3$ and $400 \cdot 10^3$ individuals of different species were found at different sites in Europe (Kaestner, 1973, Petersen & Luxton, 1982). Springtail species can make up 50 – 60 % of the total number of arthropods in the soil and leaf litter layer of rain forests (Stork, 1988; Stork & Blackburn, 1993), but they are very small. Depending on the species their body length ranges between 0.25 – 10 mm. Despite their abundance the relative contribution of springtails to the total animal biomass of the soil is usually only 1 – 5 % due to their small size. When an ecosystem adapts to environmental changes, the assemblage of species changes. During the early changes the relative contribution of springtails to the soil fauna can reach up to 33% (Petersen, 1994). They are however very important for the ecology and the texture of the soil. The humus layer of certain alpine ecosystems –of about 0.2 m in depth- is made completely from collembolan faeces (Kubiena, 1953). Many springtails feed on dead plant material and graze on fungi, which may grow on dead vegetation. The partially digested faeces is subsequently excreted and further decomposed by microorganisms. This may increase the availability of nutrients e.g. nitrates for plants.

Collembola in pine forest soils e.g. were able to increase the bioavailability of nitrates 2.4 times (Teuben & Verhoef, 1992b). In the presence of *O. cincta* as the only animal species in a field enclosure the total nitrogen in the soil was leached. So it could trickle through the soil to reach the fine roots of the plants. In the absence of any animal in the enclosure (control) a gain in total nitrogen was observed (Faber & Verhoef, 1991).

The importance of Collembola for decomposition processes was demonstrated with microcosm experiments (small model populations or communities on lab-scale or field enclosures that simulate the true circumstances in the field) with and without Collembola. When Collembola were absent decomposition rates were lower than in the presence of Collembola (Hågvar, 1988; Teuben & Verhoef, 1992a). In soils however, where earthworms are abundant, the relative contribution of Collembola to the decomposition processes may be small (Petersen & Luxton, 1988). In polluted or acid soils, where earthworms are missing, they may be more important (Stebaeva, 1989).

1.1.6 Collembola in Ecotoxicology

"Ecotoxicology is concerned with defining the potential or adverse effects of chemical agents ... on natural ecosystems ..." (Hopkin, 1997). Springtails are used in ecotoxicological experiments to predict the effects of toxicants on whole soil ecosystems because of their role in these ecosystems. For the purpose of such experiments springtails often represent a whole soil ecosystem.

Heavy metals constitute one of the most intensively studied classes of pollutants. Once enriched by human activity metals persist in the environment, they cannot be broken down to less harmful compounds. The toxic effects of heavy metals on soil ecosystems had therefore been extensively studied on springtails in the past. Springtails can influence the environmental fate of heavy metals in the soil. 1) Where Collembola are present in e.g. heavy metal polluted soil, they may increase the bioavailability (water solubility) of the pollutants (Van Straalen & van Meerendonk, J.H., 1987). 2) Fungi can accumulate elements (as e.g. metals) to levels of about 10 times -or more- higher than present in the soil (Bååth, 1991). Also green algae at polluted sites can take up considerable amounts of heavy metals (Posthuma, 1990). While springtails feed on fungi and green algae they take up the accumulated metals along with their food. Because springtails suffer from high levels of predation (Van Straalen & De Goede, 1987), this food chain is an important pathway for metals in terrestrial ecosystems. (Consult appendix C in Hopkin (1997) for more references)

For many of these studies *Orchesella cincta* was used as a model organism representing other collembolan species. *Orchesella cincta* lives in the leaf litter layer and on the bark of trees, preferably in pine plantations on sandy grounds (Joosse, 1981) feeding on green algae as well as on fungi (Verhoef et al. 1988). It can be easily reared under controlled

conditions in the laboratory and it is amongst the largest collembolan species (up to 5mm in length). This makes it well suited for experimental manipulations –compared to other Collembola.

1.1.7 Use of *Orchesella cincta* Midguts

Because the intestinal epithelium is regarded as the first barrier against poisoning through ingested food (Walker, 1976), this organ is of particular interest for ecotoxicological research. Not surprisingly the midgut of *O. cincta* has therefore already been studied with respect to metal accumulation and excretion (Joosse & Verhoef, 1983; Posthuma et al., 1992; Lupetti et al., 1992; Pawert et al. 1996). Basic information about the midgut physiology of *O. cincta* however is still lacking.

All living cells exhibit electrical potential differences across their membrane. Cells can use this potential difference to transport substances across their membranes. The study of these phenomena -electrophysiology- therefore describes basic properties of living organisms, their organs and tissues.

1.2 SOME ELECTROPHYSIOLOGICAL PARAMETERS DESCRIBING AN EPITHELIUM

1.2.1 The Transepithelial Electrical Resistance (R_{te})

Epithelia are barriers, which separate two different compartments from each other. The midgut epithelium separates the environment, i.e. the midgut lumen containing the food, from the animal's body fluid, i.e. the hemolymph. The collembolan midgut epithelium consists of cells, which are attached firmly to each other by smooth septate junctions (Lane, 1981; Dallai et al., 1993), which are the functional equivalent of the vertebrate tight junctions at the luminal side. They isolate the basolateral membrane from the apical membrane domain as well as the luminal space from the basolateral space. Consequently, there are two possible routes through which substances can be transported from the lumen into the hemolymph or the other way round (Fig. 1.2). Substances, which are transported through the cells, must cross the basolateral membrane and the apical membrane barriers in series. Substances, which follow the paracellular route must cross the smooth septate junctions, which all together form the barrier that shunts the cellular route of transport. When charged matter is moved across the epithelial barriers, this equals an electrical current across two serial conductive barriers in parallel with one conductive barrier, which shunts

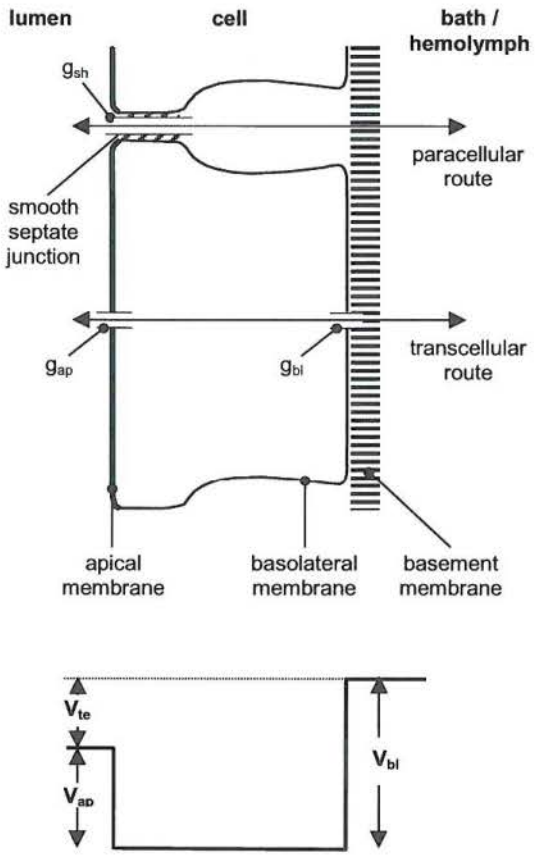

Fig. 1.2 The principal components of the collembolan midgut epithelial layer and its potential profile. $\mathbf{g_{bl}}$: conductances of the basolateral cell membrane; $\mathbf{g_{ap}}$: conductances of the apical cell membrane; $\mathbf{g_{sh}}$: conductances of the paracellular shunt in the smooth septate junctions .

$\mathbf{V_{bl}}$: potential difference across the basolateral cell membrane; $\mathbf{V_{ap}}$: potential difference across the apical cell membrane; $\mathbf{V_{te}}$: potential difference across the epithelium. V_{te} is the difference between V_{bl} and V_{ap}.

the two serial barriers (Fig. 1.2, g_{bl}, g_{ap}, g_{sh}). The electrical equivalents of the conductive barriers are electrical resistors in an electrical circuit (Fig. 1.4, R_{bl}, R_{ap}, R_{sh}).

Different epithelia differ in their ability to restrict the movement of ions across the epithelium (Frömter & Diamond, 1972). In terms of electrical properties: different epithelia have different transepithelial electrical resistances. As a rule of thumb, epithelia with high ionic permeability have low electrical resistances and epithelia with low ionic permeability have high electrical resistances. The total resistance of an epithelium depends on its surface. A large surface of a particular epithelium has a lower transepithelial resistance than a small surface of the same epithelium. If the surface is large, an electrical current encounters more possible routes for crossing the epithelium than at small surfaces. For the comparison of different epithelia, it is therefore useful to normalize them with respect to surface. The normalized transepithelial resistance, called the specific transepithelial resistance (R_{te}) expressed as $\Omega \cdot cm^2$, can than be used to classify different epithelia according to their ability

to restrict ion movement between the apical and the basolateral compartment. According to Wills et al. (1996) (p. 8, Table 1.2) epithelia can be characterized either as "leaky" or as "tight".

- In leaky epithelia the R_{te} is between 5 and 100 $\Omega \cdot cm^2$, they often have a high vectorial transport rate. These epithelia can maintain low (1-12-fold) concentration gradients for a particular substance. They are highly permeable for water. Because water can easily follow the net transport of osmotically active solutes these epithelia cannot generate significant gradients of osmotic pressure. The transepithelial potential differences across these epithelia vary between 0 and 10 mV. The proximal tubule of the mammalian kidney for instance has a R_{te} of 5 $\Omega \cdot cm^2$. It is therefore categorized as a leaky epithelium.
- In tight epithelia the R_{te} is more than 100 up to 70 000 $\Omega \cdot cm^2$. They transport substances much slower than leaky epithelia. These epithelia may generate steep concentration gradients for a particular substance (up to 10^6 fold). The water permeability is low. As a consequence the osmotic pressure of the fluids on both sides of a tight epithelium can be different. The transepithelial potential differences vary between 10 and 120 mV. The mammalian urinary bladder for instance has a R_{te} of 20 000 – 50 000 $\Omega \cdot cm^2$. It is categorized as a tight epithelium.

Thus, the estimation of R_{te} provides information about the type of epithelium under study. Small tubular structures as for instance the midgut of *O. cincta* require cable analysis for the assessment of R_{te}.

1.2.2 Cable Analysis

William Thomson (later Lord Kelvin) in 1855 was the first to develop the basic cable equations, which were intended to estimate the dimensions of submarine telegraph wires and cables required for long distances. Derived from these equations more equations were developed by different authors (for references see Jack et al., 1975), to describe the electrical properties of biological cabel-like structures.

The luminally perfused midgut preparation of Orchesella cincta can be compared to a submarine cable. The electrically conductive luminal perfusion fluid can be regarded as the core conductor of a cable. It is separated from the conductive bathing solution by the epithelium, which can be regarded as the -leaky- electrical insulation against the seawater.

When an electrical current pulse is sent into the lumen, it causes voltage deflections at both ends of the midgut preparation. The current is gradually lost through the epithelium into the grounded bath while it flows through the lumen. The voltage deflections at the side of current injection are therefore higher than at the opposite end of the preparation. From the dimensions of the midgut preparation, the electrical resistance of the lumen and the ratio of the voltage deflections at both ends, the specific transepithelial resistance (R_{te}) of the midgut can be calculated with cable equations.

Sackin (1978) and Dijkstra (1993) already described the equations used in this work. A detailed step by step derivation of these equations however is lacking in literature. An exhaustive description of the derivation of the equations used in this work is therefore given in the appendix. Every necessary mathematical operation is written, to make it easily accessible to those readers, who -like the author- are not so well versed in mathematics.

1.2.3 Electromotive Forces and Potential Differences

The electromotive forces acting on ions on both sides of cell membranes are functions of

- the diffusion potentials due to an asymmetric distribution of ions on both sides of the membranes,
- the conductive properties of the membranes and of
- energy consuming processes, which can displace ions against their electrochemical gradients (pumps, active transport).

The electrical equivalents of these forces are voltage sources in an electrical circuit (Fig. 1.4). The electrical potential differences, which can be measured across the epithelium and across the basolateral membrane, are not identical with the electromotive forces at the membranes. They arise from the combination of electromotive forces, currents and resistances of the different barriers. In how far the magnitude of the basolateral potential difference (V_{bl}) for instance does reflect the electromotive force of the basolateral membrane (E_{bl}) depends on the resistances of the other barriers. The sum of the resistances of the apical membrane and the shunt ($R_{ap} + R_{sh}$) must be significantly higher than the resistance of the basolateral membrane (R_{bl}) for V_{bl} to approximate E_{bl} (see below).

The difference of the potential differences across the basolateral (V_{bl}) and the apical membrane (V_{ap}) is the transepithelial potential difference (V_{te}) (Fig. 1.2). When the shunt resistance (R_{sh}) of the paracellular route is much lower than the resistances of the transcellular route ($R_{bl} + R_{ap}$) and there is no electromotive force in the shunt (E_{sh}), the difference

between V_{bl} and V_{ap} is leveled off. Because leaky epithelia have low shunt resistances they cannot generate the high voltage differences, which tight epithelia may establish.

1.2.4 Potassium in Insect Epithelial Transport (the Electrical Model)

The insect midgut can -at least in lepidopteran larvae (caterpillars)- exhibit transepithelial K^+ secretion into the lumen against considerable electrochemical gradients of about 200mV (Wieczorek et al., 2000). This may be to counteract the high hemolymph K^+ concentration, which is a consequence of a plant diet rich in K^+ (Harvey & Nedergaard 1964). On the other hand K^+ may be used to drive the uptake of amino acids through apical K^+/amino acid co-transporters where a cell-inward transepithelial gradient for K^+ is present (Dow & Harvey, 1988). K^+ secretion is due to the activity of an apical K^+ pumping mechanism and a passive basolateral K^+ influx. The same mechanism (Fig. 1.3) is also described for the secretion of K^+ into the lumen of the Malpighian tubules of the ant *Formica polyctena* (Leyssens et al., 1992 & Weltens et al., 1992). The apical pumping mechanism is a combination of a V-ATPase and a K^+/nH^+ exchanger. The V-ATPase creates a cell-inward electrochemical gradient for H^+, which is used by the K^+/nH^+ exchanger to excrete K^+ into the lumen. As a result the apical pump displaces positive charges (K^+) from the cell across the apical membrane into the lumen. Negative charges (Cl^-) move transepithelially into the same direction. This equals a current of positive charges in the opposite direction: from the lumen into the

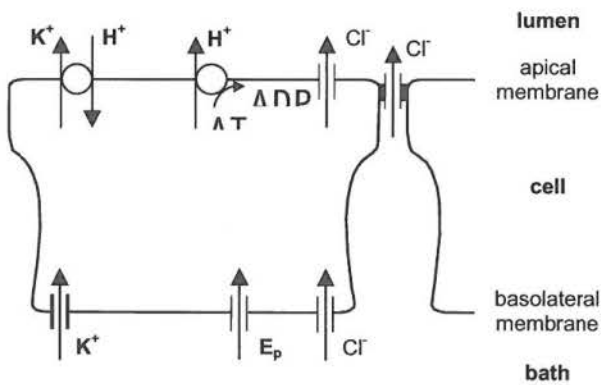

Fig. 1.3 Model of K^+ transport across an insect epithelium, adopted from Weltens et al. (1992). The V-ATPase at the apical membrane pumps H^+ into the lumen, building up a cell-inward H^+ -gradient. Driven by this gradient the apical K^+/H^+ antiport extrudes K^+ into the lumen. At the basolateral side K^+ enters the cell through highly conductive K^+ channels. Cl^- possibly moves through the paracellular shunt and/or through the cell into the lumen.

hemolymph. From the hemolymph this current flows across the basolateral membrane back into the cell. K^+ passively enters the cell through K^+ channels against its concentration gradient but driven by the high negative potential difference established by the V-ATPase. (Zeiske, 1992). These electrical phenomena can be described by using an electrical (Thévenin) equivalent circuit (Fig. 1.4 & appendix 2). The apical pump can be regarded as a current source ($I_p^0 = \frac{E_p}{R_p}$) with an internal electrical resistance R_p. In the model the total resistance of the apical membrane is made up from the diffusional resistance R_{ap} and the pump resistance R_p. The total apical resistance may be calculated as $R_t = \frac{R_{ap} \cdot R_p}{R_{ap} + R_p}$. Under experimental conditions, when the physiological solutions on both sides of the midgut epithelium (bath and lumen) are identical, there is no electromotive driving force across the shunt (E_{sh}). Therefore the basolateral potential difference (V_{bl}, see Fig. 1.3B) can be calculated without taking E_{sh} into account:

$$V_{bl} = \frac{E_{bl} \cdot (R_t + R_{sh}) \; - \; E_{ap} \cdot \frac{R_p}{R_p + R_{ap}} \cdot R_{bl} \; - \; \frac{E_p}{R_p} \cdot R_t \cdot R_{bl}}{R_t + R_{sh} + R_{bl}}, \qquad (1.1)$$

where E_{bl} and E_{ap} are the electromotive driving forces (voltage sources in the equivalent circuit) of the basolateral and the apical membrane. R_{bl}, R_{ap} and R_{sh} are the basolateral, apical and shunt resistances (resistors in the equivalent circuits) of the epithelium. $\frac{E_p}{R_p}$ is the current that the apical pump could deliver if it was short-circuited. From eq. 1.1 it follows, that V_{bl} is close to E_{bl}, if R_t is significantly higher than R_{bl}. From the same equation it follows, that V_{bl} will approximate the sum of E_{ap} and E_p, if R_{bl} is increased. Provided that R_{bl} is mainly determined by K^+ conductances (basolateral K^+ channels), blocking the basolateral K^+ channels with e.g. Ba^{2+} can increase R_{bl}. In this case the basolateral application of Ba^{2+} can reveal other conductances in the basolateral membrane and electrical phenomena at the apical membrane (E_{ap} & E_p). In the case of *Formica* Malpighian tubules a strong, immediate hyperpolarisation of V_{bl} due to the apical extrusion of positive charges (K^+) can be observed upon basolateral Ba^{2+} application (Weltens et al., 1992).

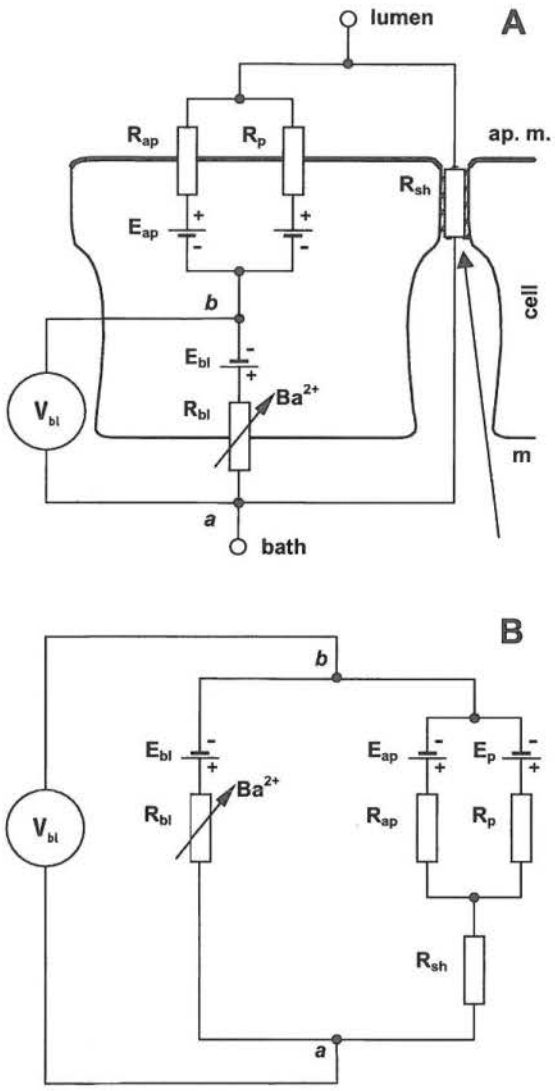

Fig. 1.4 Thévenin electrical equivalent circuit of an epithelium as shown in Fig. 1.3. A: ap. m.: apical membrane; **bl. m.:** basolateral membrane; **R_{bl}, R_{ap} and R_{sh}:** diffusional resistances of the basolateral membrane, the apical membrane and the paracellular shunt. R_{bl} is mainly determined by the conductive properties of K^+ channels. Ba^{2+} is an unspecific blocker of K^+ channels, it can therefore modify R_{bl}. **R_p:** internal resistance of the pump (Fig. 1.3). **E_{bl}, E_{ap} and E_p:** electromotive driving forces of the basolateral membrane, the apical membrane and the pump. Note that there is no electromotive driving force (E_{sh}) across the shunt because lumen and bath contain the same solutions. Between "*a*" and "*b*" the basolateral potential difference (V_{bl}) can be measured.
B: the same circuit as in **A**, redrawn: when V_{bl} is measured, E_{bl} and R_{bl} are in parallel with E_{ap}, E_p, R_{ap} R_p and R_{sh}. From that it follows, that the currents in both limbs ($I = E/R$) must be summed up. V_{bl} must therefore be calculated as in eq. 1.1).

1.3 OBJECTIVES OF THIS WORK

The objectives of this work were:

To study some functional properties of the midgut.

1) First of all some essential information was needed on the electrophysiological properties of the midgut of *O. cincta*.

1a) To start with, an elemental analysis of *O. cincta* hemolymph was performed and an adequate physiological saline was composed, based on the hemolymph composition.

1b) Furthermore we wanted to study the electrical potential differences at the basolateral and the apical membrane, i.e. to assess the importance of the conductance of the basolateral membrane for K^+ and to make an estimate of the relative basolateral versus apical membrane resistance. If the basolateral resistance is lower than the apical resistance V_{bl} approximates E_{bl} (see chapter 1.2.4). If the basolateral resistance can be increased, for instance by the application of Ba^{2+}, we could take advantage of this situation to learn more about the electrical events at the apical membrane. (electrogenic pumping mechanisms or conductances of other ions).

1c) The measurement of pH in the hemolymph, in the cell and in the lumen, should allow to calculate the electrochemical gradient across the basolateral and the apical membranes. This is important information because pH is an important factor either regulating transporters or offering a gradient across the cell membrane, energizing secondary active transport.

The items 1a, 1b and 1c are covered in chapter IA.

2) to determine the specific transepithelial resistance (R_{te}) of the midgut epithelium. Despite its small size, the midgut of *Orchesella cincta* must fulfill all needs of digestion and uptake of nutrients. Inevitably, the composition of the food composition changes as a consequence of digestion and uptake of food, while it moves through the midgut. Transport processes in the epithelium might therefore be adapted to a gradual change in the luminal content at different sites along the midgut. Consequently the R_{te} might be unequally distributed along the midgut. Because of the small size of the animal the R_{te} had to be determined with cable analysis. One assumption of cable analysis is, that the R_{te} is uniformly distributed along the tissue.

2a) Because this may not necessarily be the case, we tried to evaluate, whether it is nevertheless possible to find a good estimate of the true R_{te}, if it changes along the midgut and

2b) whether it is possible to distinguish between artifacts due to electrical leakage in the set-up and a true unequal distribution of R_{te} along the midgut.

The items outlined in 2), 2a) and 2b) are covered in chapter IB.

3) Furthermore, a technique for direct measurement of Cd^{2+} fluxes was introduced at the lab to explore the possibility of a simple self-referencing ion-selective electrode set-up to

detect Cd^{2+} fluxes at the basolateral side of the midgut, which is known to accumulate cadmium. This item is covered in chapter IIA.

2 Part I A: General Electrophysiological Properties of the Midgut

2.1 INTRODUCTION

Although *Orchesella cincta* has been used as a model in ecotoxicological studies since the early eighties (Hopkin, 1997), a description of the basic physiological features of the midgut tissue in these animals is still wanting. Transport processes through epithelia almost always involve concentration gradients across the cell membrane as well as membrane potentials. Information about them is therefore essential in understanding transport phenomena. Transporting epithelia mostly have a basolateral K^+ conductance (gK), ATP consuming pumps and ionic conductances and transporters, depending on the specific substances to be transported by the epithelium under study (Wills et al., 1996).

K^+ -conductances are important for epithelial transport, because they generate the membrane potentials, which contribute to the driving forces for transport of charged matter and serve as paths for K^+ transport across epithelia (Wang et al., 1992). In several transporting insect epithelia e.g. *Manduca* midgut (Zeiske et al., 2002) and Malpighian tubules (Pannabaker, 1995) an electrogenic V-ATPase, often located at the apical membrane, has been described. In some of these epithelia the basolateral membrane conductance is so high, due to the high gK, that it masks electrogenic phenomena, other than the K^+ diffusion potential at the basolateral membrane. For a more extensive description of the model, see Weltens et al. (1992) and chapter 1.2.4. These authors also showed that reducing gK, in the presence of the K channel blokker Ba^{2+} unmasked the presence of the apical electrogenic V-ATPase.

The aim of the present study was to provide some essential information on the electrophysiological properties of the midgut of *O. cincta*. Initially we performed an elemental analysis of *O. cincta* hemolymph and made up an adequate physiological saline, based on this hemolymph composition. We studied the presence of a basolateral gK and made an estimate of the relative basolateral versus apical membrane resistance. Ba^{2+} was applied in an attempt to find out whether an electrogenic pump was present. pH is also an important factor either by regulating transporters or by offering a gradient across the cell membrane, energizing secondary active transport (Azuma et al., 1995; Wieczorek et al., 1991). pH was measured in the hemolymph, in the cell and in the lumen, and the electrochemical gradient across the basolateral and the apical membrane was calculated.

2.2 MATERIAL AND METHODS

2.2.1 Specimens and Rearing

Specimens of *O. cincta* were kindly provided by the Department of Animal Ecology, Vrije Universiteit Amsterdam, Amsterdam, The Netherlands. They originate from animals collected at Roggebotzand, The Netherlands, which is regarded as an unpolluted reference site with respect to heavy metals (Posthuma, 1990). All measurements were done on animals derived from this initial culture. The animals were kept in PVC containers (diameter 16 cm) with a moistured plaster of Paris bottom and closed with a gauze lid. The containers were placed in an incubator set at 20 °C at 12 h light / 12 h dark regimen, the relative humidity was set at 90%. The animals were fed with green algae and molds growing on twigs of *Pinus sylvatica* from Zutendaal, Belgium, a site regarded as non-polluted area. Animals used for measurements were between 1.5 - 2.5 mm long, (total body length of living specimens in natural posture, measured with graphic paper under liquid paraffin). This body length corresponds with instar number 5 onwards. The sample therefore comprises older juveniles as well as adults (Mertens & Blancquaert, 1980; Mertens et al., 1982 and Janssen & Joose, 1987).

2.2.2 Distinguishing Between Different Molting Stages

O. cincta molts every 5 - 6 days throughout life (Mertens & Blancquaert, 1980; De With & Joose, 1971). In between two molts foraging is limited to 3 days (Joose, 1981; Joose & Testerink 1977). Then it takes 2 fasting days to prepare a new midgut epithelium before the old one is shed along with the cuticle. It seems reasonable to assume that the midgut undergoes physiological changes during the molting cycles. Therefore a method was developed by which the different physiological states of the midgut during the molting cycle could be distinguished by inspection of its morphological traits. Visible traits of dissected midguts were evaluated as follows. Animals were reared individually in small glass containers (45 ml) with a moistured bottom layer of plaster of Paris. The animals were fed with freeze-dried baker's yeast twice a week. The containers were examined daily for shed cuticles. Animals were sacrificed for dissection at day 1, 2, 3 or 4 after molt. The midguts were evaluated for transparency of the epithelium, content, and consistency of the content. The results were used to divide the midguts into 4 different stages, which possibly represent different physiological states (Fig. 2.2, Fig. 2.3).

2.2.3 Collecting Hemolymph Samples

Samples of hemolymph were analyzed for pH, osmolality, elemental composition, and chloride concentrations. The animals were rather small (1.5 - 2.5 mm in length) and samples were pooled except for the analysis of the chloride content. At 22 occasions samples of 1.6 - 6.5 µl with a total of 77 µl were obtained from 2804 animals in all. The average yield at any occasion was 27 ± 1.7 nl per individual (n = 22). Samples were collected from the animals by pushing them into liquid paraffin and tearing off one metathoracal leg. The droplet of hemolymph, which appeared, was taken up with a steel needle and added to the sample collected earlier. When a volume of a few µl was collected, the droplet was aspirated into a 5 µl microcapillary (Drummond) silanized with hexamethyldisilazane (Janssen Chimica). One end of the microcapillary was sealed with wax for hematocrit tubes (Hirschmann Labordgeräte) and the sample was spun down at 3800 rpm for 10 min in a swinging-bucket bench top centrifuge (Jouan B3.11) to clear the hemolymph from cells. Next the capillary was broken above the debris and blown out into liquid paraffin saturated with water. The loss of sample due to that procedure was 7.8 ± 2.4% (n = 14). Taking this loss into account it took 199 animals to obtain a pooled sample of 5 µl. In order to minimize evaporation all samples were kept under water-saturated liquid paraffin at 4 °C until analysis. Care was taken not to touch any of the tools used during the procedure with bare hands.

2.2.4 Osmolality

Osmolality measurements of 5 µl hemolymph samples on filter disks with a vapor pressure osmometer (Wescor 5100C) gave reproducible results. The meter was calibrated with 290 mOsmol and with 1000 mOsmol standard solutions (Wescor) on averages of at least 3 measurements each.

2.2.5 Elemental Analysis

Three samples that had been used for determining osmolality were left to dry on the filter disks and prepared for ICP-OES (Inductively Coupled Plasma - Optical Emission Spectometry) analysis of the Na, K, Ca, Mg and P contents (Table 2.2). They were extracted in 5 ml 0.14 M HNO_3 (Fluka, TraceSelect, >69.5%). This solution together with the filter disks was stored in polypropylene vials until analyzed. Samples of demineralized water were treated in the same way and served as blanks.

2.2.6 Micropotentiometry of Chloride

The hemolymph chloride content was determined potentiometrically on samples from 11 animals (for details about this technique see: Ramsey et al., 1955). Hemolymph samples (8.96 nl) not older than 1 min were mixed with aliquots (0.68 nl) of 0.2 M hydrazine monohydrate (Janssen Chimica) to give a final hydrazine concentration of 0.015 M. Chloride concentrations were corrected for the dilution afterwards. The volumes could be determined exactly by means of laboratory-made, silanized volumetric pipettes of 0.68 ± 0.012 nl ($n = 6$) and 8.96 ± 0.24 nl ($n = 6$) respectively. Handling and measurements were done under liquid paraffin saturated with water. From each of the hemolymph samples (8.96 nl) at least 3 subsamples (0.68 nl each) were drawn and measured using a microtitrator device (WPI, Microtitrator FT-2230). The potentials were recorded by a pen recorder (Sefram, Servofram). The means of 3 subsamples from each hemolymph sample were used to calculate the overall mean chloride content of one individual animal (Table 2.2).

2.2.7 pH of Hemolymph Samples

To obtain a rough estimate of the hemolymph pH, the first determination of hemolymph pH was done using indicators. Solutions of neutral red and 1-naphtholphtalein (0.68 nl) were injected into buffer droplets and samples of approximately the same diameter each. Comparing the indicator colors of the buffers and the color difference between a sample injected and a sample without indicator (hemolymph of *O .cincta* was slightly yellow, sometimes almost colorless). The hemolymph pH estimated by using indicators ranged between 6.8 and 7.1 ($n = 3$). The pH of the physiological salines was adjusted at 6.8 (Table 2.1).

2.2.8 Saline Composition

The physiological salines (Table 2.1) were composed taking into account the results of the elemental analysis, osmolality measurements and the pH estimated as described above. Solutions with different $[K^+]$ were prepared by mixing the solution containing 70 mM K^+ with the K^+ free solution. NaCl was replaced by KCl for the preparation of the 70 mM K^+ solution. Because citrate and phosphate can form complexes with double cations such as Ca^{2+}, Mg^{2+} and Ba^{2+}, the speciation of these elements in the salines was calculated with the MINEQL$^+$ 3.01b computer program (Environmental Research Software, Hallowell, ME, USA). The calculated, actual free concentrations in the control solution were 45 µM Mg^{2+}, and 2.7 µM

Ca^{2+}. They were 3.02 mM and 1.79 mM in the solution containing 2.2 mM $BaCl_2$, where the actual free concentration of Ba^{2+} was 0.86 mM. The resistivity of the control solution (7 mM K^+) was 70.8 ± 0.55 Ω·cm at 23.8 ± 0.3 °C (n = 40) with a slope of -2.1 Ω·cm/°C.

Table 2.1 Nominal millimolar concentrations in different physiological salines

saline / component	0 mM K^+	7 mM K^+ (control)	70 mM K^+	2.2 mM Ba^{2+}
Na^+	**161.7**	**154.7**	**91.7**	**152.5**
K^+	**0**	**7**	**70**	**7**
Ca^{2+}	6	6	6	6
Mg^{2+}	4	4	4	4
Ba^{2+}	0	0	0	2.2
Cl^-	**114**	**114**	**114**	**116.2**
$H_2PO_4^-$	2.8	2.8	2.8	2.8
PIPES	8	8	8	8
pyruvate$^-$	8.5	8.5	8.5	8.5
succinate^{2-}	8.5	8.5	8.5	8.5
citrate^{3-}	8.5	8.5	8.5	8.5
glucose	10	10	10	10

pH: 6.8, osmolality: 300 mosmol/kg

2.2.9 Midgut Dissection Technique

O. cincta is rigged with long pointed setae, which are readily lost whenever the animal is handled. To prevent the setae piercing the midgut epithelium, dissection was done under liquid paraffin. After decapitation with fine scissors, the abdomen was incised between the third and the fourth abdominal segment leaving gut and anus intact (Fig. 1.1). The gut including the last two segments, i.e. rectum and pylorus, the midgut and the remainder of the foregut was then gently pulled out of the animal grasping the furca with the forceps. Following dissection the preparation was placed in saline, re-cut behind the pylorus, and the adjacent tissue was removed from the saline. A second dissection technique was applied to avoid excessive stretching of the tissue. First the head was cut off with a shearing movement, so that the anterior part of the midgut was pulled out of the thorax. Next the abdo-

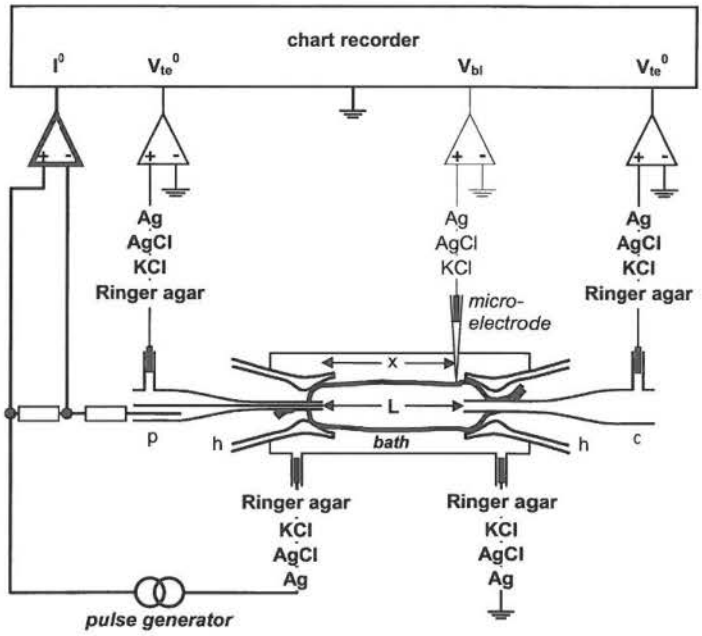

Fig. 2.1 Luminal perfusion: electrical circuits and experimental set-up. c: collection pipette, **p**: perfusion pipette, **h**: holding pipette, **L**: perfused length, **x**: distance between perfusion pipette and impalement site, I_0 was sent into the lumen by a home-made perfusion pipette and measured with a Keithley 616 Digital Electrometer, V_{te}^0 and V_{te}^L were measured with WPI 750 amplifiers, channels "A" and "B", V_{bl} was measured with WPI Duo 773 at channel "B" (10^{11} Ω), the bath was perfused with physiological saline

men was cut between the 5th and the 6th segment. The midgut was then pushed out of the thorax by gently squeezing the abdomen. Eventually, both preparations consisted of the whole midgut and short ends of the foregut and the hindgut, leaving the *valvula cardiaca* as well as the *valvula pylorica* intact, which kept the midgut closed at opposite ends. From the *valvula cardiaca* to the pylorus, the midguts were 1132 ± 31 µm long (SEM, n = 59). Their outer diameter was 230 ± 4 µm (SEM, n = 102), their inner diameter was 186 ± 3 µm (SEM, n = 50).

2.2.10 Luminal Perfusion and Electrical Setup

For a detailed description of this technique see Burg et al. (1966) and Greger and Hampel (1981), a diagrammatic illustration of the set-up is given in Fig. 2.1. Briefly, the setup

consisted of two holding pipettes with a constriction behind the orifice, a double-barreled perfusion pipette and a single barreled collection pipette. The complete midgut was mounted in between the holding pipettes. The electrical insulation between the midgut wall and the inner surface of the holding pipettes was improved with Sylgard® 184 (Dow Corning). The inner surface of the holding pipettes was coated with Sylgard ® 184. Sylgard® 184 -base and -curing agent were mixed and than diluted about 5 times with acetone. This mixture was sucked up into the mouth of the pipette. After evaporation of the acetone the Sylgard layer was cured. Curing was accelerated by heating the mouth of the pipette in the microforge. Prior to the mounting of a midgut, the mouth of the holding pipettes was filled with fluid Sylgard® 184 base agent (Sylgard oil). The coating enhanced the adhesion of the Sylgard oil to the glass surface. The ends of the midgut preparation were gently sucked into the Sylgard oil. The outer surface of the midgut epithelium was then embedded in Sylgard oil, which in turn stuck to the inner surface of the holding pipettes.

The perfusion pipette as well as the collection pipette was pushed through the midgut wall. All midguts were perfused from the oral side to the anal side by gravity feed from a fluid reservoir above the setup through the perfusion pipette. Both barrels of the perfusion pipette were filled with physiological saline. Through one of the barrels, current pulses were sent, the other served as a voltage-sensing electrode. The voltage-sensing pipette was filled with control saline. The current pipette served to change the luminal fluid if necessary. A change in perfusion fluid was accomplished by releasing the perfusion pressure on one barrel and by bringing pressure on the other. Under experimental conditions, but without a preparation mounted, the perfusion rate was estimated to be 0.3 $\mu l \cdot min^{-1}$ by measuring the loss of fluid in the reservoir through the pipette opening during 24 h. Through the other barrel 1 s current pulses of 102 $\pm$ 1.2 nA (n = 71) were sent every 10 s, the bath served as the current sink. The pulse generator was connected to earth via the bath, which was grounded by an agar-bridge and an AgCl - Ag wire in 3 M KCl (Fig. 2.1). The pulses caused voltage deflections at the perfusion (ΔV_{te}^{0}) and at the collection pipette (ΔV_{te}^{L}) as well as at the level of a microelectrode impaling the basolateral membrane (ΔV_{bl}) or when it was pushed further through the apical membrane into the lumen (ΔV_{te}^{x}). Offset voltages were 1.74 $\pm$ 0.11 mV (n = 71) at the perfusion side and 0.71 $\pm$ 0.06 mV (n = 70) at the collection side, they never exceeded 4.7 mV. The bath volume was kept between 0.6 and 1 ml. The bath flow rate was kept between 0.3 and 0.6 $ml \cdot min^{-1}$. The temperature of the bathing solution was measured with a thermistor temperature probe at a distance of

1.5 mm from the preparation. The average temperature of the bathing solution was 23.1 ± 0.23 °C (n = 65). Recordings were done with a pen recorder Servofram SRM (Sefran, Paris, France).

2.2.11 Recording of Electrical Potential Differences

Routinely, transepithelial potential differences were recorded by using the voltage sensing barrel of the perfusion pipette and the collecting pipette as voltage electrodes, the highest of both recordings was regarded as V_{te}. Measurements of V_{te} were accepted, whenever 1) there was a sudden change in potential recording upon pushing the perfusion pipette and the collection pipette into the lumen, 2) there was no visible leak of gut contents into the bath. In Fig. 2.5 the registration of V_{te} during an experiment is shown.

Basolateral potential differences were recorded with glass microelectrodes filled with 3 M KCl. Measurements of V_{bl} were accepted, whenever 1) there was a sudden decrease in potential recording upon impalement resulting in a stable reading for at least 1 min, 2) the tip of the electrode could not be seen in the midgut lumen. Whenever the potential deflections due to injected current (ΔI) showed a pronounced increase upon impalement and the tip could be seen in the midgut lumen, the recorded potentials were considered to be V_{te}. In Fig. 2.4 the registration of V_{bl} during an experiment is shown. The relative impalement site for a particular recording (x_{rel}) was calculated with respect to the total length of the midgut before mounting. At the entrance of the midgut $x_{rel} = 0$, at the opposite end $x_{rel} = 1$.

2.2.12 Calculation of Fractional Resistance

Whenever measurements of ΔV_{bl} and ΔV_{te} were done on the same preparation at the same impalement site (ΔV_{bl}^{x} and ΔV_{te}^{x}), the fractional resistance of the basolateral membrane (f_{bl}) was calculated as:

$$f_{bl} = \frac{\Delta V_{bl}^{x}}{\Delta V_{te}^{x}} \cdot 100 \qquad (2.1)$$

where ΔV_{te}^{x} and ΔV_{bl}^{x} are the deflections of the transepithelial and the basolateral potential due to a current pulse measured at site x.

2.2.13 pH Measurements with Microelectrodes

2.2.13.1 Construction of Double-barreled pH Microelectrodes

pH-electrodes for intracellular and luminal measurements were made from double-barreled, filamented borosilicate glass (Hilgenberg, OD1 = 1.5 mm, ID1 = 0.87 mm, OD2 = 0.75 mm, ID2 = 0.35 mm), with a horizontal puller (DMZ Universal Puller, Zeitz Instrumente, München, Germany). The wider of the two barrels was silanized and filled with hydrogen ionophore II - cocktail A (Fluka 95297) in the tip. The barrel was back-filled with a buffer solution containing 1M citric acid and 10 mM NaCl set at pH 6.0 with NaOH. This technique has been described earlier by Weltens and Pirotte (1987) and Zhang et al. (1994). The smaller barrel was filled with 3 M KCl. Both barrels were connected to a high-impedance electrometer via chlorinated silver wires.

For measurements of the hemolymph pH *in situ*, these electrodes were modified to facilitate the penetration of the animal's body wall: the taper of the electrode tip was made steeper so that it became shorter and more rigid. After silanization the outermost tip was broken to give an over-all diameter of 10 - 20 µm. To prevent the ion-sensitive membrane from trickling out through that opening, the ion-selective membrane was solidified. An aliquot of the hydrogen ionophore was blended with 20% w/w PVC high molecular density (Fluka 81392) together with about four times the volume of tetrahydrofuran (Fluka 87369). This mixture was introduced into the silanized barrel with a fine glass capillary. After evaporation of the tetrahydrofuran a gellified column between 0.5 and 1 mm long remained in the tip. The smaller of the barrels was back-filled with a plug of 3% agarose low melting point (Bio Rad) in 3 M KCl to prevent leakage of the 3 M KCl backfilling solution into the hemolymph.

Before and after the measurements, a calibration was done in physiological salines accurately set at pH 6.50, pH 7.00 and pH 7.50 with HCl or NaOH. Readings were accepted when a slope of at least 50 mV/decade was obtained. When necessary, measurements were corrected for a drift read at pH 7.00.

2.2.13.2 Intracellular and Luminal pH Measurements In Vitro

The pH-sensitive barrel of the electrode was connected to input channel "A" ($10^{15}\ \Omega$) of the high impedance electrometer (WPI Duo 773). The KCl-filled barrel of the microelectrode was connected to input channel "B" ($10^{11}\ \Omega$) of the same electrometer. Recordings were done with a pen recorder Servofram SRM (Sefran, Paris, France). The bathing solution was

grounded via an agar-bridge (3% agar in 3 M KCl). The midguts were mounted in the bathing solution with holding pipettes without perfusing them luminally. The midgut content was therefore not diluted with experimental solutions.

2.2.13.3 In Vivo pH Measurements of the Hemolymph

The pH-sensitive barrel of the electrode was connected to the high-impedance input (10^{15} Ω) of the electrometer (WPI Duo 733). The smaller barrel served as the reference half-cell of the electrode, it was connected to earth.

The animals were narcotized with diethyl ether for 1 min. They were transferred with a small brush soaked with ethanol and mounted onto a microscopic slide coated with water-soluble insect mounting glue. The ethanol dissolved the glue where the brush touched it, while the animal was placed onto the glue. At the time the animals began to show movements, the ethanol had evaporated leaving the glue dried up again. This immobilized the animals without killing them. The electrodes were impaled longitudinally through the intersegmental cuticle from the caudal end towards the head-end. To avoid penetration of the midgut, one impalement was done ventrolaterally between the 4th and the 5th abdominal segment into one of the ventrolateral flaps, where the midgut is absent. A second impalement was done dorsolaterally between the 5th and the 6th abdominal segment above the hindgut. After the measurements 3 animals were dissected to confirm that this impalement technique had not damaged the midgut.

2.2.13.4 Electrochemical Driving Forces

The electrochemical driving force acting on H^+ was calculated as the sum of the equilibrium potential for H^+ across the cell membrane and the membrane potential:

$$\frac{\tilde{\mu}_{(H^+)}^{o\to i}}{z\cdot F} = \underbrace{\frac{R\cdot T}{z\cdot F}\cdot 2.303\cdot \log\frac{[H^+]_o}{[H^+]_i}}_{E_{H^+}} + \underbrace{(\psi_o-\psi_i)}_{E_m} \qquad (2.2)$$

Where R is the gas constant, T is the absolute temperature, which was 296 K on average during the experiments, z = +1, the charge number of the proton, F is the Faraday constant, Ψ_i is the basolateral or the apical membrane potential and Ψ_o is the reference potential (earth or lumen respectively), suffixes "o" and "i" denote the proton activities outside and inside the cells respectively. A positive sign indicates a cell inward driving force.

2.2.14 Electrochemical Equivalent Model of an Epithelium

In order to understand electrophysiological events in an epithelium it is helpful to use a model (see for instance Weltens et al., 1992). At least three barriers should be taken into consideration: the basolateral membrane, the apical membrane and the intercellular shunt barrier. Each barrier has a certain electrical resistance. The three barriers are in series and because of the electromotive forces (E_{bl}, E_{ap}, E_{sh}) existing across these barriers (diffusion potentials and/or, across the membranes, possibly electrogenic pumps) a circular current (I) will be present.

Therefore the actual, measured potential across a barrier is determined, not only by its electromotive forces, but also by the circular current across its resistance. Briefly, as explained previously, the larger the barrier's resistance (R), the larger the influence of the circular current will be, and the more the actual potential may deviate from the electrogenic forces across the barrier:

$$V_{bl} = E_{bl} + I \cdot R_{bl} \tag{2.3}$$

$$V_{ap} = E_{ap} + I \cdot R_{ap} \tag{2.4}$$

$$V_{sh} = E_{sh} + I \cdot R_{sh} \tag{2.5}$$

2.2.15 Statistics

Results are presented as means ± SEM (n = sample number) unless indicated differently. Prior to significance testing, sample distributions were tested for normality with the Shapiro-Wilk's W test. Statistical significance of paired measurements was evaluated by the two-tailed Wilcoxon matched-pairs signed-rank test. The Mann-Whitney U test was used for unpaired measurements. Relationships between variables were tested with multiple linear regression. For each preparation V_{te} and V_{bl} were measured at different $[K^+]_{bath}$, meaning that the samples were not independent. Therefore a mixed model multiple regression was performed when $[K^+]_{bath}$ was analyzed for its effect on V_{te} and V_{bl}. For all statistical calculations SAS ver. 8.02 was used.

2.3 RESULTS

2.3.1 Molting Intervals and Intermolt Stages

The average molting interval of individually reared animals lasted 3.5 ± 1.1 (S.D.) days (n = 82) for the first molting interval after the animals had been separated. The second interval was longer: 4.5 ± 1.0 (S.D.) days (n = 29). The midgut epithelium of a particular preparation was categorized either as "transparent" or as "opaque". The fraction of transparent midguts changed gradually from 80.8% at day 1 to 4.8% at day 4.

During the first day after molt, 80.8% of all midguts were filled with fluid, no peritrophic matrix (PM) could be distinguished. The remaining 19.2% were filled with compact food, in some cases a PM could be clearly identified. In 65.4% of all midguts a gut pellet (Fig. 2.2, "gp") was found. No gut pellets were observed during the next days. During the second

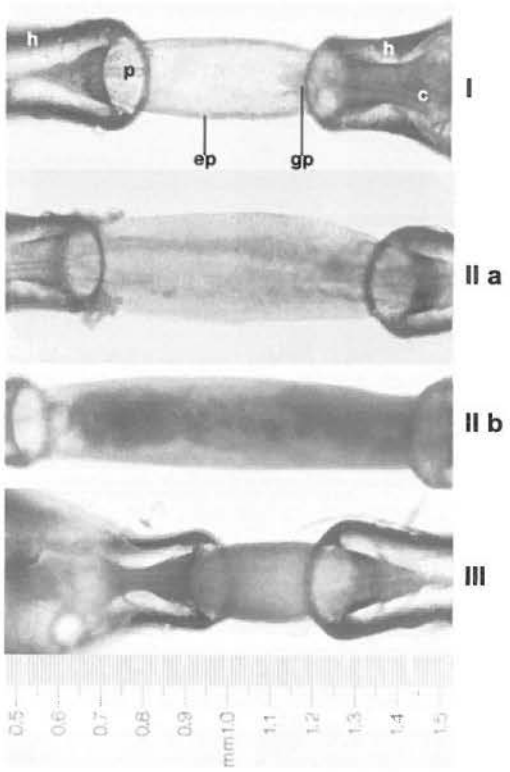

Fig. 2.2 Luminal perfusion, mounting of preparation. p: perfusion pipette, **c**: collection pipette, **h**: holding pipette, **ep**: midgut epithelium, **gp**: gut pellet (shed midgut epithelium), stages are indicated as designated in Fig. 1.1 (I, IIa, IIb, III)

day after molt 87.0% of all midguts were filled with compact food. During the third day this was 72.0% and at day 4 it was 81.0%. Accordingly the preparations were divided into 3 stages (Fig. 2.2 & 2.3). Stage "I": transparent midguts without food, stage "II" more or less opaque midguts containing food and stage "III": undoubtedly opaque midguts without food sometimes with the old epithelium locally delaminated. At those places, where the old epithelium was found detached, the new epithelium was as transparent as in type "I" midguts. These were the only occasions, where two epithelial layers could be distinguished without any doubt. Stage "II" was subdivided into "IIa" and "IIb". "IIa" midguts were more or less opaque containing dense, brownish or greenish fluid and only small pieces of food if at all. "IIb" midguts were more or less opaque containing a strand of compact food.

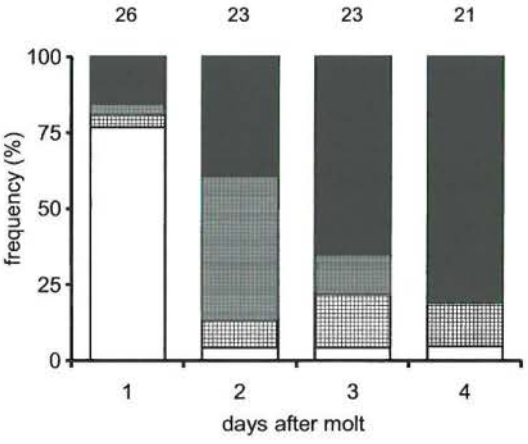

Fig. 2.3 Midgut morphology changes between molts.

Numbers at top: numbers of animals;

: transparent epithelium, fluid contents (stage I);.

: change from transparent to opaque epithelium, fluid food (stage IIa);

: change from transparent to opaque epithelium, compact contents (stage IIb);.

: opaque epithelium with compact food (stage III).

2.3.2 Elemental Analysis of the Hemolymph

The results of the elemental analysis were summarized in Table 2.2. The sum of all positive charges of the analyzed ions was 187 meq, whereas the sum of all negative charges was 124 meq. The algebraic difference between both, i. e. the anion gap, therefore was 63.3 meq. Hemolymph osmolality was 296 $\pm$ 1 mosmol / kg (SEM, n = 5).

Table 2.2 Elemental analysis of hemolymph

element	Na	K	Ca	Mg	P	Cl
concentration (mM)	153.6	7.0	9.8	3.5	6.7	113.8
SEM (± mM)	2.2	1.2	3.5	1.1	0.6	4.1
n	3	3	3	3	3	11

The net charge of P at pH 7 was assumed to be -1.5, because at this pH half of the P is supposed to be $H_2PO_4^-$, the other half as HPO_4^{--}. Samples, except for Cl, were pooled from 199 animals. pH: 6.8 – 7.1; osmolality: 296 ± 1 mosmol/kg (n = 5)

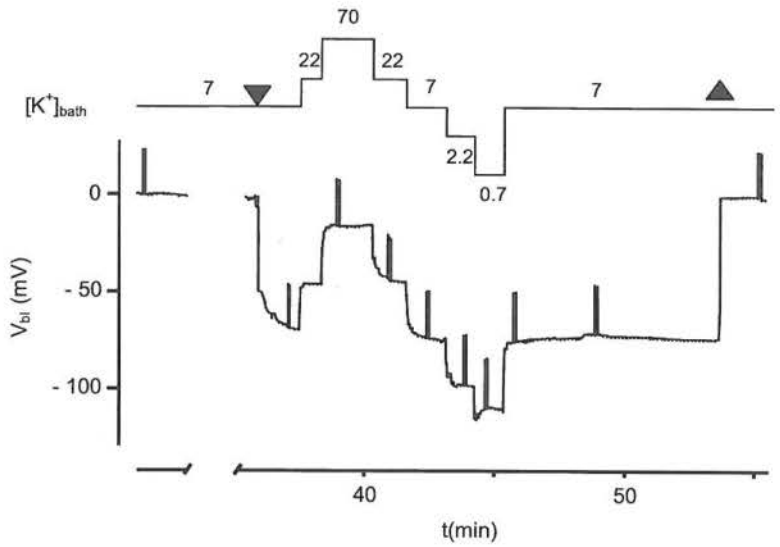

Fig. 2.4 Influence of different $[K^+]_{bath}$ on V_{bl}, representative recording. Above: experimental protocol, luminal perfusate $[K^+]$ was 7 mM; numbers: millimolar concentrations of $[K^+]_{bath}$; arrowheads: impalement and retraction of microelectrode; abscissa: time after decapitation; upright deflections in the trace are due to microelectrode resistance testing with 1 nA current pulses (± 25 MΩ); the regular, very small, downward deflections are due to 1 s current pulses of 98 nA injected into the lumen for the determination of the transepithelial resistance.

2.3.3 Basolateral and Transepithelial Electrical Potential Differences at Different $[K^+]_{bath}$

V_{bl} showed an almost perfect Nernstian behavior, when $[K^+]_{bath}$ was increased (Fig. 2.6). It depolarized with 50 mV/decade from -63.8 ± 1.17 mV at 7 mM K^+_{bath} (n = 51) to -13.2 ± 4.17 mV at 70 mM K_{bath} (n = 14). Together with a low fractional resistance of the basolateral membrane ($f_{bl,}$ results follow later on) this Nernstian behavior implies a high K^+ conductance ($E_{bl} \cong E_K$). Therefore the influence of the circular current ($I \cdot R_{bl}$ in eq. 2.3) on V_{bl} was negligible. This allowed to estimate $[K^+]_{cell}$ from V_{bl} using the Nernst equation. Under control conditions, at 23.1°C, this was 85 mM. V_{bl} hyperpolarized with 31 mV/decade from -63.8 mV at 7 mM K^+_{bath} to -95.0 ± 3.67 mV (n = 21) at 0.7 mM K^+_{bath}. V_{te} was less sensitive to

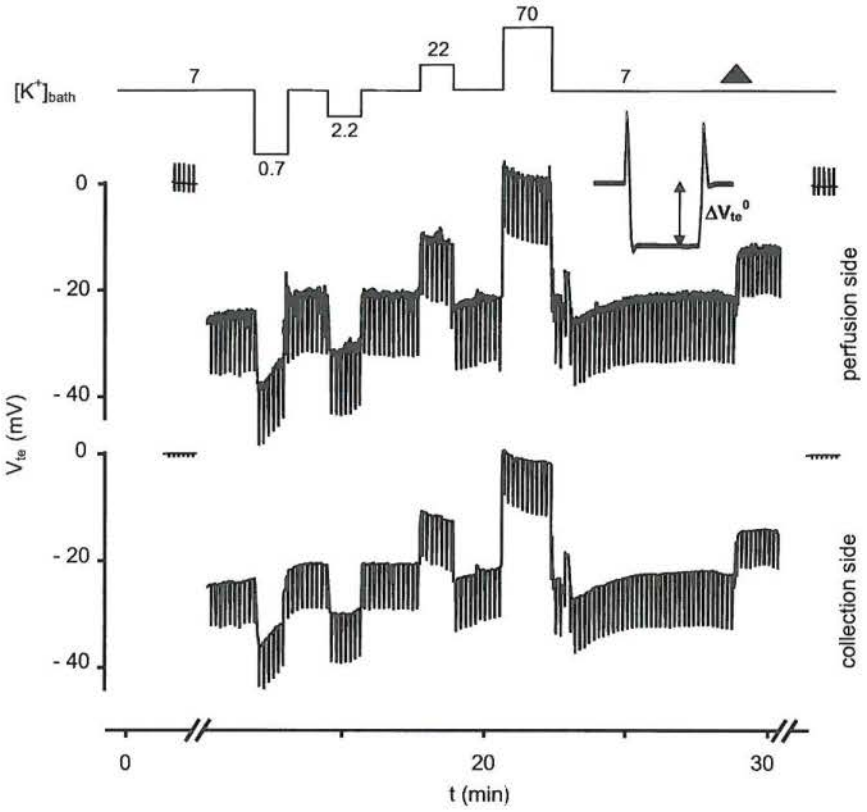

Fig. 2.5 Influence of different $[K^+]_{bath}$ on V_{te}, representative recording. Above: experimental protocol, luminal perfusate $[K^+]$ was 7 mM; numbers: millimolar concentrations of $[K^+]_{bath}$; Abscissa: t: time after decapitation; upper trace: V_{te} recorded at the perfusion side; lower trace: V_{te} recorded at the collection side; insert: detail from upper trace, see text; arrowhead: retraction of an intracellular microelectrode from the epithelium induced a drop in V_{te}

$[K^+]_{bath}$. It depolarized with 9.6 mV/decade from -10.6 ± 0.73 mV at 7 mM K_{bath} (n= 59) to -1.0 ± 0.74 mV at 70 mM K_{bath} (n = 20). V_{te} hyperpolarized with 3.5 mV/decade from -10.6 mV at 7 mM K_{bath} to -14.1 ± 1.37 mV at 0.7 mM K_{bath}. Under control conditions the average apical membrane potential (V_{ap}), calculated as the arithmetic difference between V_{bl} and V_{te}, therefore was -53.2 mV, cell negative with respect to lumen. Analyzed with multiple linear regression, the influence of $[K^+]_{bath}$ on V_{bl} and V_{te} was highly significant when tested along with other variables described below. The slope of V_{bl} was 0.52 ± 0.11 mV/mM ($p < 0.0001$, n = 46). The slope of V_{te} was 0.19 ± 0.04 mV / mM ($p < 0.0001$, n = 68).

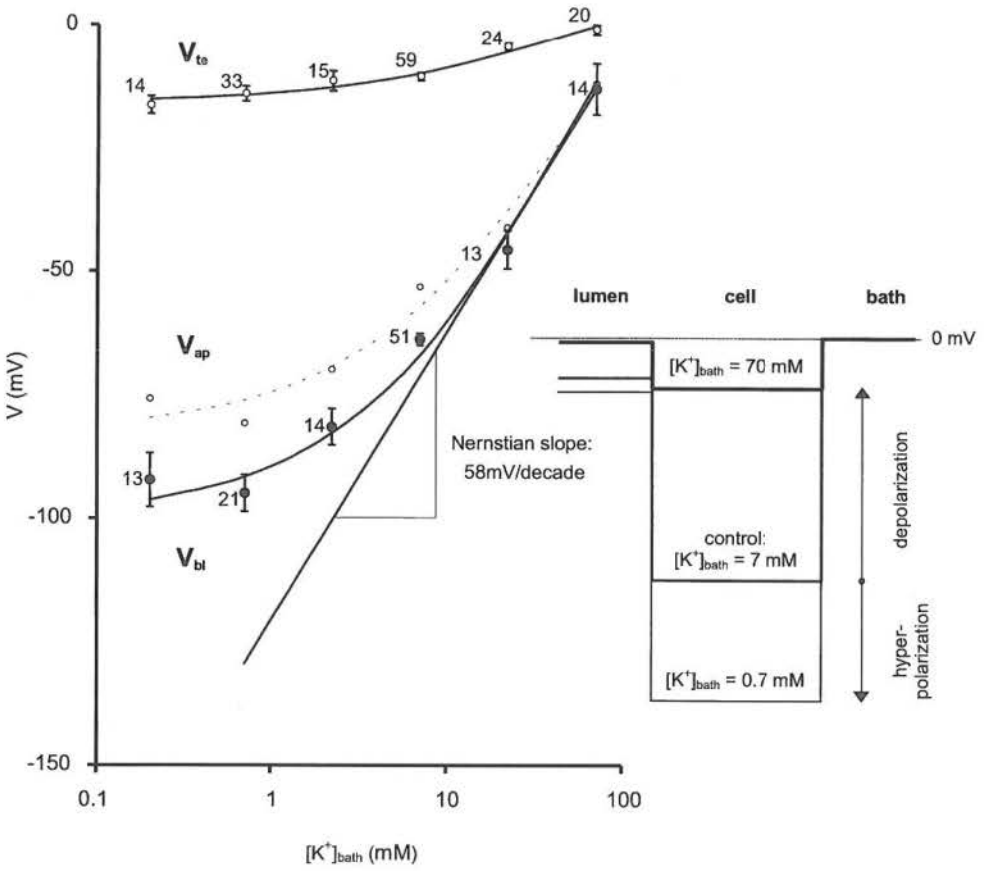

Fig. 2.6 Dependence of potential differences on $[K^+]_{bath}$. The straight line indicates the theoretical, maximal response of V_{bl} per decade, based on the Nernst equation; numbers: number of measurements; empty circles: V_{te}; filled circles: V_{bl}; small, empty circles: V_{ap}, calculated as $V_{bl} - V_{te}$; whiskers: SEM. Insert: same data presented as potential profiles for different $[K^+]_{bath}$

2.3.4 Transepithelial Electrical Potential Differences at Different $[K^+]_{lumen}$

Changing the luminal fluid from control solution containing 7 mM K^+ to 70 mM K^+, V_{te} depolarized from -6.4 ± 1.1 mV (n = 13) to -4.4 ± 1.6 mV (n = 7). When changed to 0.7 mM K^+, V_{te} hyperpolarized to -10.4 ± 1.4 mV (n = 6) (Fig. 2.7). Tested with Kruskal-Wallis ANOVA these differences were not statistically significant (p = 0.64, n = 26), suggesting that V_{te} was not dependent on $[K^+]_{lumen}$. In this series of experiments, the basolateral side was bathed in control solution containing 7 mM K^+, the basolateral potential difference (V_{bl}) was not measured.

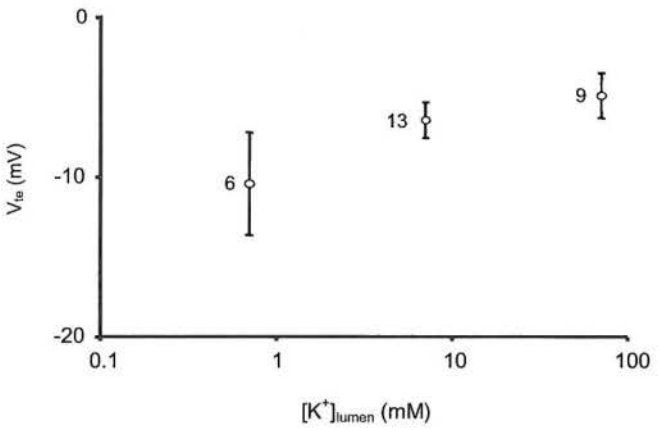

Fig. 2.7 Reaction of the transepithelial potential difference (V_{te}) on $[K^+]_{lumen}$.
Numbers: number of measurements, whiskers: SEM.

2.3.5 Basolateral and Transepithelial Potential Differences and Barium

Ba^{2+} applied basolaterally at a nominal concentration of 2.2 mM depolarized the cells from -63.7 ± 2.7 mV (n = 7) in Ba^{2+} free bathing solution to -43.2 ± 5.0 mV (n = 7), (p = 0.018). The transepithelial potential was depolarized by Ba^{2+} from -7.8 ± 1.2 mV (n= 10) to -4.5 ± 1.0 mV (n= 10), (p = 0.0051) (Fig. 2.8). Hence V_{ap} depolarized from -54.2 ± 5.0 mV (n = 5) to -38.8 ± 7.3 mV (n = 5), cells negative with respect to lumen. The potential profiles illustrate, that the apical membrane depolarized almost as much as the basolateral membrane, when Ba^{2+} was applied at the basolateral side of the midgut (Fig. 2.8).

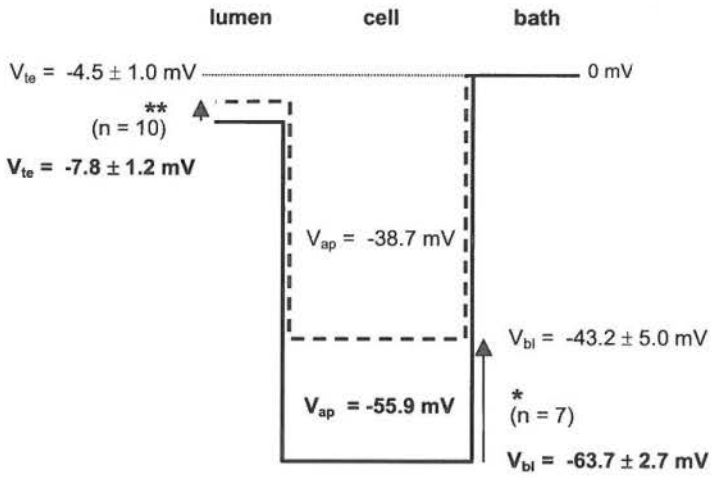

Fig. 2.8 Influence of basolateral Ba^{2+} on the basolateral, the transepithelial and the apical potential differences (V_{bl}, V_{te} and V_{ap}). Full line: control conditions, bath and lumen 7mM K^+, 0M Ba^{2+}; dashed line: 7mM K^+, 2.2mM Ba^{2+} in the bath (basolateral side) and 7mM K^+, 0M Ba^{2+} in the lumen (apical side) (all nominal concentrations); whiskers: SEM;*: p = <0.05; **: p<0.01.

2.3.6 Fractional Resistances

Under control conditions, the fractional resistance (f_{bl}, eq. 2.1) of the basolateral membrane was estimated to be 17 ± 5% (n = 12), ranging from 4% to 59%. The f_{bl} of preparations at intermolt stage I was 8 ± 1% (n = 5), whereas it was 24 ± 7% (n = 7) for stages IIa, IIb and III all together. This difference was not significant (p = 0.46; n = 12).

2.3.7 Other Variables Affecting V_{bl} and V_{te}

Other variables besides $[K^+]_{bath}$ such as intermolt stage, temperature and electrode impalement site may have an influence on V_{bl} (Table 2.3). Therefore these variables were tested for their influences on the potential differences under control conditions where $[K^+]_{bath}$ was 7 mM. Possibly V_{bl} and V_{te} change between two molts, reflecting some underlying physiological changes due to the transition from molting to feeding and vice versa. During the experiments the temperature could not be controlled. Because temperature affects active transport processes, the correlation between temperature and potentials was tested for.

Additionally, there might be differences in the spatial distribution of physiological functions along the alimentary channel. Therefore the relationship between the relative impalement site (x_{rel}) of the microelectrode and V_{bl} was tested. Provided that the axial electrical resistance of the luminal fluid is lower than the resistance across the epithelial wall, V_{te} at both sides of the preparation should be the same. The simulations performed on the equivalent circuit described in the next chapter confirmed that this was the case. Because the quality of electrical insulation at both ends of the preparation obviously biasses the measurement of V_{te}, the correlation between the extent of leakage and V_{te} was tested. The variable "leakage" was estimated as the factor by which the measurements

Table 2.3 Multiple linear regression analysis summary: relationships between different variables and the basolateral potential V_{bl} at $[K^+]_{bath}$ = 7 mM.

Variable	$\beta_{st.} \pm$ SE	$\beta \pm$ SE	part r^2	p-level	
Temperature	-0.44 ± 0.22	-2.77 ± 1.40	0.10	0.063	n.s.
Stage	0.91 ± 0.22	8.15 ± 1.96	0.42	0.0006	
X_{rel}	0.49 ± 0.17	18.32 ± 6.28	0.21	0.009	

Overall $r^2 = 0.56$, $p < 0.0016$, $n = 22$

$\beta_{st.}$: standardized regression coefficient = standardized estimate, β : regression coefficient = parameter estimate, part r^2: part correlation coefficient, indicates that part of the overall r^2, which is attributable to a particular variable, n.s.: statistically not significant

of V_{te} differed from each other at the perfusion and the collection end of the preparation. Because measurements of V_{te} were never exactly identical at both ends of the preparation, V_{te} was defined as the higher of both voltages. To reveal the relationships, these variables were entered in a multiple linear regression procedure.

The data were not pre-selected with respect to the variable "leakage". No data were excluded because of large differences between measurements of V_{te} on both sides of the setup. The average ratio of V_{te} measurement values at the opposite ends of the preparation was 1.6 ± 0.1 (SEM, n = 70) ranging from 1.0 up to 6.0. The data were however not complete for every experiment. That is to say the variables "temperature", "stage" and "leakage" were not recorded all together for every experiment. This explains the low number of cases (n = 24) in Table 2.4, compared to the number of V_{te} measurements presented in Fig.

2.6. Within this set of data (Table 2.4) the average ratio of V_{te} measurement values at the opposite ends of the preparation was 1.3 ± 0.1 (SEM, n = 24), ranging from 1.0 to 2.4. Within this subset of data V_{te} was −10.34 ± 0.9 mV (SEM, n = 24). This value did not differ much from the average V_{te} of the overall sample, which was −10.6 ± 0.7 mV under control conditions (see chapter 1.3.3).

If V_{bl} was the dependent variable, intermolt stage, temperature and x_{rel} were entered as independent variables. The numerical results of this statistical analysis are shown in Table 2.3. If V_{te} was the dependent variable, intermolt stage, temperature and leakage were entered as independent variables. The results of this analysis were summarized in Table 2.4. After controlling for the effects of all other variables, the remaining proportion of the overall variance that could be accounted for by one particular variable alone is given in the columns "part r^2". In either case there were no statistically significant interactions between the independent variables. The relationships between intermolt stage and x_{rel} on the one hand and V_{bl} on the other turned out to be highly significant; i.e. - besides the effect of $[K^+]_{bath}$ - V_{bl} becomes also less negative with increasing time after molt as well as with increasing distance from the midgut entrance. The aspect of spatial differences in electrophysiological parameters is analyzed in the following chapter. In contrast to V_{bl}, V_{te} is not influenced by the variables intermolt stage and temperature. The variable "leakage" did not influence V_{te} either.

Table 2.4 Multiple linear regression analysis summary: relationships between different variables and the transepithelial potential V_{te} at $[K^+]_{bath}$ = 7 mM.

Variable	β_{st} ± SE	β ± SE	part r^2	p-level	
Temperature	0.36 ± 0.22	0.87 ± 0.55	0.11	0.13	n.s.
Stage	-0.20 ± 0.22	-0.86 ± 0.98	0.04	0.39	n.s.
Leakage	0.33 ± 0.22	4.73 ± 3.20	0.09	0.16	n.s.

Overall r^2 = 0.15, p = 0.34, n = 24

$\beta_{st.}$: standardized regression coefficient = standardized estimate, β: regression coefficient = parameter estimate, part r^2: part correlation coefficient, indicates that part of the overall r^2, which is attributable to a particular variable, n.s.: statistically not significant

2.3.8 pH and Driving Forces Acting on Protons

In vivo measurements of hemolymph pH with H^+ sensitive microelectrodes revealed the following results: in the lateral abdominal flaps it was 7.33 ± 0.12 (n = 8), at the dorsolateral site above the hindgut it was 7.19 ± 0.12 (n = 7). In 6 individuals, both measurements could be done consecutively without killing the animals. The difference between both measurements was not statistically significant (p = 0.35, n = 6). On average hemolymph pH was 7.26 ± 0.10 (n = 9).

Under control conditions the midguts were bathed in a physiological solution with pH 6.8. The cell pH under control conditions was measured as 6.81 ± 0.08 (n = 8), the luminal pH just above the apical border of the epithelium was 6.73 ± 0.09 (n = 17). We could not detect spatial differences in pH along the longitudinal axis of the midgut.

With these values, the electrochemical driving force acting on H^+ was calculated for the control conditions according to eq. 2.2. At the basolateral side, with Ψ_i = -63.8 mV, this was +64.4 mV, at the apical side, with Ψ_i = -53.2 mV, it could be calculated to be +57.9 mV. Hence, at both membranes the driving forces for protons were directed cell inwardly. Under control conditions the average V_{te} was -10.6 mV, therefore the transepithelial driving force for protons could be calculated to be –6.5 mV, directed from bath to lumen.

2.4 DISCUSSION

2.4.1 Inorganic Ion Content

The inorganic ion content of *O. cincta* hemolymph resembles the body fluid of other evolutionary ancient hexapod orders as for example *Orthoptera* and *Odonata*. This is also true for the relative contributions of Na^+, K^+, Ca^{2+} and Mg^{2+} to the inorganic cation load in *O. cincta* which are 88.3%, 4.0%, 5.6% and 2.0% respectively. The Na:K ratio in *O. cincta* is 22, which is comparable to adults of *P. americana (Blattodea),* 20.6 and *Acheta domesticus* (*Ensifera*), 21.4. In evolutionary younger orders the Na:K ratio usually is only a few multiples of 1 or even lower (Florkin & Jeuniaux, 1974). The Ca:Mg ratio in *O. cincta* is 2.8. In ancient orders, the Ca:Mg ratio is typically about 1 whereas it is less than 1 in younger orders. In *O. cincta* hemolymph the total Ca concentration was 9.8 mM which is comparable to 10.1 mM found in adults of *B. fusca (Blattodea) or* 7.6 mM in adults of *L. migratoria (Ensifera)*. But both species have higher Mg concentrations (7.9 and 13.5 mM respectively) than *O. cincta*, which has 3.5 mM Mg. The high Ca:Mg ratio therefore is mainly due to a low

Mg concentration. Both cations usually are complexed to other components of the body fluids. Therefore the actual free concentrations and ion activities cannot be estimated exactly. However, all midgut preparations stay viable for at least one hour in the artificial saline, which was based on the measured hemolymph ion concentrations. Most preparations even showed contractions, though in antiperistaltic direction, indicating that the actual free concentrations in the saline were approximately the same as *in vivo*. The chlorine content of *O. cincta* was 113.8 mM which is comparable to that of adults of *L. migratoria*, 118.6 mM and *P. americana*, 174.2 mM. The phosphorus content was 6.7 mM in *O. cincta*, which is within the range of the highly variable values found for other insects, ranging from 4 mM to 40 mM. The data for comparison were retrieved from Florkin & Jeuniaux (1974) and Nation (2001). The average hemolymph osmolality measured on pooled samples of 199 animals was considerably lower than the average osmolarity (sic!) reported for the same species by Verhoef and Witteveen (1980) and by Verhoef (1981). Where they found 351 and 320 mosmol·l^{-1} respectively, we determined hemolymph osmolality on pooled samples comprising all intermolt stages to be 296 mosmol·kg^{-1}. But this falls within the range Verhoef (1981) reported for this species: during one intermolt the hemolymph osmolarity of fully hydrated animals increased from about 310 to 350 mosmol·l^{-1} during the first two days after molt and it decreased to 280 mosmol·l^{-1} at day 5.

2.4.2 Molting Intervals

The duration of an average molting interval (3.5 and 4.5 days) is somewhat shorter than reported by others. Under laboratory conditions similar to those in our lab and fed with *Pleurococcus sp.*, *O. cincta* juveniles molted every 4.3 ± 0.6 days (Janssen & Joosse 1987). As long as they were reared individually, the animals were fed with freeze-dried baker's yeast instead of green algae, which perhaps could account for the difference. The first molting interval (3.5 days) is significantly shorter than the second one (4.5 days). This is perhaps due to a synchronizing effect of transferring the animals from the mass-cultures to the containers for individual rearing. The manipulations necessary for the transfer most likely disturbed the animals. This perhaps made the animals cease feeding, empty their guts and molt synchronously thereafter, comparable to the synchronizing effect of transient starvation (Joosse & Testerink, 1977).

2.4.3 Intermolt Stages

The epithelium opaqueness observed by light microscopy is probably due to the mineral concretions inside the epithelial cells, which increase in size during the intermolt cycle (Humbert, 1979). He divided the intermolt cycle of the springtail *Tomocerus minor* into an alimentary period, which coincided with a single-layered epithelium, and a fasting period, which corresponded with a double-layered epithelium. The generation of the new epithelial layer overlaps with the feeding period. *A priori*, we assumed that the shift from a single-layered epithelium engaged in the uptake of nutrients to a double layered epithelium engaged in the preparation of the following molt was accompanied by significant physiological changes within the epithelium. We found that the basolateral potential became less negative with increasing time. This may be due to shutting down transport activity of the old, degenerating epithelium at the end of an intermolt cycle.

2.4.4 Potassium Concentration and Electrical Potential Differences

The curve of V_{bl} levels off at $[K^+]_{bath}$ lower than 7 mM (Fig. 2.6). This is because cell electromotive forces (E_{bl} and E_{ap} in eq. 2.3 and 2.4) are the sum of the equilibrium potentials of all ions present at both sides of the membrane times their relative conductances. When the $[K^+]_{bath}$ was decreased, the relative influence of the K^+ equilibrium potential on V_{bl} decreases along with it. It seems that, as in symmetrical cells, the membrane must be permeable not only to K^+, but to (an)other ion(s) as well (Hodkin & Horowicz, 1959). When $[K^+]_{lumen}$ was changed while $[K^+]_{bath}$ was left at 7 mM (Fig. 2.7) V_{te} was not affected. This suggests that there is no significant contribution of K^+ conductances to V_{ap} or to V_{sh}. If there was, increasing $[K^+]_{lumen}$ would have hyperpolarized V_{te} either via V_{sh} or via V_{ap}: V_{ap} would have been decreased thereby making $V_{te} = V_{bl} - V_{ap}$, more negative.

2.4.5 Barium and Electrical Potential Differences

Barium is an unspecific blokker of K^+ conductances in cell membranes. As described by eq. 2.3, the V_{bl} is the sum of the electromotive force E_{bl} across the basolateral membrane and the circular current $I \cdot R_{bl}$, which runs through the basolateral membrane, the apical membrane and then through the intercellular cleft back to the basolateral membrane. Part of the circular current could be due to a mechanism, which pumps electric charges across the apical membrane. The presence of such a pump explains why the electrochemical gradi-

ent for K^+ in insect epithelia is often cell inward (for detailed discussion see Weltens et al., 1992). Closing of K^+ channels for instance by Ba^{2+} may therefore cause a hyperpolarisation. Although that paper deals with the Malpighian tubules of an ant, the same reasoning should hold for insect midguts. In the posterior part of mosquito midguts for instance, there is a V-ATPase at the apical membrane (Boudko et al., 2001). If a V-ATPase was also active at the apical membrane of *O. cincta* midguts, blocking the basolateral K^+ channels would have revealed, that positive charges, namely protons, were pumped out of the cell and V_{bl} therefore should have hyperpolarized. But instead, Ba^{2+} depolarized V_{bl} by 32.2% (from -63.7 mV to -43.2 mV) and V_{ap} by 30.8% from (-55.9 mV to -38.7 mV). This suggests that in *O. cincta* midguts Ba^{2+} affected both membranes to the same extent, because R_{ap} was much higher than R_{bl}. This was confirmed by determining the fractional resistance of the basolateral membrane (f_{bl}). Consequently, the electromotive forces at the basolateral side rather than those at the apical side determined V_{ap}.

Ba^{2+} clearly had a depolarizing effect, although it may not have blocked the K^+ channels completely. Therefore it seems reasonable to assume that the [Ba^{2+}] applied in our experiments was too low to block all K^+ channels. The nominal concentration of barium in the artificial saline was 2.2 mM. Because the saline contained citrate, which forms complexes with double cations, the free concentrations were calculated with MINEQL. As a result, the main fraction of barium (1.35mM) was calculated to be bound to citrate as [Ba-citrate]$^-$. The calculated free concentration of Ba^{2+} was 0.86 mM. The concentration of K^+ was almost 8 times higher (7 mM), K^+ could therefore compete with Ba^{2+} for entering the K^+ channels. Exposed to bathing solutions with approximately the same ion concentrations as the solutions used for our measurements the K_D for a Ba-block in HERG channels (inward rectifier in the human heart) was 0.6 mM, which implies that at this concentration half of the K^+ channels were open (Trudeau et al., 1995). The calculated free [Ba^{2+}] in our experiments was of the same order of magnitude.

2.4.6 Intermolt Stages and Potential Differences

With increasing time after molt V_{bl} became less negative while there was no effect on V_{te}, suggesting that V_{bl} as well as V_{ap} depolarized approximately to the same extent. This may be due to the degeneration of the old epithelium towards the end of the intermolt. Because the old epithelium is thicker than the underlying new epithelium (Humbert, 1979; Thibaud, 1976), it is more likely that cells of the old epithelium were impaled with a microelectrode

than cells of the new one. Hence we assume that the change in potentials reflects the developmental stage of the old epithelium rather than the physiological state of the new one.

2.4.7 Impalement Site and V_{bl}

Towards the caudal end V_{bl} became less negative. As demonstrated in the next chapter, this is possibly -at least partially- due to a decrease in the relative basolateral K-conductance from the head end to the caudal end.

2.4.8 Insulation and V_{te}

The degree to which the measurements reflect the true values of V_{te} depends on the degree of electrical insulation at both ends of the preparation. In this particular set of data, the variable "leakage", defined as the ratio of measurements of V_{te} at opposite ends of the preparation, had no significant effect on V_{te}. It was therefore concluded, that this particular set of data provided reliable estimates of the true V_{te} values in the preparations. Because the V_{te} values in the overall sample were almost the same as in the sub-sample, we concluded, that the average value for V_{te} in the whole sample was also a reliable estimate of the true value of V_{te}. That is to say, the electrical seals were tight enough to give reliable measurements of V_{te}.

2.4.9 pH and Driving Forces Acting on Protons

There was no detectable spatial distribution in pH in the midgut lumen. If such a distribution existed, it might have been dissipated during dissection. Dadd (1975) found that the luminal pH of dissected midguts of midges declined from pH 10 to pH 7 almost instantaneously. He did not specify, whether the preparations were placed in physiological saline or not. However the dissection did apparently disturb the physiological distribution of pH along the midgut lumen.

Hemolymph pH values *in vivo* differed with 0.14 - though not statistically significant- at two different sites within the animal. The pH above the hindgut was slightly less basic than in the ventrolateral flaps of the abdomen. This may have been due to repeated contractions of the muscles flexing the furca away from the abdomen in an attempt to escape from the experimental manipulations. These muscles are specialized for bursts of anaerobic activity (Zinkler & Schroff, 1989) which may acidify the surrounding body fluid. In the locust *Melanoplus bivittatus* for example, forced jumping lead to an acidification of the

hemolymph with 0.13 pH not completely returning to resting values after 15 min recovery (Harrison et al. 1991).

The average hemolymph pH measured with microelectrodes was 7.3. This corresponds to 1/3 of the proton activity in the artificial salines used in the experiments (pH 6.8). Nevertheless the midgut preparations showed peristaltic movements and stayed viable during the experiments. This indicates that the tissue is not too susceptible to variations in pH.

Protons are a substrate for some transporters in the cell membrane of lepidopteran midgut epithelia, e.g. the electrogenic $K^+/2H^+$ antiporter of goblet cells (Azuma et al. 1995). The co-transport of Ca^{2+}, Fe^{2+}, Zn^{2+} (and others) and protons is performed by secondary active transporters using an electrochemical H^+ gradient which is large enough to overcome the uphill gradient for the divalent cations (Knöpfel et al. 2000). In midguts of *O. cincta*, the average driving force for protons from lumen to cell unde control conditions (*in vitro*) is 58 mV. From bath (hemolymph side) to cell this is 64 mV. In both cases this is almost exclusively due to the electrical potential difference, which pulls positive charges into the cell. Protons could therefore concentrate neutral substances into the cell from both sides by secondary active cotransport. If the transport of a charged substance needed to be driven, transporters would be needed with an adapted stoichiometry, for instance $cation^+/2H^+$ antiport, as mentioned above. Such a antiport would be electrogenic and could make use of the inward electrical potential driving force.

2 Part I B: Spatial Distribution of the Electrical Transepithelial Resistance (R_{te})

3.1 INTRODUCTION

Since the early eighties, *Orchesella cincta* has been used as a model in ecotoxicological studies (Hopkin, 1997). Though uptake and excretion of xenobiotics by *O. cincta* has been studied (van Straalen, van Meerendonk 1987; Posthuma et al., 1992), no studies have been done so far on the physiological properties of the transport epithelia, which are involved. In *O. cincta*, the midgut is the major site of uptake and storage-excretion for at least some pollutants (Posthuma et al., 1992). It seems obvious, that the concentrations of food components will change as they are taken up by the midgut epithelium. The gradients of these substances from midgut lumen to hemolymph across the epithelium may change accordingly from the oral to the aboral end. As long as charged matter is concerned, electrophysiological properties of the midgut may change with length. As shown in the preceding chapter, there is a statistically significant, positive correlation between the magnitude of V_{bl} and the distance between the entrance of the midgut and the impalement site of the microelectrode. Towards the hindgut V_{bl} becomes less negative. This suggests that there are indeed functional differences in the membrane properties between cells at the head end and at the caudal end of the midgut. As demonstrated in the preceding chapter, the Nernst potential for K^+ and the K^+ conductance are the major determinants of V_{bl}. Therefore we examined whether there was a difference in the relative K_+ conductance between the head-end and the caudal end of the midgut epithelium. This would be additional proof for a functional differentiation of the epithelium along the midgut axis.

Although we could not confirm this for *O. cincta* for reasons mentioned in the preceding chapter, Humbert (1974) demonstrated that there is a pH gradient in the midgut lumen of living specimens of the springtail *Sinella coeca*. It is acid at the head end and alkaline at the caudal end. Zinkler (1969) found different pH optima for the collembolan carbohydrases saccharase and maltase. From that, Humbert (1974) hypothesized that the gut pH regulates the spatial distribution of carbohydrase activity within the midgut. Because differences in function are usually reflected by differences in morphology, spatial differentiation in function is expected to be accompanied by spatial differentiation in structure. However, reports about spatial morphological differentiation of midgut epithelium are lacking. For example, in his paper about the midgut ultrastructure of *Orchesella villosa* Dallai (1966) did not report any apparent morphological zonation of the epithelium. However, functional differentiation between both ends of the midgut seems likely. There might be mass transport against low gradients at the head end as shown for the small intestine of

vertebrates. And there might be transport against steep electrochemical gradients in the caudal part of the midgut as in the colon of vertebrates. One electrophysiological parameter, which - amongst others - describes the transporting activity of an epithelium, is its specific electrical resistance R_{te}. A low R_{te} (< 100 $\Omega \cdot cm^2$) indicates, that high transport rates of charged matter against low electrochemical gradients can be realized. A high R_{te} (> 100 $\Omega \cdot cm^2$) indicates, that low transport rates of charged matter can be sustained against steep electrochemical gradients.

For small tubular tissue structures the determination of R_{te} requires cable analysis and luminal micro-perfusion techniques. Cable analysis is based on the assumption that -as in a technical transmission line- the electrical resistance of the insulation surrounding the core conductor is distributed continuously and uniformly along the cable. Therefore, this method is *in se* not suitable for the determination of R_{te} in tubules where R_{te} might change with length. We suggest a way to overcome this problem by extending the method with a simple, discrete, compartmental electrical model of the tubule. This approach resembles the method Redman et al. (1987) used to explain their experimental results on dendrites of rat ganglion cells. They performed computer simulations, i.e. cable analysis of simple electrical equivalent circuits, to track down the location of K^+ conductances on the dendrites. Briefly, if the membrane resistance was increased by Ba^{2+}, the input resistance of the dendritic cable increased not as much as the time constant. From that, they concluded that there was an unequal distribution of the membrane resistance along the dendrites. Simulations on an equivalent circuit yielded the best agreement with the experimental results, when they introduced a variable leakage resistor representing the K^+ conductances at the distal end of the model dendritic cable. Without giving the details, the same authors reported that they used compartmented models, "... when more elaborate nonuniform resistance changes were investigated ...".

But cable analysis has another major shortcoming. It is based on the assumption that there are no significant electrical leakages at the points of connection between the perfused tubule and the measurement devices. These resistances are in parallel with the electrical resistance of the perfused tubule. When they are small relative to the transmural resistance of the tubule, the transepithelial voltage measurements are affected and so are the resistance calculations based on them. To our knowledge, no one before did try and find an estimate of these electrical leakage resistances. In this study we therefore suggest to use the relationship between length and input resistance (R_{input}) to assess the leakage

resistances. We made an estimate of the electrical leakage resistances and assessed whether there was a non-uniform spatial distribution of R_{te} along the *O. cincta* midgut.

3.2 MATERIALS AND METHODS

3.2.1 General

The technical details of specimen rearing and dissection, the setup and details of the saline composition were already described in the preceding chapter. The control saline contained 7 mM K^+ and 155mM Na^+ whereas the saline with 70 mM K^+ contained 92 mM Na^+. Additionally both salines included (in mM l^{-1}) Ca^{2+} 6, Mg^{2+} 4, Cl^- 114, $H_2PO_4^-$ 2.8, PIPES 8, pyruvate$^-$, succinate^{2-}, citrate^{3-} 8 each and glucose 10. The pH was 6.8, the osmolality was 300 mosmol·kg^{-1}.

3.2.2 Coloration of the Epithelium

Whether the midgut epithelium was colored or not was evaluated qualitatively by eye. For any preparation the remainders of the foregut and the hindgut were invariably transparent. When there was a difference in color between the foregut and the midgut as well as between the midgut and the hindgut, those midguts were considered to be "colored". When the latter showed a color difference between the oral side and the aboral side with a distinct transition zone in between, this was called a "color difference".

3.2.3 Stageing

Midgut preparations were grouped into four different intermolt stages according to the criteria described in the first chapter.

3.2.4 Experimental Set-Up

The experimental setup used for the measurements has already been described in the first chapter. Sylgard® 184 (Dow corning) was used to improve the electrical insulation between the inner face of the holding pipettes and the midgut preparations. For those experiments where the midguts were perfused from the oral towards the aboral end, the holding pipettes at the perfusion side were made to fit the oral curvature of the midguts (Fig. 3.2). By sucking up the remainder of the foregut through the constriction of the holding pipette,

the midguts were centered in the pipette in a fixed position. Hence the mouth of the perfusion pipette in the midgut lumen was approximately 50 – 150 µm from the cardiac valve in all experiments. Because, on the other hand, the smallest diameter of the holding pipette at the collection side was wide enough to suck up the midguts to any desired length, it was possible to perfuse oral fractions of different lengths. For those experiments where the midguts were perfused in the opposite direction i.e. from the aboral towards the oral end, the holding pipette at the perfusion side was made to fit the curvature of the pylorus. The midgut – pylorus border was near the mouth of the holding pipette.

When the length of the midguts - from cardiac valve to the midgut - pylorus border - could be measured before mounting, the relative length (L_{rel}) of the perfused piece with respect to the total length of the midgut was determined. At the entrance of the midgut $L_{rel} = 0$, at the opposite end $L_{rel} = 1$.

3.2.5 Calculation of R_{te}

Briefly, the calculation of the specific transepithelial resistance was based on cable theory; for the derivation of equations see: Boulpaep & Sackin (1979) and appendix. In the model, the fluid inside the midgut was considered to be a conductor enclosed by the epithelium. The latter was regarded as the equivalent of the leaky electrical insulation between the conductive core of a cable and the conductive environment i.e. the bathing fluid. It is noteworthy to point out again, that all equations were based on the assumption, that the electrical insulation between the core conductor and the surrounding fluid was continuously and uniformly distributed along the cable. Accordingly, the specific transepithelial resistance (R_{te}) was calculated as:

$$R_{te} = 2 \cdot \pi \cdot r \cdot R_{input} \cdot \lambda \cdot \tanh\left(\frac{L}{\lambda}\right) \qquad (3.1)$$

where r was the luminal radius of the midgut measured halfway between the perfusion and the collection pipette, L was the distance between the perfusion and the collection pipette and R_{input} was the ratio of the current pulse (ΔI_0) sent into the lumen over the voltage deflection (ΔV_{te}^0) measured at the mouth of the perfusion pipette, where L = 0:

$$R_{input} = \frac{\Delta I_0}{\Delta V_{te}^0}. \qquad (3.2)$$

The length constant (λ) was calculated as:

$$\lambda = \frac{L}{\operatorname{arccosh}\left(\frac{\Delta V_{te}^{\,0}}{\Delta V_{te}^{\,L}}\right)} \qquad (3.3)$$

An example for an experimental recording is given in the first chapter (Fig. 2.5). As shown in the insert of this figure, ΔV_{te} was measured as the difference between the base-line V_{te} and the plateau of the voltage deflection. The composition of the luminal perfusion solution and the bathing solution was the same. So no transepithelial diffusion potentials were present.

3.2.6 Simulation with Equivalent Circuits, the Model

Measurements were simulated by modeling the midguts by a virtual chain of 10 resistors (R_c) in series representing the core conductance and 10 parallel resistors (R_m) representing the transmural resistance of 1/10 of the epithelium (Fig. 3.1). Every loop was the equiva-

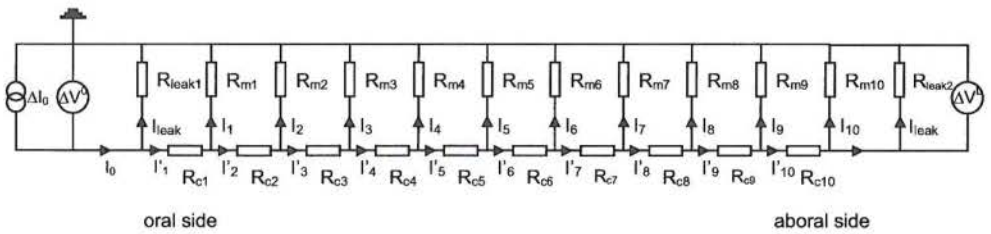

Fig. 3.1 Equivalent circuit of the midgut tube. R_m represents the transmural resistance of a particular section of the midgut epithelium; R_c represents the resistance of the luminal fluid in one of the sections of the midgut lumen. I and I': see text for explanation.

lent of one particular, discrete section of the midgut. At both ends of the model midgut resistors in parallel to the transmural resistors represented the resistances of the seals between the pipettes and the midgut (R_{leak}). Midgut pieces of different relative lengths were modeled by circuits with different numbers of loops. On average the actual preparations were 1132 µm long and 230 µm in diameter. According to these dimensions the values for the modeled resistors were calculated assuming a tubule of 1mm length with a uniform diameter of 0.25 mm, divided into 10 loops of 0.1 mm each. While the R_m of each loop was given a different value, each R_c was given the same value. Knowing that the volume resistivity of the perfusion fluid was 71 Ω·cm, each R_c was calculated to be 1445 Ω.

3.2.7 Simulation with Equivalent Circuits, Calculations

Fig. 3.1 shows the model of the midgut used for the simulations. First the resistance of the last loop consisting of the resistors R_{m10} and R_{leak2} was collapsed into one single resistor (R'_{10}): $R'_{10} = \frac{R_{m10} \cdot R_{leak2}}{R_{m10} + R_{leak2}}$. R'_{10} and R_{c10} are series resistors, they were summed up as $R_{10} = R_{c10} + R'_{10}$. R_{10} and R_{m9} are parallel resistors, they were collapsed into one accordingly: $R'_9 = \frac{R_{m9} \cdot R_{10}}{R_{m9} + R_{10}}$.

These calculations were applied to all loops of the model midgut, until the whole network of resistors was collapsed into one single resistor "R_{input}". The latter is the equivalent of the electrical resistance encountered by the current I_0 when it enters the midgut lumen (see eq. 3.2). Next, the currents running through the different branches of this network were calculated stepwise, starting at the oral side of the model midgut. At the first node the current injected into the model (I_0) splits into one component running through R_{leak1} (I_{leak1}) and a second one, which follows the axial way (I'_1). I_{leak1} was calculated accordingly: $I_{leak1} = \frac{R_1}{R_{leak1} + R_1} \cdot I_0$, where R_1 is the total resistance of all loops beyond the first node to the aboral end of the model midgut. The current reaching the next node was calculated as the difference $I'_1 = I_0 - I_{leak1}$. The current running through R_{m1} was calculated as: $I_1 = \frac{R_2}{R_{m1} + R_2} \cdot I'_1$, where R_2 is the total resistance of all resistors beyond the second node to the aboral end of the model midgut. At all nodes of the model midgut the currents were calculated in the same manner.

The R_{input} was used to calculate the voltage deflections $\Delta V_{te}^{\ 0}$ in response to current pulses I_0 with an amplitude of 100 nA (see eq. 3.2). To determine the voltage deflections at the opposite end ($\Delta V_{te}^{\ L}$), the loss of current through R_m at each node was calculated first. With the current left at the last loop, the voltage deflection at R_{leak2} was calculated. To calculate the total R_{te} of this – discrete - model, the L-, r-, R_{input}, $\Delta V_{te}^{\ 0}$- and $\Delta V_{te}^{\ L}$- values resulting from the model were then entered into the cable equations (eq. 3.1 & 3.3), which are continuous models of the midgut tubule, in the same way as were the actual measurements. For all calculations Microsoft® Excel worksheets were used. The calculations were performed

stepwise as described above and each step was written as a formula within a separate cell of an Excel worksheet. The midgut model without performing cable analysis was checked for correctness with the PSpice program (OrCAD®, Beaverton, Oregon USA). As a final verification a simulation was done assuming uniformly distributed R_m of 637 kΩ on midgut models of different relative lengths. Expressed as R_{te} this corresponds to 500 Ω·cm². R_{leak1} and R_{leak2} were set at 10^{15} Ω each. The simulated results showed, that R_{te} was correctly recalculated by the simulation and independent from length (Fig. 3.2). When R_{leak1} and R_{leak2} were set at 500 kΩ, keeping the values for R_m, the simulated R_{te} increased with increasing length, its maximum value was 397 Ω·cm².

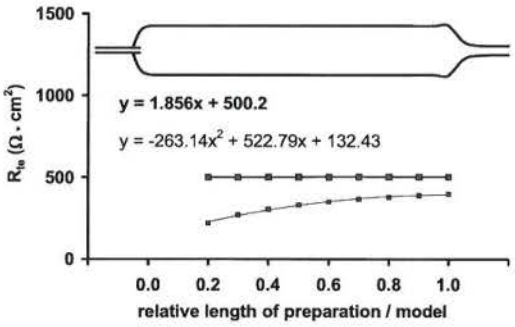

Fig. 3.2 Validation of the midgut model. Each R_m = 500 Ω·cm²; each R_c = 1445 Ω; thick line and large squares: $R_{leak1, 2} = 10^{15}$; thin line and small squares: $R_{leak1, 2}$ = 400 kΩ

3.2.8 Calculation of I_{sc}

The equivalent short circuit current (I_{sc}), defined as the current necessary to reduce V_{te} to zero, was calculated by dividing V_{te} by R_{te}.

3.2.9 Statistics

Relationships between variables were tested with multiple linear regression. After performing multiple regression analysis, a residual analysis was performed. In no case there were serious deviations from a normal distribution of the residual values. (Residual values are the differences between the observed and the predicted values.) Unless indicated differently, results are given as mean ± standard error of the mean. Statistical significance of differences between means was tested with the Mann-Whitney U test. Differences in percentages between samples were tested for significance with the X^2test. For all statistical calculations SAS ver. 8.02 was used.

3.3 RESULTS

3.3.1 Coloration of Epithelium

In 84% of all examined animals, the midgut epithelium was found to be colored (n = 114). (The orange color of most midguts resembled the color of the shed midgut epithelium. Very rarely the epithelium was bright green.) In 94% of those animals (n = 107), the colored part of the epithelium was confined to the oral 2/3 of the midgut, showing a sharp border between the colored and the uncolored part (Fig. 3.3). The results are presented in Table 3.1: between two molts, the highest percentage of colored midguts was found in animals in stage IIb. When compared to stage I, this difference was statistically significant. When the midgut epithelium was colored, the intermolt stage had no significant effect on the frequency of color difference between the oral and the aboral end.

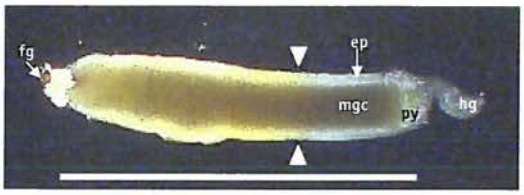

Fig. 3.3 Freshly dissected midgut preparation, darkfield. fg: remainder of the foregut with adjacent tissue; **ep**: midgut epithelium; **mgc**: midgut content; **py**: pylorus; **hg**: hindgut; arrowheads: border between differently coloured midgut regions; scale bar: 1 mm

Table 3.1 Spatial differences in epithelial color as judged by eye.

		Colored		color difference	
stage	n	(%)	P	(%)	p
I	13	54	/	100	/
IIa	13	77	n.s.	100	n.s.
IIb	76	91	0.0007	90	n.s.
III	34	82	0.056	100	n.s.
All	136	84		94	

Colored: percentage of "n" showing coloration, color difference: oral ¾ colored, aboral ¼ colorless, percentage of those preparations found colored, p: significance of differering from stage I, X^2 test

3.3.2 Relative K^+ -Conductances

The change of the basolateral potential (ΔV_{bl}/decade) in response to a tenfold change in $[K^+]_{bath}$ from 7 mM to 70 mM was taken as a measure of the relative influence of the basolateral K^+-conductance on the diffusion potential across the basolateral membrane. This approximation is justified, because the basolateral membrane has a high relative conductance and a low fractional electrical resistance (R_{bl}/R_{cell}) as was demonstrated in the first chapter. The latter result allows us to consider E_K as the major determinant of the diffusion potential across the basolateral membrane (see first chapter). When plotted against the distance of the microelectrode impalement site from the entrance of the midgut, a decrease of the relative K^+-conductance could be observed (Fig. 3.4). The linear regression explained 35% of the variance in ΔV_{bl}/decade ($p = 0.027$, $n = 14$). The data did not contain any outlier (a re-

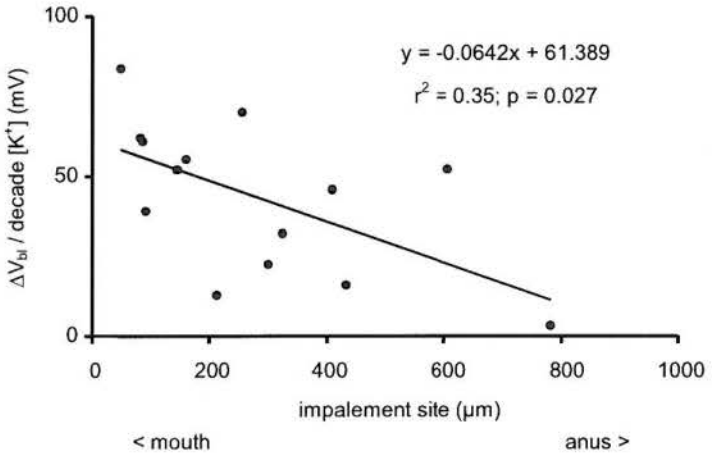

Fig. 3.4 Responsiveness of V_{bl} to changes in $[K^+]_{bath}$ from 7 to 70 mM as a function of impalement site. Impalement site: distance between perfusion pipette and microelectrode

sidual value, which deviates more than 2 times the standard deviation from the regression line). Because conductance is the inverse of resistance, this lead us to assess whether the total transepithelial resistance also increased from the head end towards the caudal end of the midgut.

3.3.3 Specific Transepithelial Resistance, Oral to Aboral Perfusion

In a first set of experiments the midguts were perfused from the oral towards the aboral end. When plotted against the actual length (L) of the perfused piece of midgut, R_{te} showed an increase from about 70 $\Omega \cdot cm^2$ at 250 µm to about 900 $\Omega \cdot cm^2$ at 1500 µm (Fig. 3.5A). On average R_{te} was 389 ± 35 $\Omega \cdot cm^2$ (n = 69). From these data we selected those where the relative length (L_{rel}) could be determined and a reasonable electrical insulation

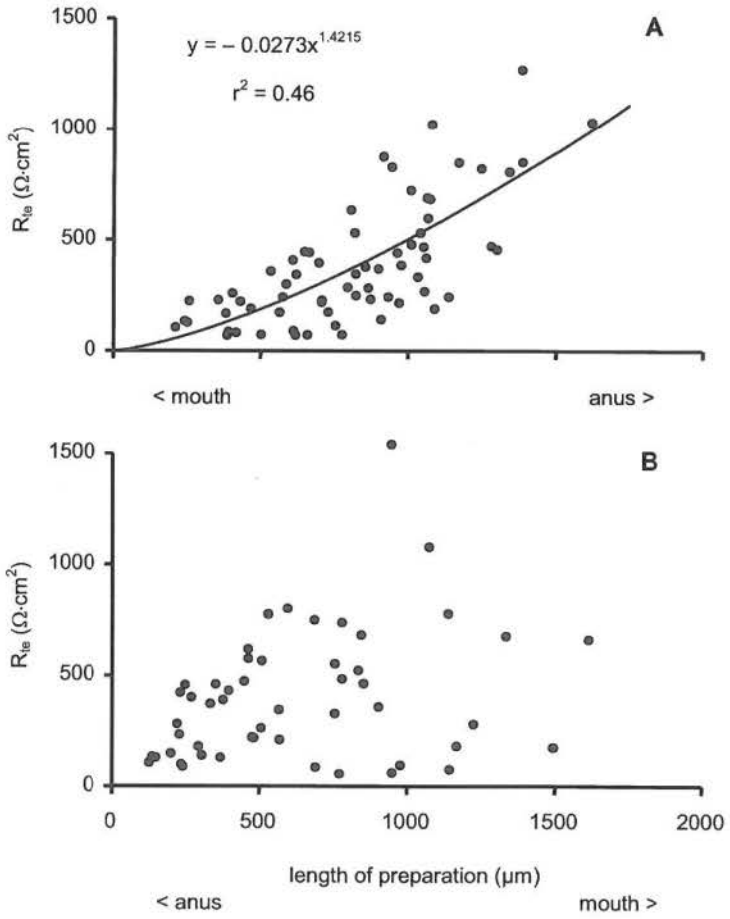

Fig. 3.5 Specific transepithelial resistance (R_{te}) of midgut pieces with different lengths. **A**: midguts were perfused from the oral to the aboral side. The origin in this graph corresponds to a point in the midgut 50 – 150 µm away from the cardiac valve. A non-linear curve-fit was chosen, to avoid negative values for R_{te} while extrapolating for very short pieces. **B**: midguts were perfused from the aboral towards the oral side. The origin of the graph represents the midgut – pylorus border.

was achieved at the perfusion side as well as at the collection side. "Reasonable electrical insulation" was arbitrarily defined as a ratio less than or equal to 1.4 between the measurements of V_{te} at opposite ends of the preparation. For perfect electrical insulation of the midgut lumen from the bath the V_{te} at both ends should be the same. The low electrical resistance of the luminal fluid would level off possible differences between V_{te}^{0} and V_{te}^{L}. Simulations of the experimental results (see below) confirmed this assumption afterwards. When plotted against L_{rel}, which was defined as the ratio of L over the total length of the midgut before mounting in the setup (Fig. 3.7A), R_{te} was 397 ± 77 $\Omega \cdot cm^2$ (n = 14); the average L_{rel} was 0.56 ± 0.07 (n = 14). For L_{rel} 0.56, R_{te} was 231 ± 44 $\Omega \cdot cm^2$, for $L_{rel} > 0.56$, R_{te} was 564 ± 105 $\Omega \cdot cm^2$. This difference was tested to be statistically significant (p = 0.035, n = 7). After curve-fitting, almost half of the variation in R_{te} could be explained by the variation in length (p = 0.016, n = 14). The finding that R_{te} became smaller with decreasing length of the perfused piece of midgut could be an artifact due to leakage at both sides of the preparation, where the epithelium was in contact with the pipettes. Because in short pieces the epithelial surface is smaller than in longer pieces, the overall resistance of a short piece should have been larger than the overall resistance of a longer piece.

3.3.4 Specific Transepithelial Resistance, Aboral to Oral Perfusion

The leakage resistances were in parallel with the overall resistance of the midgut. Therefore the ratio of leakage resistances over the overall resistance of the midgut determined how much of the injected current was lost through the leakage resistance and how much passed into the lumen of the midgut. To examine whether the relation between length and R_{te} indeed reflected an underlying spatial difference in R_{te} between both ends of the midgut or whether it was due to leakage, a second series of experiments was conducted. The midguts were perfused in the opposite direction, i. e. from the aboral to the oral side. When plotted against the actual length (L) of the perfused piece of midgut, R_{te} showed an increase from about 260 $\Omega \cdot cm^2$ at 250 µm to about 530 $\Omega \cdot cm^2$ at 1000 µm. From 1000 µm to 1500 µm it decreased to 430 $\Omega \cdot cm^2$ (Fig. 3.5B). The polynomial curve-fit through the data explained 14% of the variation (p = 0.006, n = 51). On average R_{te} was 399 ± 41 $\Omega \cdot cm^2$ (n = 51). From these data we selected those where the relative length (L_{rel}) could be determined and a reasonable electrical insulation was achieved at the perfusion side as well as at the collection side. "Reasonable electrical insulation" in this case was arbitrarily defined as a ratio

less than or equal to 1.4 between the measurements of V_{te} at opposite ends of the preparation. When plotted against L_{rel} (Fig. 3.7B), R_{te} was 447 ± 65 $\Omega \cdot cm^2$ (n = 27). The average L_{rel} was 0.47 ± 0.05 (n = 27). The curve fitted through this subset of data explained 23% of the variation in R_{te} by the variation in L_{rel} (p = 0.0125, n = 27). The estimate of the quadratic coefficient in x of the polynomial function (see equation in Fig. 3.7B) was statistically not significant (-1922 ± 1037 Ω, p = 0.08). The estimate of the linear coefficient in x on the other hand was statistically significant (2474 ± 1131 Ω·cm, p = 0.039). Unlike for the results plotted against L (Fig. 3.5B), the intercept parameter is negative (-151 ± 248 $\Omega \cdot cm^2$, p = 0.55). This would imply a negative R_{te} for very short pieces. Nevertheless the curve was assumed to reflect the underlying relationship between R_{te} and L_{rel}, because the latter parameter estimate was not statistically significant. If there was no influence of leakage resistances, the R_{te} should have been higher for short pieces than for longer pieces, which apparently was not true. Therefore leakage resistances - at least to some extent - influenced the measurements. If the leakage resistances were lower than the resistances of the perfused midgut pieces, the direction of perfusion should have had no statistically significant influence on R_{te}. The relationship between the length of the perfused piece of midgut and R_{te} - i. e. the resulting curves - should be the same for both perfusion directions, if R_{te} was equally distributed alond the midgut.

3.3.5 Comparison Between Perfusion Directions

To answer the question whether or not both sets of data were essentially the same, they were analyzed with a multiple linear regression procedure. There were three independent variables. The length of the perfused piece of midgut was entered in the procedure as µm values. The direction of perfusion was entered as the value 1 for the oral to aboral perfusion and as the value -1 for the opposite direction. The interaction between length and direction was entered as the product of both values. R_{te} was the dependent variable. All independent variables significantly influenced R_{te}. The p – value for the influence of the length of perfused piece of midgut on R_{te} was < 0.000001, confirming the relationship between length and R_{te} shown in Fig. 3.5A and Fig. 3.5B. The p - value for the influence of the direction of perfusion on R_{te} was 0.0011 meaning that the outcome of the R_{te} measurements depended on whether the midguts were perfused from the oral towards the aboral end or the other way round. The p – value of the influence of the interaction variable on R_{te}

was 0.0013. The direction in which the midguts were perfused therefore influenced the effect of the length of the perfused pieces on R_{te}. This suggests that the relationship between length and R_{te} was different for both directions of perfusion. However, the mere fact that for short pieces the R_{te} was about the same in both series of experiments indicated that leakage influenced the measurements considerably.

From the above we concluded, that there were regional differences in R_{te} between the oral and the aboral end of the midguts, but that these differences were to some extent concealed by leakage.

3.3.6 Leakage Resistances

To estimate the extent of leakage at both ends of the perfused midguts we used the relation between the R_{input} and the length of the perfused piece of midgut. Only R_{input}-data from experiments, where a reasonable electrical insulation could be achieved according to the criteria specified above, were used. When the midguts were perfused from the oral towards the aboral end (Fig. 3.6A), the regression line through the data points was not statistically

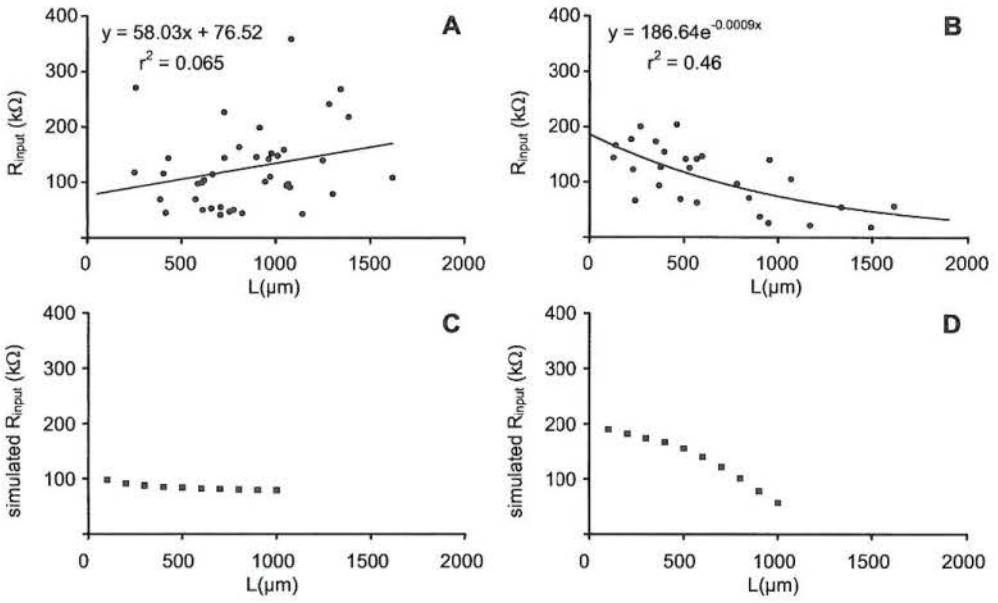

Fig. 3.6 Input resistances change with the length of the perfused piece of midgut. Left hand side: oral to aboral perfusion, (regression line not significant, p = 0.11), right hand side: aboral to oral perfusion (regression line significant, p = 0.00011). **A, B**: experimental values; **C, D**: result of simulations $R_{leak1, 2}$ = 400 kΩ, all R_m were the same as used for the simulations shown in Fig. 3.7.

significant ($p = 0.11$, $n = 40$). When the midguts were perfused the other way round (Fig. 3.6B), the regression line explained 46% of the variation in R_{input} by the variation in length ($p = 0.00011$, $n = 27$). The R_{input} value (186 ±23 kΩ, $p < 0.00001$) extrapolated for $L = 0$ was considered to be an approximation of the total leakage resistance. This resistance was assumed to be the sum of the leakage resistances at both ends of the preparation. Because they are in parallel, and they were assumed to be the same, the value of the leakage resistance at one side was estimated to be twice that value (372 kΩ).

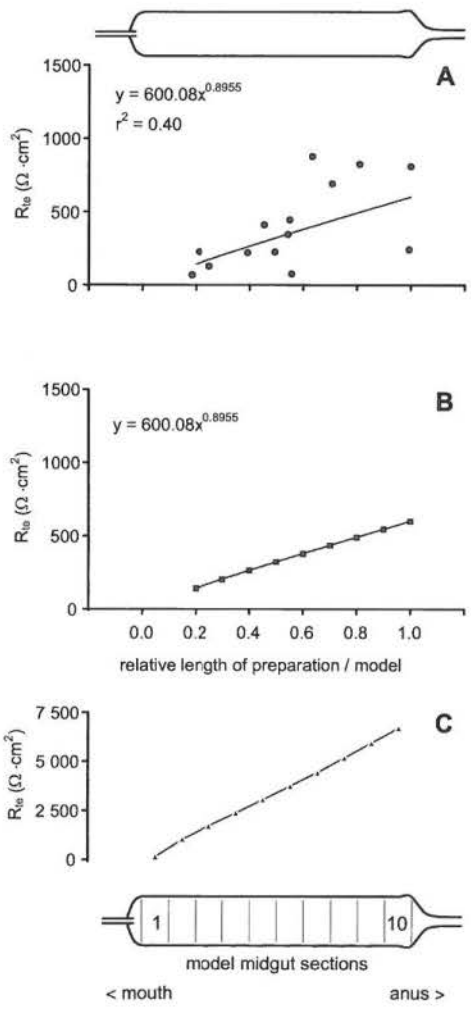

Fig. 3.7 Simulations with model midgut. Mimicking the experimental results with the model shown in Fig. 3.1. Midguts were mounted and perfused from the oral to the aboral end.

A: experimental results, subset of the data shown in Fig. 3.5A, for selection criteria see text;

B: introducing different values for R_m in the model and calculating R_{te} for midgut pieces of different lengths. The best simulation for curve fitting in A was sought. ■ : every datapoint represents the R_{te} calculated for one particular length of the model midgut, consisting of one or more sections (1/10).

C: Estimate of actual R_{te} as distributed along the midgut. ▲: every datapoint represents the R_{te} of one particular section (!) of the model midgut, which had to be entered into the model, to mimic the experimental results.

3.3.7 Simulation, Oral to Aboral Perfusion

Consequently the values of the leakage resistors in the model midgut (R_{leak1} and R_{leak2}) were set to 400 kΩ each. To find out which values for the transmural resistances may explain the results, different values for R_m were introduced into the discrete model (Fig. 3.1). R_{te} was then calculated for pieces of midguts with different lengths. The mathematical functions that fitted the experimental results (Fig. 3.7A) were used to try and fit these simulated R_{te} values. When calculated values for R_{te} were introduced, that were almost linearly increasing from the oral towards the aboral end, a good simulation was obtained (Fig. 3.7A, B, C). The R_m resistor values chosen were 189 kΩ for the first 1/10 and 1.32 MΩ for the second 1/10. From the second 1/10 on the values were increased linearly up to 8.5 MΩ in the most aboral 1/10. Expressed as R_{te}, these values correspond to 148 $\Omega \cdot cm^2$, 1035 $\Omega \cdot cm^2$ and 6699 $\Omega \cdot cm^2$ respectively. The equivalent short circuit currents (I_{sc}) calculated from these values were -71.5, -10.2 and -1.6 $\mu A \cdot cm^{-2}$ respectively. This implies that there was an active net transport of positive charge from the lumen to the hemolymph. This transport was 7 times higher in the first 1/10 of the midgut than in the second 1/10 and 45 times higher than in the last aboral 1/10.

3.3.8 Simulation, R_{input}

For the aforementioned simulations the R_{input} was also calculated, the results were plotted against the virtual length of the model midgut pieces (Fig. 3.6C, D). The simulated values closely resembled the experimental values (Fig. 3.6A, B).

3.3.9 Transepithelial Potential Differences of Short Ends

From what is reported above, it is evident, that the core resistance is much lower than the transmural resistance of the midgut. Any variation in the spontaneous transepithelial potential difference (V_{te}) therefore would be leveled off. To get information about possible differences in electromotive force between both ends of the midgut, we compared the V_{te} of pieces from the oral third with the V_{te} of pieces of the aboral third of the midgut. As mentioned in the preceding chapter, the average length of the midgut preparations was 1132 µm. One third of the length of the midgut therefore was defined as a piece being shorter than 377 µm. The V_{te} of such an oral 1/3 was -10.6 ± 0.5 mV (n = 5), where it was -5.0 ± 2.0 mV (n = 17) for an aboral piece of 1/3 of total length. The difference was

statistically significant, ($p = 0.031$). In two cases slightly positive V_{te} were found in aboral 1/3 pieces (+1.0 mV and +2.2 mV).

3.3.10 Simulation, Transepithelial Potential Differences of Short Ends

We then simulated the V_{te} values found for both ends of the midgut. For that purpose we used the same R_m and R_{leak} values as for the simulation of oral to aboral perfusions. The midgut model shown in Fig. 3.1 was cut down to 3 loops to simulate 1/3 of a midgut. The model was extended with one voltage source (E) at each loop (Fig. 3.8). Each voltage

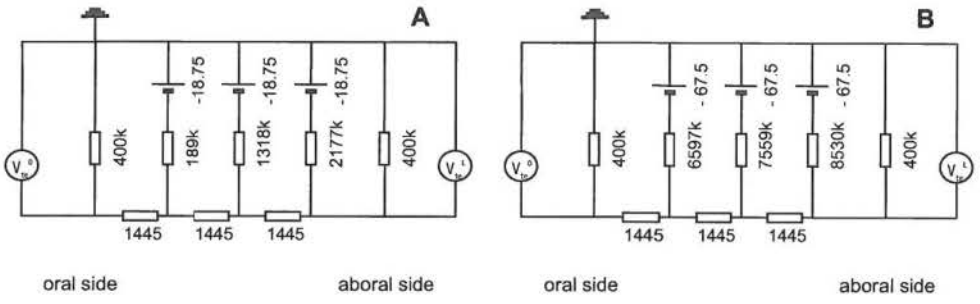

Fig. 3.8 Simulations, perfusion of short oral and aboral pieces of midgut. Numbers near resistors: values (Ω), the values of the parallel resistors are therefore in kΩ; numbers near voltage sources: values (mV); **A**: oral 1/3, simulated $V_{te}^{0} = -10.59$ mV, simulated $V_{te}^{L} = -10.57$ mV; **B**: aboral 1/3, simulated $V_{te}^{0} = -5.01$ mV, simulated $V_{te}^{L} = -5.02$ mV

source represented the transepithelial electromotive force of one particular 1/10 of the midgut. The simulations were done with PSpice. To simulate the experimental results of the perfusions of short oral pieces (-10.6 mV), E had to be set at -18.75 mV each (Fig. 3.8A). The experimental results for short aboral pieces (-5.0 mV) were simulated with E set at -67.5 mV (Fig. 3.8B).

3.3.11 Simulation, Differences between V_{te}^{0} and V_{te}^{L}

With these results further simulations were done to examine the influence of differences in leakage resistances between both ends of the model midgut. As described above, the midgut model shown in Fig. 3.1 was extended with one voltage source at each loop (Fig. 3.9). The voltage sources of the first three oral 1/10 were set at -18.75 mV, in last three aboral 1/10 they were set at -67.5 mV. The remaining voltage sources were set at the intermediate value of -43.13 mV. Simulations were performed with R_{leak} set at 400 kΩ, 40 kΩ, 4 kΩ

and 0.4 kΩ. The ratio by which the simulated V_{te}^{0} and the simulated V_{te}^{L} differed from each other was called "leakage". The results are shown in Table 3.2. When both R_{leak} were set at 400 kΩ, the resulting V_{te} did not differ from each other. At both ends of the whole model midgut V_{te} was -14.2 mV. When one R_{leak} was set at 400 kΩ, while the other was set 10 times lower, V_{te} ranged from -4.9 mV to -5.9 mV. The "leakage"- factor was 1.1 and 1.2. For comparison, the experimental values from oral to aboral perfusions were: V_{te}^{0} = -9.9 ± 0.7 mV, n = 71; V_{te}^{L} = -8.5 ± 0.7 mV, n = 70. The average "leakage" was 1.66 ± 0.12, n= 70.

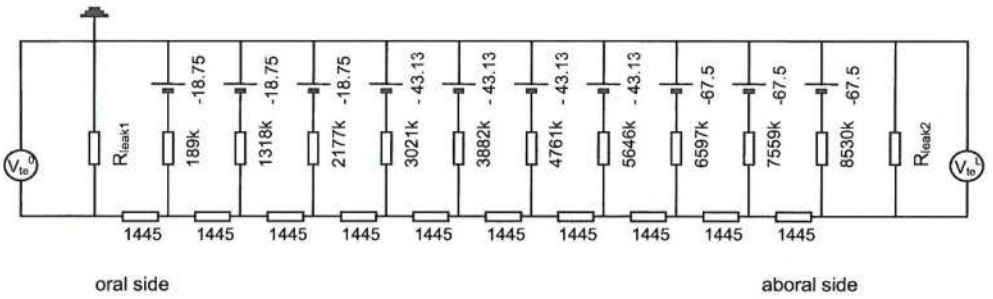

Fig. 3.9 Simulation, equivalent circuit of the midgut tube with voltage sources. Numbers near resistors: values (Ω), the values of the parallel resistors are therefore in kΩ; numbers near voltage sources: values (mV); values for R_{leak} see text and Table 3.2

Table 3.2 Simulation of transepithelial potential differences for differences in leakage.

R_{leak1} (kΩ)	R_{leak2} (kΩ)	V_{te}^{0} (mV)	V_{te}^{L} (mV)	"leakage"
400	400	-14.2	-14.2	1
400	40	-5.9	-4.9	1.2
400	4	-2.2	0.65	3.4
400	0.4	-1.7	-0.07	24.3
40	400	-5.1	-5.6	1.1
4	400	-0.69	-1.5	2.2
0.4	400	-0.07	-0.87	12.4

3.3.12 Other Factors Affecting R_{te}

In the preceding chapter the influence of the variables "leakage", "stage" and "temperature" on V_{te} was analyzed under control conditions for oral to aboral perfusion with multiple regression analysis. The same variables were analyzed for their influence on R_{te}. There were no statistically significant interactions between these variables. The results are presented in Table 3.3: the major contribution (squared partial correlation) to the overall variation in R_{te} is due to the variation in length. Additionally temperature shows a statistically significant, negative correlation with R_{te}, suggesting that R_{te} is decreasing with increasing temperature.

Table 3.3 Multiple linear regression analysis summary: relationships between different variables and the specific transepithelial resistance R_{te}, oral to aboral perfusion.

variable	$\beta_{st.} \pm SE$	$\beta \pm SE$	part r^2	p-level	
leakage	-0.12 ± 0.10	-34.59 ± 28.73	0.013	0.234	n.s.
stage	-0.20 ± 0.10	-52.89 ± 26.65	0.036	0.052	n.s.
length	0.75 ± 0.10	0.68 ± 0.09	0.467	< 0.00001	
temperature	-0.24 ± 0.10	-34.96 ± 14.88	0.050	0.023	

Overall $r^2 = 0.53$, $p < 0.00001$, $n = 57$

$\beta_{st.}$: standardized regression coefficient = standardized estimate, β: regression coefficient = parameter estimate, part r^2: part correlation coefficient, indicates that part of the overall r^2, which is attributable to a particular variable, n.s.: statistically not significant

3.4 DISCUSSION

3.4.1 R_{te} and Length of Midgut: is the Spatial Distribution of R_{te} Real?

The specific transepithelial resistance (R_{te}) was dependent on the relative length of a luminally perfused midgut of *O. cincta*. We hypothesize that R_{te} increased along the length of the midgut from the oral to the aboral side. There is one objection that could be made against this. The actual R_{te} could be distributed equally, and the length dependence of R_{te} could be an artifact due to a systematic leak at the perfusion side or at the collection side,

where the pipettes were pierced through the midgut wall. This can be explained in terms of the model shown in Fig. 3.1. With all transmural resistors (R_m) being the same, the introduction of a low-resistance "leakage"-resistor (R_{leak}) at the oral and at the aboral side in parallel to the transmural resistors (R_m) would lead to an increase in the simulated R_{te} with increasing length. This is indistinguishable from a true increase in R_m - and therefore in R_{te} - when R_{leak1} and R_{leak2} are e.g. 10 times higher than the first R_m in the model. Therefore we mounted the midguts backwards and perfused them from the aboral towards the oral side, to decide whether a systematic leakage in the set-up or a true spatial difference in R_{te} was responsible for the observed relationship between length and R_{te}. The fact that the direction of perfusion had a statistically significant effect on the relationship between length and R_{te} confirmed the assumption that the specific transepithelial resistance (R_{te}) was indeed unevenly distributed along the midgut. However it can not be overlooked that leakage considerably influenced the outcome of our experiments at least when the midguts were perfused from the aboral towards the oral end.

The accuracy of our simulations of R_{te} (Fig. 3.7) depends on the correct estimation of the leakage resistances (R_{leak}). If our estimate is higher than the actual R_{leak}, the low experimental values for short midgut pieces were due to R_{leak} and at the oral side, the actual R_{te} would be higher than the simulated R_{te}. If for instance our estimate of R_{leak} (400 kΩ) is halved, the R_{te} of most oral 1/10 would be 2847 $\Omega \cdot cm^2$, in the second 1/10 it would be 1032 $\Omega \cdot cm^2$ (!) and in the most aboral 1/10 it would be 6647 $\Omega \cdot cm^2$. The actual increase in R_{te} along the midgut would be lower than the simulated increase if we underestimated R_{leak}.

But our estimate of the R_{leak} by extrapolating the input resistance (R_{input}) for zero length is rather the lowest possible estimate than an overestimate. The R_{input} is the total resistance of the transmural resistance of the midgut and the R_{leak} in parallel, neglecting the low resistance of the luminal fluid for that purpose. The total resistance of parallel resistors cannot be higher than the smallest of them. That is to say, the actual R_{leak} has to be at least as high as the R_{input} for short midgut pieces. As shown in Fig. 3.6B, the extrapolation of R_{input} yields a value, which is somewhat smaller than the highest values measured between 200 – 500 µm. In other words, the R_{leak} values we used might be too low. If the actual R_{leak} for instance is 1000 times the estimated value of 400 kΩ, the simulation of the experiments would result in slightly lower values for R_{te}. The R_{te} of the most oral 1/10 would be 76 instead of 148 $\Omega \cdot cm^2$ and for the most aboral 1/10 it would be 5913 instead of 6699 $\Omega \cdot cm^2$. The actual increase in R_{te} along the midgut would be higher than the estimated increase.

From that we conclude, that our estimate of the leakage resistance is a sufficient approximation of the -average- actual leakage resistance. As a consequence, our simulation should be a good approximation of the actual distribution of R_{te} along the midgut. There is another clue for the spatial differences in R_{te}. The relationship between R_{input} and length is different for both perfusion directions. Midguts perfused from the aboral towards the oral end showed the usual decrease of R_{input} with length. (With increasing length the total surface increases, the total resistance decreases; see chapter 1.2.1.) On the contrary, in the midguts perfused from the oral end towards the aboral end there was a tendency, though statistically not significant, of R_{input} to increase, but certainly not to decrease, with length. If the R_{te} was equally distributed along the midgut, the R_{input} would have decreased exponentially (see equation 3.1).

3.4.2 Simulations of V_{te} Depend on the Estimate of Leakage Resistance

If our estimated value, i.e. 400 kΩ, for the leakage resistances is correct, it follows, that the voltage sources in our model (Fig. 3.8 & Fig. 3.9) must generate high voltages at the aboral end (-68mV). Each voltage source in the model represents the V_{te}, which would be observed if only one single 1/10 was measured. As shown in the preceding chapter, we found that the basolateral potential difference (V_{bl}) was less negative at the aboral side than at the oral side. Furthermore, we measured the average V_{bl} to be -64 mV. That implies that the actual apical potential difference (V_{ap}) under control conditions at the most aboral side of the midgut must be slightly positive or at least about zero!

From measurements of the V_{te} at different luminal K^+ -concentrations (see chapter 2.4.4) we can assume that K^+ conductances do not significantly contribute to V_{ap}. If they would the V_{ap} must be negative: the luminal [K^+] is about 10 times lower than the cell [K^+]. Other ions in the perfusion fluid should therefore determine the magnitude of V_{ap}. Because we do not know the actual ion composition of the luminal fluid of unperfused midguts, we are not able to tell whether a zero V_{ap} at the aboral side reflects the true situation in the living animal.

As mentioned above (chapter 3.4.1), our estimate of the leakage resistance (R_{leak}) might be too low. Though this does not influence our R_{te} simulations very much, the V_{te}-simulations might be more seriously affected. If for instance the actual R_{leak} was 1000 times higher than the estimate, the values of the voltage sources in the model are almost identical to the voltages that can be measured. Leakage in that case is negligible. The voltages,

which must be introduced into the model to generate the same V_{te} as were measured in our experiments, are close to the experimental values. From the statistical comparison of the results obtained with different perfusion directions, however, we know that electrical leakage considerably influenced the results of the aboral to oral perfusion. However, from linear regression analysis (preceding chapter, table 2.4) we concluded that the measurements of V_{te} , when the midguts were perfused from the oral to the aboral side, was not significantly influenced by leakage. From the above we conclude 1) that the simulated V_{te} values were overestimations of the true V_{te} in the preparations and 2) that the true V_{te} in the preparations were nevertheless higher (more negative) than the experimental values.

3.4.3 Other Differences between Oral and Aboral End of the Midgut in *O. cincta*

Besides the differences in R_{te}, there are other indications, that there are indeed differences between the oral end and the aboral end of the midgut.

1) The basolateral membrane potential (V_{bl}) and the relative K^+ conductance of the epithelium decreases with increasing distance from the entrance of the midgut as reported in the first chapter. (Both parameters of course are independent from the electrical insulation, suggesting that there is indeed a spatial differentiation of function along the longitudinal axis of the midgut.)
2) The oral 1/3 of midguts showed spontaneous transepithelial potentials (V_{te}), which were more negative than the V_{te} of aboral 1/3. The higher potential difference (-10.6 mV) was found where the R_{te} was supposed to be low (100 - 200 $\Omega \cdot cm^2$) and the lower of both V_{te} (-5.0 mV) was found, where the R_{te} was supposed to be high (6700 $\Omega \cdot cm^2$). At first sight this finding is somewhat contradictory, because a high V_{te} usually coincides with a high R_{te} and a low V_{te} with a low R_{te}. But the low value perhaps does not reflect the physiological electromotive force of the aboral end of the gut. The leakage resistance of the setup, near the high transmural resistance of the tissue, partly shortcircuits the epithelium. This problem is technically difficult to overcome. Nevertheless, taking into account the high R_{te} of the aboral end and the fact that we could still measure a substantial V_{te} is a further proof that the aboral end is physiologically different from the oral end, and has a rather high electromotive force coupled to a high transmural resistance.
3) We demonstrated that there are differences in coloration between both ends of the midgut. Besides its differential coloration, the epithelium between the *valvula cardiaca* and

the pylorus did not exhibit any spatial morphological differentiation, when viable preparations were observed with the light microscope. This is in line with the fact that in ultrastructural studies on springtail midgut no such differences were mentioned (Pawert et al., 1996; Humbert, 1979; Lupetti et al., 1992; Dallai, 1966). The green color of the epithelium found in some cases and the orange color in most cases suggests, that the epithelium most likely consecutively takes up chlorophylls from the food and degrades them. The waste is then shed along with the old epithelium. This process seems to be confined to the oral ¾ of the midgut (Fig. 3.3). The highest percentage of colored midgut epithelium was found during intermolt stage IIb, which is the advanced alimentary phase of the intermolt. This indicates that the coloration is most likely due to uptake of matter from the food. Therefore the differential coloration may reflect a difference in physiological activity between the head end and the back end of the midgut epithelium.

Functional differentiation within an epithelium without any structural differentiation as found in *O. cincta* midguts is not unique. In the Malpighian tubules of *Drosophila* for example there are at least two different types of principal cells showing different expression patterns within a morphologically uniform subregion of the tubule (Sözen et al., 1997). In the springtail *Tetrodontophora bielanensis,* the oral part of the midgut is less active in secretion than the aboral part (Jura, 1958). This shows that within the systematic group of the collembola there can be morphologically uniform as well as morphologically and functionally differentiated midgut epithelia.

3.4.4 Functional Differences Along the Midgut that have been Found in Other Hexapods

It is therefore not unlikely that there are functional differences along the length of the *O. cincta* midgut. The differences in R_{te}, found by us in these preparations, indicate that there are differences in ion transport mechanisms between both ends of the midgut. If our model reflects the actual situation correctly, it takes a distance of less than 1 mm to develop huge differences in R_{te} in the *O. cincta* midgut. At the aboral end of the midgut R_{te} may be almost 45 times higher than at the very entrance of the midgut. We are not aware of any report about similar spatial differences in R_{te}. Differences in other parameters than R_{te} have been reported. In *Aedes aegypti* and *A. canadensis* midguts the direction of transepithelial H^+ transport changes from outward to inward within a distance of about 5mm (Budko et al., 2001). This change in transport properties is due to a different localization

of the V-ATPases. At the oral side the V-ATPases are situated basolaterally at the aboral side they are located apically, causing a 100fold gradient for protons within the peritrophic space. For *A. aegypti* Clark et al. (1999) presented evidence for spatial differentiation in ion transport. The V_{te} in the oral part is lumen negative, whereas it is lumen positive in the aboral part, indicating that ion transport differs fundamentally between both regions. Moreover the ion transport in both parts is regulated differently, the V_{te} is stimulated by phorbol 12,13-diacetate (PE) in the oral part and not in the aboral part. (PE is an agonist of the protein kinase C.)

3.4.5 The R_{te} Values Found for *O. cincta* were Uncommonly High

At first glance the R_{te} values at the aboral end of the midgut of *O. cincta* seem extraordinary high compared to those found for e.g. *Manduca sexta* where it is 217 $\Omega \cdot cm^2$ in the aboral one third of the midgut (Chamberlin, 1990). The surface of this particular part is heavily folded (Figs. 4 and 9 in Cioffi, 1979). Judging by what is shown in this paper the epithelial surface is enlarged about 8 times by these folds. To compare the values we found for *O. cincta*, with those found by Chamberlin (1990) for *Manduca*, therefore the surface enlargement by the epithelial foldings of the *Manduca* midgut must be taken into account. Then the R_{te} in the aboral part of the midgut of *Manduca* amounts to almost 2000 $\Omega \cdot cm^2$. This is somewhat closer to the value we postulated for the most aboral part of the *O. cincta* midgut (6700 $\Omega \cdot cm^2$). Moreover, the values we found for *O. cincta* were corrected for the electrical leakage, which we were able to estimate. Consequently, this leakage should be taken into account when our data are compared to those from other tissues and other species. Usually R_{te} values reported in literature are based on the assumption, that electrical leakage in the experimental setup is negligible. Here we showed that this assumption should be made with the greatest care at least when high R_{te} values are involved. In other words, high values for R_{te} might actually be even higher than reported in literature.

As shown above (chapter 3.4.1), the high R_{te} values found by simulation on the model were likely to be a good approximation of the R_{te} under experimental conditions. That does not mean that the R_{te} in the living animal is as high as under control conditions. Physiological solutions neccessarily are a poor imitation of body fluids -and the midgut content in this case. The hemolymph of *O. cincta* may for instance contain hormones, which can alter the midgut functions and adapt them to the needs of molting or reproduction. The midgut

content most likely contains the products of digestions as for instance amino acids. In insects they are transported into the cell by K^+ dependent cotransport (Dow & Harvey, 1988). Active electrogenic sugar transport, as for instance Na^+/glucose transport, deserves no consideration in this case: insects lack sugar transporters in the midgut. Sucrose glucose and fructose cross the midgut epithelium by facilitated diffusion, following their concentration gradient (Crailsheim, 1988b; Turunen, 1985). If amino acid transporters are present in the aboral part of the *O. cincta* midgut, the absence of amino acids in the perfusion fluid may perhaps be responsible for the high R_{te}. If the aboral part of the midgut was specialized in secondary active amino acid transport -this is of course highly speculative- a lack of the transported substrate would result in less displacement of charges across the epithelium. Less displacement of charges means less current across the epithelium: when V_{te} is not altered, this would cause an increase in resistance (R_{te}). In other words, the differences in R_{te} along the midgut may reflect differences in the expression of transportes along the midgut. Some transport mechanisms for instance may be confined to the aboral or the oral part of the midgut.

The short circuit currents (I_{sc}) - calculated with the measured V_{te} - fell within the range of other hexapod gut epithelia. For the hindgut of the roach *Leucophaea* this was 150 $\mu A \cdot cm^{-2}$, for the midgut of some lepidopteran species this ranges between 500 and 1000 $\mu A \cdot cm^{-2}$ (all values from the review of Dow, 1986). However, in the light of recent findings, that Hexapoda are unlikely to be a monophyletic group (Nardi et al., 2003), prudence is in order when comparing data from Collembola with those from other hexapods (e.g. insects).

It should be noted that the basolateral resistance (R_{bl}) does not significantly contribute to R_{te} because it is almost 5-10 times smaller than the apical resistance (R_{ap}) as demonstrated in the preceding chapter. The major contribution to R_{te} therefore should come either from R_{ap} or from the paracellular resistance (R_{sh}). R_{te} was susceptible to temperature, this may be an indication for the temperature dependent stimulation of active rheogenic transport mechanisms at the apical membranes.

4 Part II: Cadmium Fluxes at the Basolateral Face of the Midgut: a Preliminary Study

4.1 INTRODUCTION

Cadmium is a natural substance, it occurs as CdS or $CdCO_3$ together with zinc minerals or e.g. as $Cd_3(PO_4)_2$ in phosphorous minerals. It has mainly become a pollutant due to human activity, 89% of the global turnover of cadmium is due to industrial activity (Walker et al., 2001). Today cadmium concentrations in the soil increase with 0.2%/year (Järup et al., 1998). Along with soil concentrations crops and cattle show increasing cadmium levels, inevitably leading to higher concentrations in human tissues. On the basis of human autopsy specimens the cadmium concentrations in the kidney cortex increased 47 fold from the turn of the centuries (1897 – 1939) to 1980 (Drasch, 1983). Järup et al. (1998) and Klaassen et al. (1999) suggested that cadmium accumulating in the kidney eventually leads to renal injury in 7% of the general population. Therefore the environmental fate of cadmium especially in the soil is important for our understanding of human non-occupational exposure to this toxicant. The environmental fate of cadmium in the soil is determined by the degree to which the soil-living organisms take it up, accumulate it and eliminate it. That implies that there are mechanisms by which the organisms can cope with the toxic effects of cadmium. Some soil-living organisms as for instance springtails can even increase the bioavailability (water solubility) of the heavy metals (Van Straalen & van Meerendonk, J.H., 1987).

Cadmium unlike the so-called trace elements iron, zinc, vanadium etc. is not required for the regular functioning of organisms, it has no beneficial effects at whatever concentration. Instead it is toxic to organisms. It readily reacts with sulphydryl groups (-SH in Cys) on proteins. This can change the three-dimensional structure of a protein obstructing its regular function. Moreover, it can compete with essential metals for their position at the active center of metalloenzymes. And it can impair the activity of the enzymes (Coleman, 1967).

Cadmium is a metal, it is therefore non-biodegradable. Organisms are unable to break it down into less harmful compounds. Possible detoxification strategies followed by organisms therefore involve the formation of insoluble cadmium complexes, which precipitate intracellularly, or hiding cadmium by complexing it with proteins rich in Cystein.

In *Orchesella cincta* the midgut is the major site of uptake and excretion of cadmium (Posthuma et al., 1992). Cadmium is ingested with contaminated food and accumulated in the body, but it is strongly located within the midgut epithelium (90%) whereas the tissue only constitutes about 4% of the whole animal (Fig. 4.1). At molt the old midgut epithe-

lium is exfoliated and 35% of the total body cadmium is excreted along with it. (The authors point out, that this was apparently due to a partial re-uptake of cadmium by the new epithelium from the degenerating epithelium.) Because the animals molt throughout their life this provides an effective means of cadmium excretion.

Posthuma et al. (1992) found, that animals descending from populations at a clean reference site and at cadmium polluted sites, differed in their ability to excrete cadmium, which they had ingested. While the cadmium accumulation rate did not differ in both populations, the excretion was improved in animals from polluted sites. The animals from the polluted site were genetically adapted to high heavy metal loads by improvement of their excretion efficiency (Posthuma, 1990; Posthuma et al., 1992; Posthuma et al., 1993).

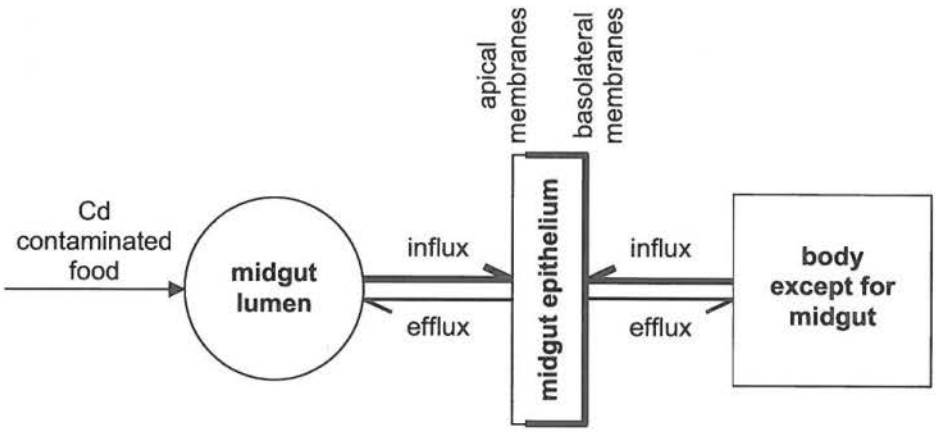

Fig. 4.1 3-compartment model for the cadmium accumulation and excretion in *Orchesella cincta*. Modified from Posthuma et al. (1992). The reabsorption kinetics determine the net cadmium flux across the basolateral membrane of the midgut epithelium. In cadmium adapted animals the balance between release from the epithelium compartment into the body compartment and re-entry into the epithelium may be changed in favor of net reabsorption of cadmium across the basolateral membranes of the epithelium. Excretion of cadmium is accomplished by voiding the (old) midgut epithelium at molt.

This implies, that the basolateral cadmium transport rates differed in both populations. That should be observable as a difference in net cadmium fluxes across the basolateral membrane of the midgut. We tried to confirm this by direct measurements of Cd^{2+} fluxes. We expected inward net fluxes across the basolateral border of the epithelium, which would be higher in animals from polluted than in animals from the reference site.

The cadmium fluxes may be measured as changes in intracellular Cd^{2+} activity with simple intracellular Cd^{2+}-selective electrodes. The detection limit of the Cd^{2+} selective ionophore restricts the use of the electrode to Cd^{2+} activities above 1 µM (Piñeros et al., 1998). An estimate of the maximum cadmium concentration in the midgut epithelium can be calculated for animals from a cadmium polluted site in Stolberg, Germany. (Animals from the same population were used for our experimants too.) For those animals -with emptied guts- Posthuma (1990) reports a whole-body cadmium concentration of 17.4nmol · g^{-1} dry weight. With an average water content of 73.1% (Verhoef & Li, 1983) this becomes 4.7nmol· g^{-1} fresh weight[1]. Taking into account that 90% of the cadmium is present in the midgut epithelium and that the epithelium constitutes 4% of the total body volume, the total epithelial cadmium concentration can be calculated as 105 µM. Cadmium entering the cell may be caught by metallothioneins (MT) and other proteins and phosphate (Hensbergen et al., 2000; Walker et al, 2001). In HCO_3^- -free artificial salines containing phosphate, more than 99% of the cadmium would precipitate as $Cd_3(PO_4)_2$ (own calculations with the MineQl program, for reference see part IA). Even in animals from the polluted site, the intracellular Cd^{2+} activity therefore should be considerably lower than the total cadmium concentration. Most likely, the expected Cd^{2+} activity within the cytosol was near or below the detection limit of the Cd^{2+}-selective ionophore. Moreover, we experienced that Cd^{2+}-selecitive microelectrodes for intracellular measurements (with tip diameters of less than 0.5 µm) had detection limits higher than 1 µM and tended to give instable responses. Therefore we considered that intracellular Cd^{2+}-selective electrodes were not advisable for measurements of Cd^{2+} activities. Instead, we decided to assess the Cd^{2+} fluxes directly with an extracellular vibrating Cd^{2+}-selective electrode. This was advantageous for the following reasons. Because the electrode operated in the artificial saline, the Cd^{2+} activity in the saline could be adapted to the detection limit. Because there was no need for extremely small tip diameters, the electrode tip could be made wider resulting in stable electrode responses. Because there was no need for impaling the cells, artifacts due to damage caused by impalement were avoided. Because the vibrating electrode measured differences in Cd^{2+} activity at well-defined distances away from the midgut, fluxes could be calculated directly from the differential measurements.

[1] nmol · g^{-1} eaquals µmol · kg^{-1} ≅ µmol · l^{-1}

Workable Cd^{2+}-selective electrodes were characterized and implemented in a simple vibrating electrode-setup. The efficiency in detecting a known artificial Cd^{2+} gradient was determined. Measurements were done on control animals as well as on animals from a polluted site in Stolberg, Germany. Intact midgut whole-mounts were exposed to $CdCl_2$. Close to the midgut epithelium Cd^{2+} fluxes were measured to get some insight on the basolateral cadmium transport.

The experiments described in the first part of the thesis suggest, that there are spatial differences in transepithelial resistance and other parameters. Consequently, we examined, if there were spatial differences of Cd^{2+} fluxes along the midgut.

4.2 MATERIALS AND METHODS

4.2.1The Self-Referencing Ion-Selective Micro-Electrode (SERIS): Principle of Operation

Fluxes of ions across cell membranes cause gradients of ion activity in the extracellular fluid. These gradients can be measured as differences in ion activity between different sites in the extracellular fluid. This can be achieved by moving the electrode from one measurement site to the other and reading the potential or by using two electrodes measuring the ion activities at different sites in the fluid. The difference in the recorded potential should reflect the difference in ion activity. But ion selective microelectrodes share one problem: virtually any electrode shows a long-term baseline drift. Superimposed upon that drift, the baseline potential may show unpredictable short-term fluctuations. Especially these fluctuations can mask true differences in ion activity or fake them. As shown in Fig. 4.2A, the amplitude of baseline fluctuations can be higher than differences between particular measurements at different sites or at different moments in time. To minimize the influence of the fluctuating electrode potential, the electrode can be vibrated i.e. quickly moved back and forth between two fixed resting positions. The drift characteristics of a particular electrode are the same for both positions. With respect to drift and fluctuations, the electrode therefore references itself, hence the name Self-Referencing Ion-Selective probe (SERIS). The potential recordings at both extremes of electrode displacement are subtracted from each other. The potential difference is proportional to the difference in ion concentration between both positions. It is no longer masked by the drift characteristics of the electrode: the sensitivity of the electrode to small differences in ion activities is increased. Piñeros et al. (1998) claim, that the ability to detect differences between two ion activities is about 50 times higher for vibrating than for non-vibrating electrodes.

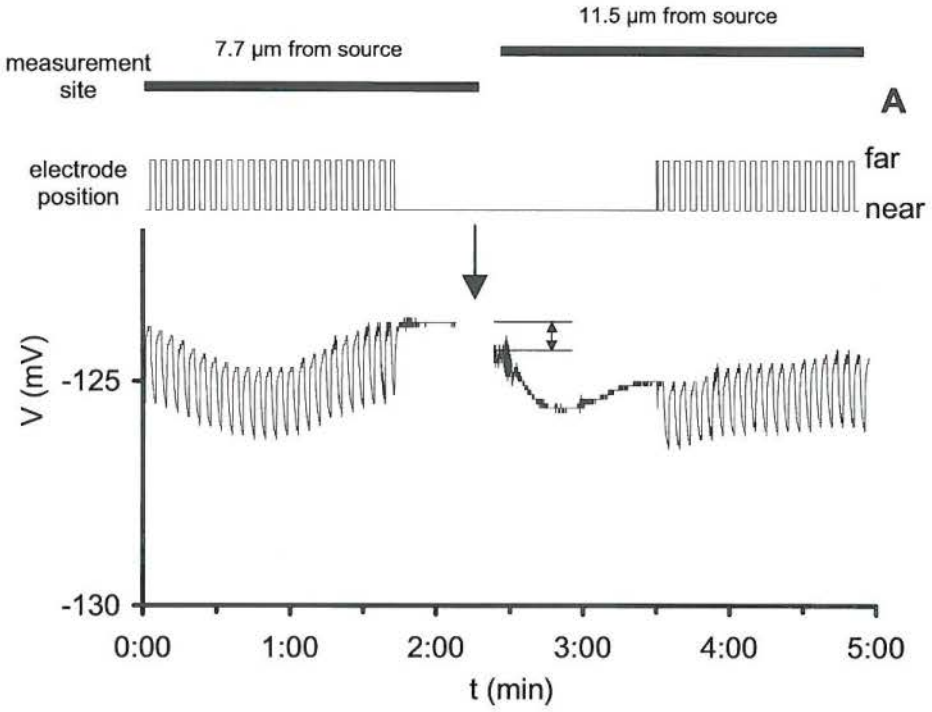

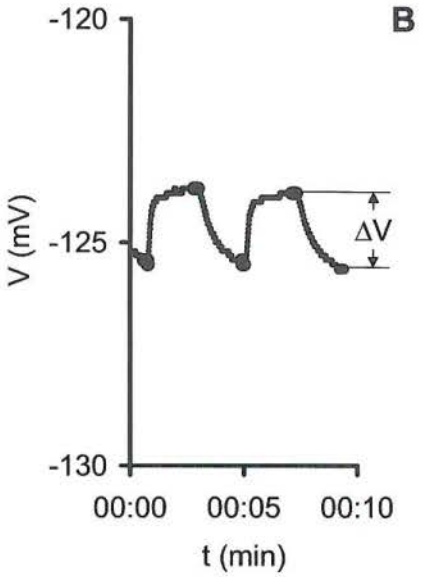

Fig. 4.2 Recording of an artificial gradient. A: upper trace: electrode position (near = near with respect to the diffusion source); lower trace: electrode potential; arrow: change of the "near" position from 7.7 µm to 11.5 µm away from the artificial Cd^{2+}-source (Fig. 4.6); double-headed arrow: voltage difference used for the coarse evaluation of the gradient (see text). The manual positioning of the electrode introduced noise. This part of the recording was discarded. The average of ca 10 s reading right before and right after the change of measurement site was used for the coarse evaluation of the artificial gradient. A more negative V means lower $[CdCl_2]$. Note that the amplitude of the potential fluctuations is higher than the potential difference due to the change in measurement site during the static recording.
B: enlarged section of the potential recording in **A**, example for calculation of ΔV from the last 20 data samples in one half-wave (bold points).

The vibrating Cd^{2+} -selective microelectrode was developed by Piñeros and co-workers (1998) to detect Cd^{2+} fluxes in roots of the Cd/Zn hyperaccumulating *Thlaspi caerulescens* as well as in nonaccumulating species. This type of electrode was based on the vibrating Ca^{2+}-selective electrode developed by Kühtreiber and Jaffe (1990). The Cd^{2+} -ionophore was first synthesised by Schneider et al. (1980). Measurements with vibrating ion-selective electrodes were usually done at vibration frequencies of about 0.3Hz with amplitudes between 5 and 30 µm.

4.2.2 The Self-Referencing Ion-Selective Micro-Electrode (SERIS): Others Studies

The SERIS is based on the vibrating electrode technique that has been developed by Jaffe and Nuccitelli in the 1970ies (Hoppe et 1982). With the vibrating electrode transmembrane ion currents can be measured, but without the ability to distinguish between different ion currents. This limitation was overcome when the vibrating electrode was extended to ion-selective microelectrodes. A concise, though clear description of the technique and some examples for experimental results and recordings can be found in the paper of Kühtreiber & Jaffe (1990) and in the review of Smith & Trimarchi (2001). A more exhaustive description of the technical details and the lay-out of the instrumentation can be found in the paper of Smith et al. (1999). A very short description of this technique was published by Smith in 1995.

The SERIS-approach can be applied to virtually every ion-selective microelectrode or other chemical sensors, like those for NO (Kumar et al., 2001; Porterfield et al, 2001) or for glucose (Trimarchi et al., 2000). The SERIS probe has already been used in a variety of different studies, on plant as well as on animal species:

H^+-selective SERIS probes were used to detect H^+ gradients near the midgut of two *Aedes aegypti* and *Aedes canadensis* (Boudko et al. 2001), H^+ fluxes in retina cells of the skate (Elasmobranchii) (Malchow et al., 1998).

K^+-selective SERIS probes were used to detect K^+ activities near rat glia cells (Shirihai et al. 1998), to examine spatial differences in K^+ transport in Malpighian tubules of *Drosophila melanogaster* (Rheault & O'Donnell, 2001).

Ca^{2+}-selective electrodes were used to demonstrate Ca^{2+}-fluxes in *Amoeba proteus*, *Nicotiana tabacum* pollen tube, *Sarcophaga bullata* and during *Phallusia mammilata* fertilization (Kühtreiber & Jaffe, 1990), to observe Ca^{2+}-influxes during "catch" contractions of

Mytilus edulis muscle (Pelc et al. 1996) and for Ca^{2+} -flux measurements recorded from neurons of *Aplysia* (Smith et al., 1999).

Cl^--selective electrodes were used to detect Cl^--fluxes in rat cerebral arteries (Doughty & Langton, 2001).

Cd^{2+}-selective electrodes were used to show Cd^{2+}-influx in *Thlaspi caerulescens* and *in Thlaspi arvense* (Piñeros et al., 1998).

For all these studies the authors used computer control of elaborate 3-dimensional positioning tools driven by stepper motors. They used custom-made computer software for motion-control and data processing during the measurements. For the purpose of the present preliminary study, we restricted the technical positioning equipment to manually driven micromanipulators and one Piezo actuator. Moreover, the data were not processed during the measurements. The raw data were analyzed with an ordinary spreadsheet program. More details follow later on.

4.2.3 Construction of Cd^{2+}-Selective Microelectrodes

Cd^{2+} -selective microelectrodes were made from the same single barrelled capillaries as the intracellular potential electrodes (Fig. 4.3). They were made lipophilic with hexamethyldisilazane (Janssen Chimica, Beerse, Belgium). The lipophilic electrodes were first backfilled to the shank with an electrolyte solution (10 mM $Cd(NO_3)_2$, 100 µm KCl). The outermost tip of the electrode was broken off, generating electrodes with an inner tip diameter of 2.8 ± 0.4 µm (n = 9). Next the electrode was completely filled by blowing the backfilling solution into the shank with a syringe. Then the tip was front-filled with the Cd^{2+}-selective cocktail (Cd^{2+}-LIX), which formed a column of 134 ± 20 µm in length (n = 11). The Cocktail contained 10% (w/w) Cd^{2+}- ionophore ETH1062, 10% (w/w) K-tetrakis-(3,5-bis (trifluromethyl)phenyl)-borate and 80% (w/w) 2-nitrophenyl octyl ether; all compounds from Fluka Chemie Ag, Buchs, Switserland. Bevelling the tip in a suspension of 0.3 µm alumina (Al_2O_3) particles in water (AB Alpha Polishing Alumina nr 2, Buehler LTD, Evanston, USA) finished the electrode. It was mounted in a holder (type MEH900R WPI, Stevenage, UK) which contained an $AgCl_2$ pellet and connected to the high impedance input of WPI Duo 773 electrometer (World Precision Instruments, Stevenage, UK). To equilibrate the electrode it was placed for two hours in a grounded bath (KCl-agar, AgCl-Ag, see chapter 2.2.10), which contained the same electrolyte solution as the electrode. After equilibration

under these conditions the standard electrode potential E_0 [2] was +202 ± 58 mV (n = 17). With the "ERT"-push button of the electrometer a pA – current pulse was sent through the electrode. The "ERT"-tool was calibrated by sending the same current through a 1 GΩ (± 5%) resistor. From the resulting voltage deflection the electrode resistance could be calculated. It ranged between 3 and 20 GΩ with an average of 8 ± 1 GΩ (n = 14).

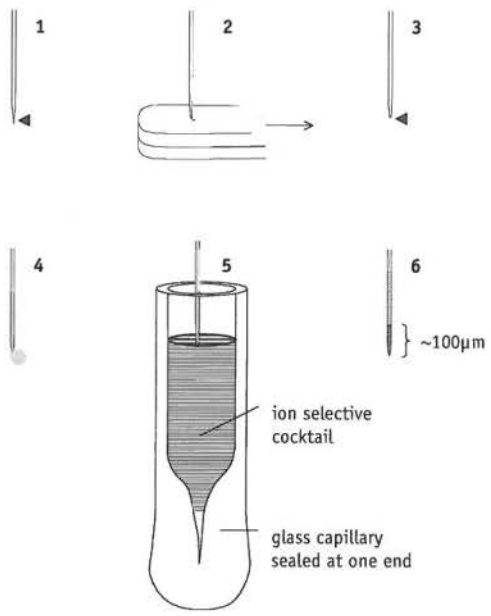

Fig. 4.3 Construction of a single-barreled ion-selective electrode. **1**: After backfilling the electrode with the appropriate electrolyte solution (see text), the tip is still empty. **2**: The outermost tip (arrowhead in "1") is broken off by pulling the back of a forceps over it (arrow). **3**: The tip opening is about 3µm now. **4**: The electrolyte solution is forced into the lipophilic tip. Some fluid has been pushed through the opening to ensure that no air bubble stays in the electrode. **5**: Dipping the electrode into a small (µl) aliquot of the ion-selective cocktail spontaneously fills the tip. **6**: The tip is filled up to the desired length with the Cd^{2+}-selective cocktail (Cd^{2+}-LIX).

4.2.4 Electrode Characterization in Static Mode

For ion-selective electrodes the relationship between the electrode potential and the (negative) decadic logarithm of the activity of the particular ion species is linear. Consequently, the response of the electrode to the addition of a small amount of the ion depends on the amount of the ion already present in the solution (background activity of the particular ion). Moreover, all LIX-microelectrodes we used tended to loose their sensitivity, when they

[2] The electrode potential of an ion selective electrode (E) is the sum of two potentials. One is due to a difference in ion activity at both sides of the ion sensing cocktail (E_{ion}), the other potential is a constant specific for every individual electrode (E_0): $E = E_0 + E_{ion}$. The E_0 of the Cd^{2+} selective electrode is the potential measured, when identical solutions were on both sides of the Cd^{2+} -sensing cocktail in the tip and therefore $E_{ion} = 0$.

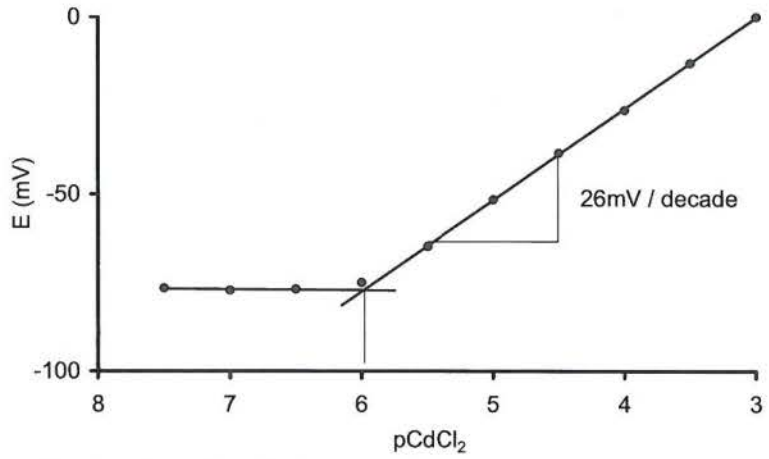

Fig. 4.4 Calibration of a Cd^{2+} -selective microelectrode, representative example. $pCdCl_2$ is the negative, decadic logarithm of the molar $CdCl_2$ concentration ($pCdCl_2 = 10^{-3}$ M $CdCl_2$). The potential recorded for $pCdCl_2 = 3$ was arbitrarily defined as 0 mV, the whole curve was then referred to 0 mV. Each data point represents the average of a 2min potential reading, when the electrode was in equilibrium.

were exposed to ion activities below their detection limit. Therefore, the background activity had to be chosen as low as possible, but it had to be above the detection limit of the electrode. The detection limit was found by calibrating the electrode in a dilution range from 10^{-3} M to $10^{-7.5}$ M $CdCl_2$ in the artificial saline (Fig. 4.4). After having changed the calibration solution, the electrode was allowed to equilibrate. The amplitude of base-line fluctuations was of the order of 1 mV (Fig. 4.2). When the electrode potential had reached its equilibrium, the average potential of approximately 2min reading was used for the calibration. All potentials were corrected for the average drift of the electrode between the start of the calibration procedure and the end of the experiments. Then the intercept of the extrapolated regression lines through the oblique and the horizontal linear parts of the calibration curve was calculated. The detection limit was determined as the molar $CdCl_2$ concentration at the intercept of both lines. On average it was $10^{-5.66 \pm 0.20}$ (n = 8). The artificial saline had 0.145 M ionic strength. The activity coefficient of a $CdCl_2$ solution of 0.145 M ionic strength is 0.198, intrapolated from the data given by Barrow (1973). $10^{-5.66}$ M (2.2 µM) $CdCl_2$ therefore corresponded to a 434 nM Cd^{2+} activity. For comparison: Piñeros and co-workers (1998) reported a loss of Cd^{2+} sensitivity at 1 µM Cd^{2+} activity in solutions with fixed Ca^{2+} background activities (50 µM and 200 µM). The Ca^{2+} background in

the *O. cincta* artificial saline used for calibration and experiments was 6mM. It was concluded that our electrodes performed at the lowest possible detection limit.

The oblique linear part of the calibration curve had an average slope of -28.6 ± 0.5 mV / decade (n = 16) at 28.5 ± 0.5 °C (n = 14). This was close to the theoretical maximum response of -29.9 mV / decade at that temperature. The average coefficient of determination (r^2) for this slope was 1.00 ± 0.003 (n = 17). The average baseline drift between the start of the calibration procedures and the end of the experiments ranged between -0.38 mV and +0.50 mV/h (n = 18).

4.2.5 Electrode Characterization in Dynamic Mode, Definition of Efficiency

Next, the response of the vibrating electrode to an artificial gradient of $CdCl_2$ was evaluated: to what extent does it reflect the actual gradient? This approach was adopted from Kühtreiber and Jaffe (1990). If a compound diffuses from a point-like source into a virtually infinite amount of solution, the relationship between ion concentration (C) and distance from the source (x) is described by

$$C = C_b + K\frac{1}{x}. \qquad (4.1)$$

Where C_b is the background ion concentration at an infinite distance away from the point source in µM and K is an empirical constant specific for a particular experiment. K is the slope in 1/x of the linear equation 3.1). It can be determined graphically: plotting C as a function of 1/x yields a line with the slope K. C and C_b are in µM, which is equivalent to 10^{-9} µmol $\cdot \mu m^{-3}$. Then K is in µmol $\cdot$ μm^{-2}. The value found for K can be used to calculate the theoretical voltage difference of an electrode vibrating with the amplitude Δx:

$$\Delta V = \frac{S}{2.303} \cdot \frac{-K \cdot \Delta x}{C_b \cdot x^2 + K \cdot x}. \qquad (4.2)$$

Where S is the slope of the electrode, as calibrated in static mode. The distance x from the point source is determined as the average of both extreme electrode positions. For the derivation of eq. 4.2 see appendix 2. With this equation it is possible to calculate the curve of the expected voltage difference ΔV at any distance x away from the source. Comparison between the theoretical and the experimental measurements will supply a measure for the ability of the electrode to detect a gradient in the ion concentration / activity. The ratio

between the experimental and the theoretical slope values of the gradient yields the efficiency of the vibrating electrode.

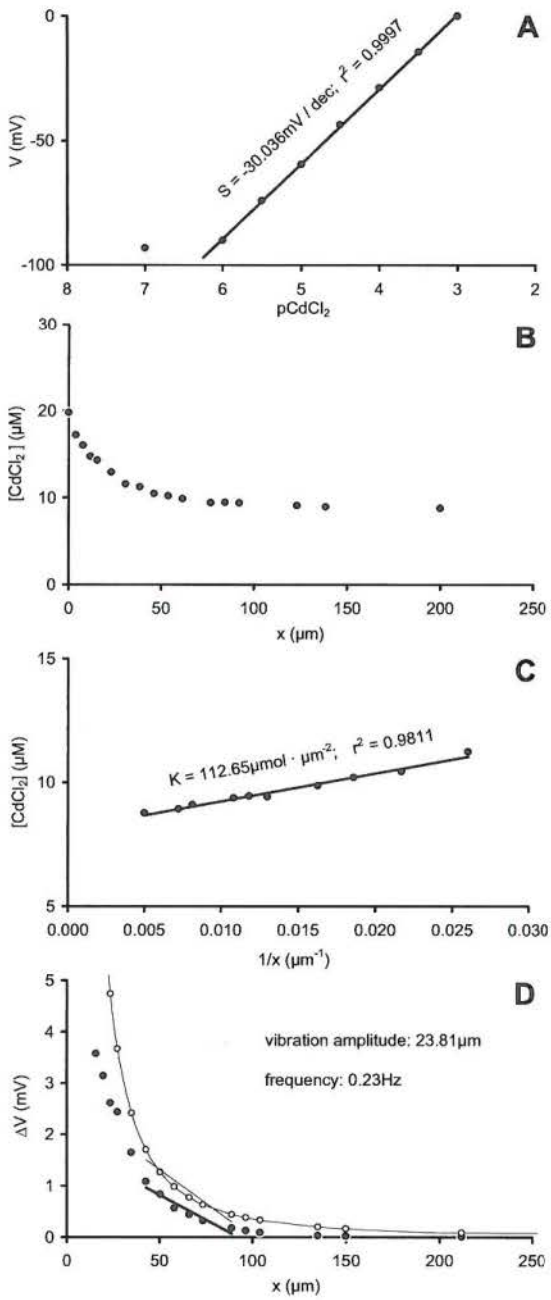

Fig. 4.5 Example of dynamic calibration.

A: determination of the Nernstian slope (S) in static mode.

B: artificial $CdCl_2$ gradient in a background concentration (C_b) of 10^{-5}M $CdCl_2$, coarsely measured with the electrode in static mode, single measurements.

C: determination of the constant "K" with a plot of the statically measured $[CdCl_2]$ values against the inverse of x. The slope of the regression line through the data points yields K:

$[CdCl_2] = C_b + K \cdot x^{-1}$

($[CdCl_2]$ values measured at distances between 0 and 38µm were omitted.)

D: electrode in dynamic mode; theoretical (○) and experimental (●) data for the artificial $CdCl_2$ gradient. The value for K was used to calculate the theoretical ΔV according to eq. 4.2:

$$\Delta V = \frac{S}{2.303} \cdot \frac{-K \cdot \Delta x}{C_b \cdot x^2 + K \cdot x}.$$

Straight lines: regression through data points between 40 and 90µm (regarded as the most reliable part of the curves); experimental (●): **y = -0.0194x + 1.79** (r^2 = 0.921); theoretical (○): **y = -0.0262x + 2.63** (r^2 = 0.908). The ratio of the slopes therefore gave a 74% efficiency of this particular electrode. The SEM-whiskers were smaller than the data points (n = 25).

4.2.6 SERIS Probe Mounting

The electrode holder was mounted on a P-2040 Piezo actuator, connected to a P-2000 controller (both: Physik Instrumente, Karlsruhe, Germany). A homemade square wave generator triggered the controller, allowing to adjust the actuator's frequency of excursions. The Piezo actuator was mounted on manually driven micromanipulators for exact 3-dimensional positioning of the electrode. The Piezo actuator vibrated the electrode between two fixed positions 23.81 ± 0.11 µm (n = 20) apart from each other at a frequency of 0.23 Hz. Via an A/D converter ("Powerlab", ADInstruments, Castle Hill, Australia) potentials were recorded at a sampling frequency of 100Hz and logged to the hard disk of a computer. By the software (Chart 4.01, also ADInstruments) the data were low-pass filtered at 2 Hz.

4.2.7 Determination of Efficiency

After the Nernstian slope was determined (Fig. 4.5A) the electrode was calibrated in the dynamic (vibrating) mode to determine its efficiency in detecting a known artificial Cd^{2+} gradient. The gradient was generated by placing a point-like source of high $CdCl_2$ concentration in a solution low in $CdCl_2$. The gradient source was made from a broken-tip microelectrode (tip diameter: 13.8 µm, Fig. 4.6). It was backfilled with a solution of 10^{-3}M $CdCl_2$ in artificial saline. The back of the pipette was sealed with dental wax to prevent bulk flow out of the tip. This source pipette was placed in the middle of a 60mm Petri dish (Falcon 1016, Becton Dickinson UK LTD, Plymouth, UK) containing approximately 15ml $10^{-5.5}$ or 10^{-5} M $CdCl_2$. The gradient was allowed to settle for 0.5 hour. It was measured at known distances away from the opening of the source pipette (Fig. 4.5B). Throughout the whole range of measurements both, static and dynamic recordings were done. While the measurement site of the electrode was changed it was not vibrated. The differences in potential recordings immediately before and after the change of site (Fig. 4.2A) were summed up and added to the potential measured at the starting position. This reduced the influence of drift and potential fluctuations on the measurements. Along with the electrode potentials, the position of the vibrating electrode was recorded from the monitor output of the Piezo controller. The data from these recordings were analyzed afterwards with MSExcel. The average of the last 20 data points recorded before the electrode was moved to the other position was calculated. The difference between this average and the previous one at the previous position was used to calculate the concentration differences between the last two

extremes of movement (Fig. 4.2B). An example of how the electrode was calibrated in the dynamic mode of operation is given in Fig. 4.5A-D. The average efficiency of the vibrating electrode system we used was 84 ± 3.5 % (n = 5). For the measurements of Cd^{2+}-fluxes had therefore to be corrected by the factor 1.19.

4.2.8 Mounting of Midgut Preparations

After dissection the midguts were immediately transferred to 3.16 µM $CdCl_2$ ($10^{-5.5}$ M) in artificial saline. To hold them in place, they were mounted between two holding pipettes (Fig. 4.7). A 60 mm Petri dish served as a bath containing approximately 15ml of the saline. Through a 3 M KCl- agar bridge and an AgCl - Ag wire in 3 M KCl the bathing fluid was grounded. The bath was not perfused to allow for the development of a stable gradient near the midgut.

4.2.9 Adjusting the Position of "Closest Approach"

Cd^{2+} fluxes near the midgut epithelium were carried out with the electrode vibrating perpendicularly to the midgut and as close to the epithelium as possible (Fig. 4.8). This position was found by slightly indenting the epithelium with the electrode tip and pulling the electrode back until the depression disappeared. This was defined as the "near" position (0 µm). When adjusted correctly, the vibrating electrode did not visibly hit the epithelium.

4.2.10 Calculation of Fluxes

The net Cd^{2+} fluxes were calculated in fmol · cm^{-2} · s^{-1} according to Fick's first law of diffusion:

$$J = -D_{Cd^{2+}} \cdot \frac{\Delta C}{\Delta x}, \qquad (4.3)$$

where $D_{Cd^{2+}}$ is 7.2 · 10^{-6} cm^2 s^{-1} (Parsons, 1959), Δx is the vibration amplitude (23.81 · 10^{-4}cm), ΔC is the difference in Cd^{2+} activity between both electrode positions. By rearranging equation 1.6 (see appendix) ΔC was calculated as

$$\Delta C = \frac{\Delta V \cdot 2.303 \cdot C_b}{S}, \qquad (4.4)$$

where ΔV and S were in mV and C_b was in 10^{-12} mol · cm^{-3}.

4.2.11 Scanning

Before scanning a midgut for spatial differences in Cd^{2+} flux, its length was measured as described in part I and divided into 10 imaginary sections. In the middle of every section, which was accessible with the electrode tip, flux measurements were done above the epithelium. Because of the oblique placement of the electrode, the holding pipette was in the way of the electrode at one end of the midgut (Fig. 4.7). This made it impossible to scan all sections of the midgut during one experiment.

4.2.12 Offset

In the bulk solution at a semi-infinite distance from the preparation a Cd^{2+}-gradient was supposed to be absent. Thus, without any difference in concentration between both electrode positions, ΔV should have been zero. Any deviation from zero was therefore regarded as system offset[3]. The ΔV values measured in the bulk solution were averaged throughout an experiment to give the offset of a particular electrode. The mean offset value for all electrodes was 21 ± 11 µV ($n = 9$). The measurements were corrected for the offset.

4.2.13 Composition of Artificial Salines

The artificial saline (Table 2.1) was modified to avoid complexation of Cd^{2+} by citrate and precipitation as $Cd_3(PO_4)_2$. The organic compounds (citric acid, succinic acid and pyruvic acid) as well as phosphoric acid were therefore omitted. In the original saline they were added as their Na-salts. Omitting them made it necessary to replace them by another Na-compound. NaOH (68 mM instead of 14.2 mM) was added to the solution and pH 6.8 was adjusted with 42.1mM PIPES[4] (free acid, Sigma-Aldrich, Bornem, Belgium).

Salines containing Cd^{2+} were prepared by adding 1 mM $CdCl_2$ (Sigma-Aldrich, Bornem, Belgium) to the above Cd^{2+} -free saline. From this 10^{-3} M stock solution a dilution range down to $10^{-7.5}$ M was made up by mixing with $CdCl_2$-free saline. The final saline compositions are shown in table 4.1. The actual relative concentrations of the different cadmium

---

[3] A possible source of offsets were the abrupt electrode displacements. They perhaps caused small pressure changes on the liquid ion-selective membrane (Kühtreiber & Jaffe, 1990).

[4] PIPES (Piperazine-N,N'-bis(2-ethanosulfonic acid) : pK_2 = 6.8, $pK/°C$ = -0.0085, metal-buffer complexation is negligible (Good et al., 1966)

species were calculated with MineQl ver. 3.01b (see part I A): Cd^{2+} 20.4%, $CdCl^{+}$ 62.7%, $CdCl_3^{-}$ 1.0%, $CdCl_2$ aq. 15.7%.

Table 4.1 Nominal millimolar concentrations in the physiological salines.

saline / component	control	1 mM $CdCl_2$
Na^+	**155**	**155**
K^+	**7**	**7**
Ca^{2+}	6	6
Mg^{2+}	4	4
Cd^{2+}	0	1
Cl^-	**114**	**115**
PIPES	42.1	42.1
glucose	10	10

pH: 6.8, osmolality: 300 mosmol/kg

4.2.14 Animals, Descent and Capture Site, Food

Animals from the same population as used in part I served as controls. Descendants of animals caught at a polluted site near a lead smelter works at Stolberg, Germany were also used because this particular population was previously described as heavy metal adapted (Posthuma, 1990; Posthuma et al., 1993). They were cultured at the lab under the same conditions as the control animals, exept for food. These animals were offered twigs overgrown with algae and molds, which served as contaminated food. The twigs were collected at the heavy metal polluted capture site and air-dried in the lab for at least two weeks before use.

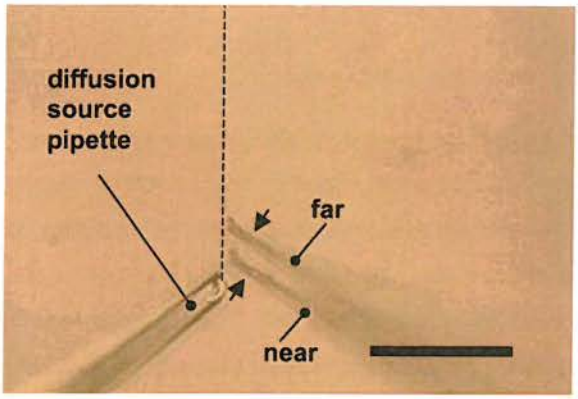

Fig. 4.6 Cd^{2+}-SERIS probe measuring Cd^{2+} activities in an artificial gradient. (2 Video stills were blended to show the resting positions "near" and "far" with Δx = 23.81 µm); arrows: height of LIX-column (68 µm); scale bar: 100 µm; the tip diameter was 2.7 µm; dashed line: line along which the electrode tip was moved to explore the gradient.

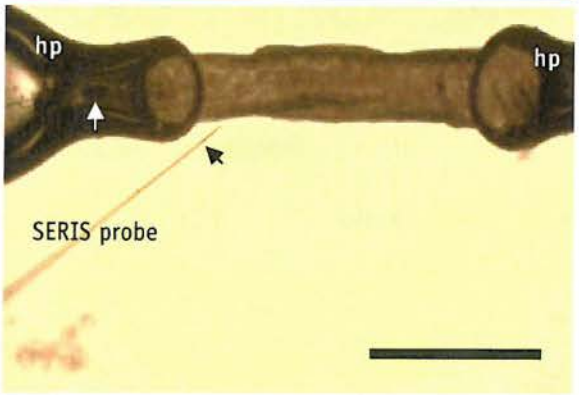

Fig. 4.7 Cd^{2+}-Seris probe measuring Cd^{2+} activities near a whole-mount midgut preparation, stage III, video still. The midgut was not perfused. The electrode is in "far-pole position". Black arrow: height of LIX-column (73 µm); white arrow: valvula cardiaca (oral side of the midgut); hp: holding pipette; scale bar: 500 µm

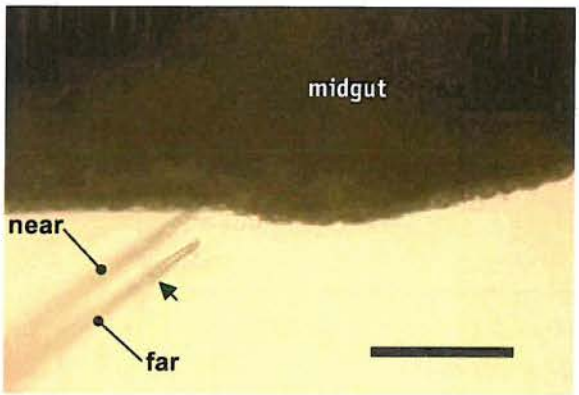

Fig. 4.8 Cd^{2+}-Seris probe measuring Cd^{2+} activities near a whole-mount midgut preparation, stage IIb. (2 Video stills were blended to show the resting positions "near" and "far" with Δx = 23.81 µm); arrow: height of LIX-column (68 µm); scale bar: 100 µm; the tip diameter was 2.7 µm.

4.3 RESULTS

4.3.1 Cd^{2+} Gradient and Fluxes in Controls and in Adapted Animals

We tried and demonstrate that the midgut preparations were able to take up detectable amounts of cadmium at the basolateral side, they were placed in 3.16 µM $CdCl_2$. During $CdCl_2$ exposure the Cd^{2+} activity above the midgut epithelium and in the bulk solution at approximately 4mm away from the midgut was statically measured with a Cd^{2+} -selective electrode. Because Cd^{2+} and the other cadmium species ($CdCl^+$, $CdCl_3^-$, $CdCl_2$ aq.) present in the artificial saline were in chemical equilibrium, a change in one cadmium species would immediately be seen as a change in Cd^{2+} activity.

One preparation from an animal coming from the cadmium-polluted site and one from a control animal were examined. Measurements were done during 41 – 47 min and during 44 – 80 min of exposure respectively. Above the midgut from the cadmium adapted

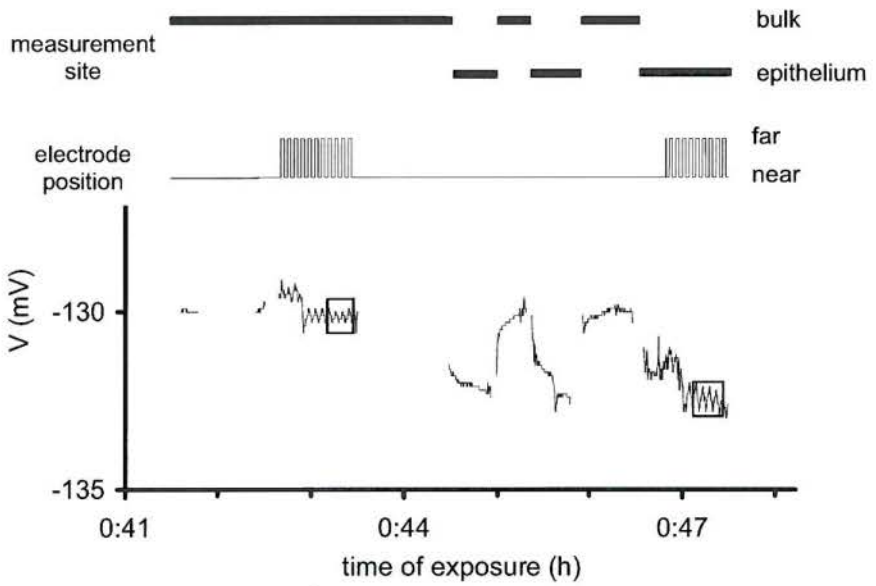

Fig. 4.9 Measurement of Cd^{2+}-activity above the midgut from a cadmium-adapted animal and in the bulk solution. Lower trace: voltage output of the electrode; middle trace: vibration position; upper trace (heavy lines): site of measurement; bulk: bulk solution, about 4 mm away from the midgut epithelium; epithelium: closest possible approach to the epithelium; near, far: near- and far-pole position of the electrode vibrating through a 23.81 µm amplitude, near = near with respect to the midgut preparation; numbers: $pCdCl_2$ values; frames: detail views in Fig. 4.10. Above the epithelium the Cd^{2+}-activity is lower than at the bulk position, more negative potentials mean less Cd^{2+}-activity.

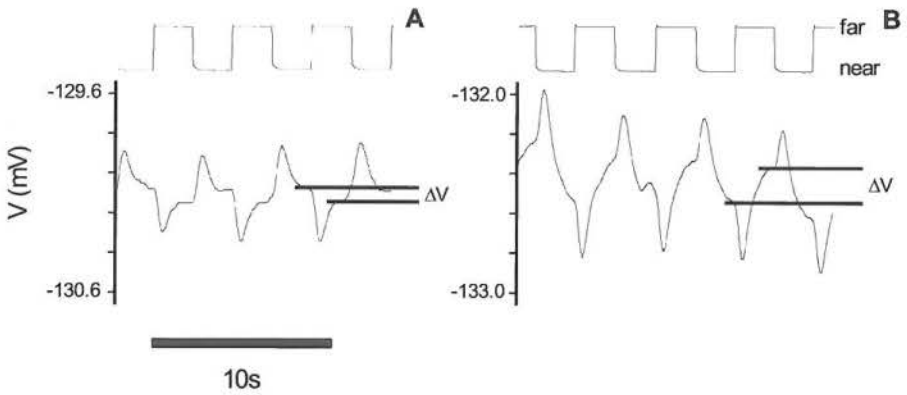

Fig. 4.10 Dynamic measurements of a Cd^{2+}-gradient in the bulk solution and near a midgut epithelium during $CdCl_2$-exposure detail view from Fig. 4.9 (frames). **A**: in the bulk solution, about 4mm away from the midgut, after 59min exposure. The Cd^{2+}-activitiy (3.16 µM nominally) in the bulk solution was supposed to be distributed homogeneously. Nevertheless there were small ΔV offsets measured in the bulk solution. **B**: above the midgut epithelium after 63 min exposure. Upper traces: electrode vibration position with respect to the epithelium, lower traces: voltage output of the electrode. When measured above the epithelium, the voltages read at the "near" epithelial position were more negative than at the "far" position. Above the epithelium the Cd^{2+}-activity was therefore lower than 23.8 µm away from it. The Cd^{2+} gradient was cell-inward. Because ΔV was determined by subtracting the "far"-value from the preceeding "near"-value (see text for details) the ΔV values were negative in **B**. Negative ΔV therefore indicated cell-inward flux. The voltage peak due to the electrode displacement had no visible influence on the measurement of ΔV: it was the same in both **A** and **B**.

animal the Cd^{2+} activity was 516 ± 31 nM (n = 5) lower than in the bulk solution (Fig. 4.9). For the control this was 308 ± 118 nM (n = 6). Dynamic measurements confirmed that there was Cd^{2+} influx at that time (Fig. 4.10). Fig. 4.10 gives a detail view of the dynamic measurements shown in Fig. 4.9 to illustrate that the cadmium fluxes measured at that time were cell inward. The net fluxes were found to oscillate (Fig. 4.11). Although the gradient measured statically only minutes before indicated a net influx of Cd^{2+}, the dynamic measurements revealed that there was net influx as well as net efflux. Similar oscillations were observed in any of the 9 preparations we examined. Although one control preparation only showed influx and another control preparation only showed efflux. Fig. 4.11 also illustrates that the preparations tended weakly towards higher Cd^{2+} efflux with increasing time. This was confirmed by linear regression analysis of the data pooled from all preparations, which

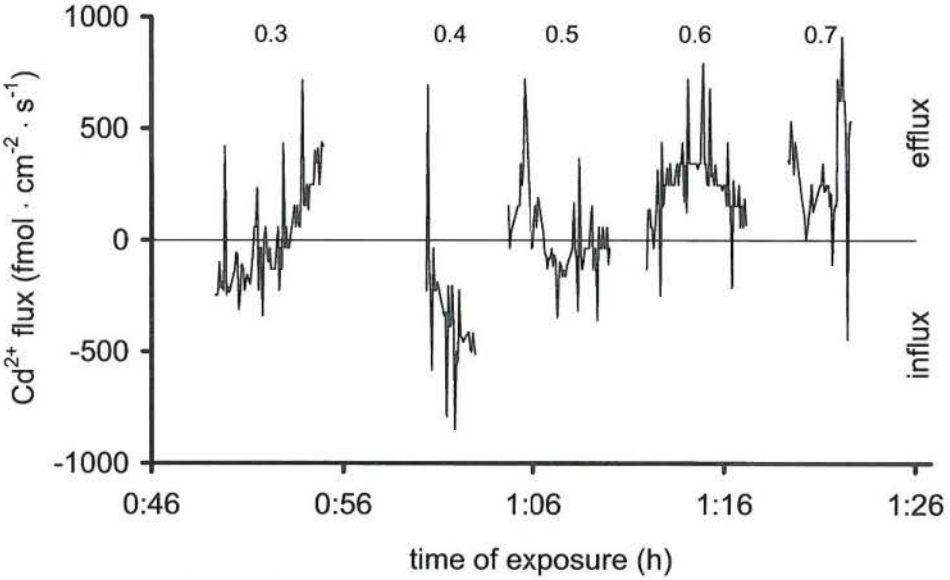

Fig. 4.11 Cd^{2+}-flux recorded from a midgut preparation from the same cadmium-adapted animal as in Fig. 4.9. Numbers at top: measurement site expressed as relative length (e.g.: 0.3 is the 3rd 1/10 of the midgut with respect to the midgut entrance). Where the trace is interrupted, the electrode was moved from one site above the midgut epithelium to the bulk solution and back to the midgut. The flux values were calculated from ΔV values corrected for the offset measured in the bulk solution as well as for efficiency (see materials and methods section).

showed that 1.5% of the variation in flux was due to an increase in time (r^2 = 0.015, $p < 0.00001$, n = 3328), graph not shown.

The mean flux values the entire measurements of all midguts from control animals and from cadmium adapted animals were 5 ± 28 fmol·cm^{-2}·s^{-1} (n = 6) and 72 ± 4 fmol·cm^{-2}·s^{-1} (n = 3) respectively. This difference was statistically not significant (p = 0.121, Mann-Whitney U). The high SEM value reflects the fluctuations in Cd^{2+} flux we found (Fig. 4.11).

3.3.2 Development of the Cd^{2+} Gradient

In the first hour after the start of exposure to $CdCl_2$ the cadmium concentration near the midgut was lower than in the bulk solution (Fig. 4.9). At 100 – 120min of exposure to $CdCl_2$ the same preparation as shown in figs 3.9 – 3.11 was again evaluated for a Cd^{2+} gradient (Fig. 4.12). From the bulk solution towards the midgut at 20 µm above it, the Cd^{2+} activity

decreased as in Fig. 4.9, but at 0 µm it was higher than in the bulk solution, suggesting that some net Cd^{2+} efflux had been activated.

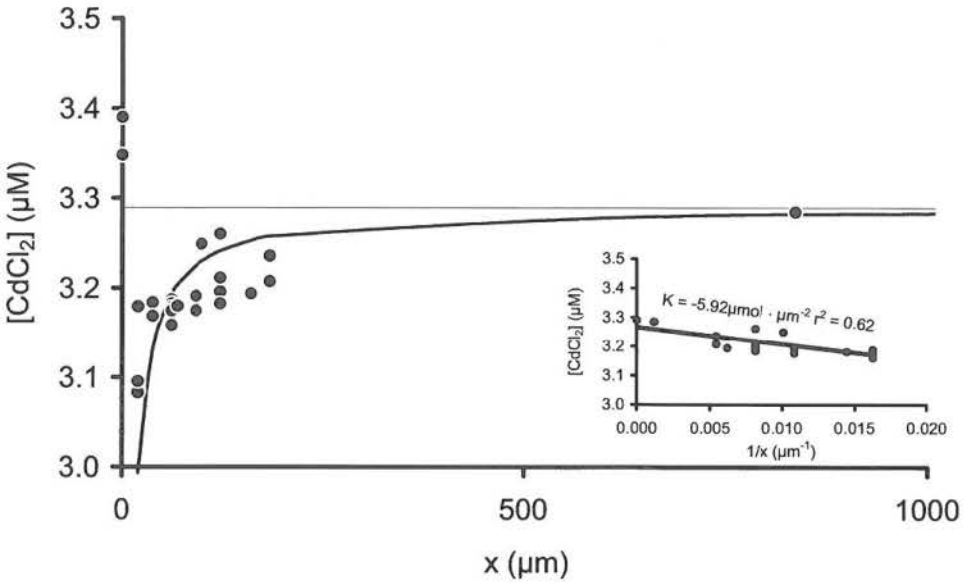

Fig. 4.12 Static measurement of $CdCl_2$ above the midgut from a Cd-adapted animal and in the bulk solution, 1:40 –2:00 hour exposure to 3.16 µM $CdCl_2$. Same preparation as in Figs 3.9 – 3.11; Heavy line: theoretical gradient for $CdCl_2$. It was calculated as $[CdCl_2] = C_b + K \cdot x^{-1}$ from static measurements of $[CdCl_2]$ between 60 µm and 4 mm (bulk solution). Insert: the constant K was determined as the slope of the regression line through the measured $[CdCl_2]$ plotted against the inverse of x. Thin line: background $[CdCl_2]$ (C_b) as measured in the bulk solution. Dynamic measurements of the same gradient gave analogous results for fluxes (not shown).

4.3.3 Eliciting Cd^{2+} Influx by Increasing the Basolateral $[CdCl_2]$

After 70min basolateral exposure to 3.16 µM $CdCl_2$, the $[CdCl_2]$ was increased to 10 µM by exchanging the whole saline volume. Before the new saline (10 µM) was added, the old saline (3.16 µM) was removed completely from the bath. The new As a result, the Cd^{2+} changed from weak efflux (+96 fmol·cm^{-2}·s^{-1}) to strong influx (app. –3000 fmol·cm^{-2}·s^{-1}). Within 5 minutes the influx rapidly decreased and eventually changed to efflux, reaching a plateau at +276 fmol·cm^{-2}·s^{-1} (Fig. 4.13). Before reaching the plateau, the influx suddenly increased for approximately 30s. After that it decreased again towards the plateau. Exactly

the same pattern was observed when the experiment was repeated with a second preparation.

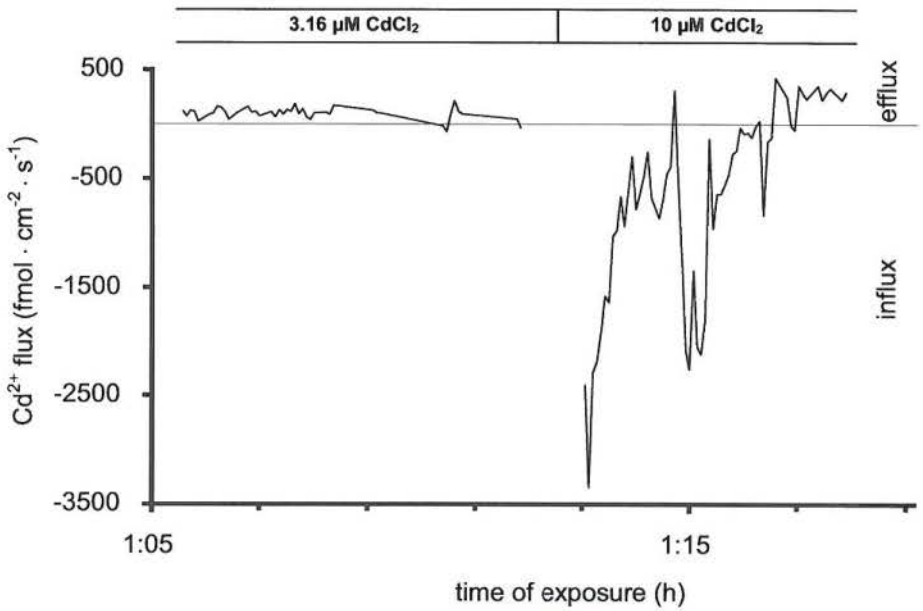

Fig. 4.13 Measurement of Cd^{2+} flux above a midgut from a heavy metal adapted animal. Above: experimental protocol; thin line: demarcation of zero flux; positive values indicate efflux and vice versa. The increase in basolateral $CdCl_2$ concentration caused a strong transient influx of Cd^{2+}. The sudden increase of Cd^{2+} influx at t = 1:15 h was also observed when the experiment was repeated with another preparation.

4.3.4 Scanning for Spatial Differences in Cadmium Fluxes

The Cd^{2+} fluxes were evaluated at different measurement sites above the midgut epithelium. The Cd^{2+} flux showed no obvious spatial differences along the midgut although the regression line through the flux data ($r^2 = 0.028$, $n = 3328$, $p < 0.00001$) pooled from all animals suggested a weak influence of the measurement site on Cd^{2+} flux. At the oral side efflux slightly prevailed influx, whereas at the aboral side in- and efflux were in balance.

4.4 DISCUSSION

Orchesella cincta is able to excrete cadmium ingested with the food by storage - excretion via the midgut epithelium. The model of Posthuma et al. (1992) predicts basolateral cad-

mium influx, which should be stronger in midguts from cadmium adapted than in midguts from not adapted animals. By measurement of Cd^{2+} fluxes and by evaluating Cd^{2+} gradients near midgut preparations we could confirm, that there was basolateral transport of cadmium into the midgut epithelium. We could however not substantiate statistically significant differences in Cd^{2+} fluxes between both populations. Piñeros et al., (1998) report similar results: they used a Cd^{2+}-SERIS to detect Cd^{2+}-fluxes near roots of two related plant species. The Cd/Zn hyperaccumulator (species able to enrich Cd and Zn in it's tissues above the concentrations found in nonaccumulating species) *Thlaspi caerulescens*, was expected to show higher influx rates of Cd^{2+} than the related nonaccumulating species *Thlaspi arvense*. Unexpectedly, they found no differences in Cd^{2+}-influx rates between the hyperaccumulator and the nonaccumulator.

4.4.2 Validation of the technique

The SERIS method in general does not need any further validation: it has already been used in many studies (for references consult chapter 4.2.2). The method implies that the electrode is calibrated in static (i. e. nonvibrating) mode as well as in dynamic (i. e. vibrating) mode. During the dynamic calibration the electrode detects an artificial gradient (see materials and method section). That implies that the direction of the gradient is known. By that the correct functioning of the electrode can be ascertained, i. e. that the electrode correctly measures the direction of the gradient. In the present study however, effluxes were found, where influxes were expected. Influxes of Cd^{2+} were expected, because there should be a cell-inward electrochemical gradient for Cd^{2+} in the midguts and because the midguts are known to accumulate reasonable amount of cadmium. That raised doubt about the correct interpretation of the measurements. Therefore the cadmium concentration was suddenly increased in two experiments to increase the cell-inward gradient for Cd^{2+}. As expected, a high influx could be measured, though only for 2 min, then it turned into efflux (Fig. 4.13). We concluded that the SERIS electrode correctly measured the direction of Cd^{2+}-fluxes near the midgut.

Oscillations in fluxes measured with a SERIS as we report here are not unusual. (see for example fig. 9C in Smith et al., 1999; fig. 3 in Porterfield et al, 2001; fig. 4A in Rheault & O'Donnel, 2001;). The amplitude of oscillations ranged between 0.5 $pmol \cdot cm^{-2} \cdot s^{-1}$ observed for NO fluxes (Porterfield et al, 2001) to more than 3 $pmol \cdot cm^{-2} \cdot s^{-1}$ observed for Ca^{2+} fluxes

(Smith et al., 1999). Our own measurements showed oscillations of about the same order of magnitude (Fig. 4.11).

Cd^{2+} flux values near roots of two *Thlaspi* species ranged between 50 and 300 fmol·cm^{-2}·s^{-1} (Piñeros et al., 1998). Ca^{2+} flux values as low as 20 – 112 fmol·cm^{-2}·s^{-1} were found in *Amoeba proteus*, background signals were 3 ± 18 fmol·cm^{-2}·s^{-1} (Kühtreiber & Jaffe, 1990). Control Ca^{2+} fluxes near neurons of *Aplysia* were about 0.5 pmol·cm^{-2}·s^{-1} (Smith et al., 1999). The fluxes we measured were within the range other authors already reported.

In many studies however the ΔV values, i. e. the difference of the two voltages measured at the extremes of electrode movement, are presented instead of flux values. Usually they are in the µV range, Boudko et al for instance measured ΔV values between 20µV and 80µV (Boudko et al. 2001). For comparison: the ΔV values we measured were in the range of 100 µV and lower. With a Nernst slope of 28 mV a ΔV of 100 µV equals a concentration difference between the both electrode positions of 26 nM at a background concentration of 3.16µM $CdCl_2$ (see eq. 4.4). From that value the flux can be calculated with eq. 4.3 as 93 fmol·cm^{-2}·s^{-1} for a vibration amplitude of 23.8 µm.

We had electrodes, which were able to detect a Cd^{2+} gradient with 84 ± 3.5% (n = 5) efficiency (see chapter 4.2.7). For comparison: the authors, who developed the Cd^{2+} vibrating electrode (Piñeros et al., 1998), reported an efficiency of 55% for their Cd^{2+} electrodes.

4.4.2 Gradient and Flux Measurements

Static measurements at different distances from the epithelium showed, that cadmium had been taken up from the solution into the cells (Figs 4.9 & 4.12). Surprisingly, close to the epithelium, measurements in dynamic mode indicated, that there was net influx as well as net efflux. If there was only one distinct mechanism of cadmium entry, a saturation of Cd^{2+} influx should have been observed, which finally should have reached zero values. But the oscillations of Cd^{2+} flux we observed (Fig. 4.11) suggested that there were at least two different mechanisms involved in basolateral cadmium transport. Apparently there were distinct in- and efflux mechanisms of cadmium at the basolateral side of the epithelium. From that we concluded, that cadmium first had been taken up by the midgut epithelium by a rapid entry mechanism in the period before the flux measurements were started. This mechanism might resemble the "fast process of accumulation" reported by Jumarie (2002) for vertebrate alveolar cell monolayers. Afterwards, during the observation period, the net

influx and the net efflux alternated. When the net cadmium influx exceeded a particular value, with a certain delay an efflux mechanism might have been activated causing these alternating net fluxes.

An entirely passive entry of cadmium would have approximated a steady-state value at the electrochemical equilibrium for cadmium, without anything but random fluctuations. At the electrochemical equilibrium the net flux would be zero. This was not observed. Instead, the net fluxes averaged over the whole observation period following a preincubation to $CdCl_2$ even had a positive sign; cadmium left the epithelium at the basolateral side. From that we concluded, that active extrusion mechanisms must exist in the midgut.

The Cd^{2+} efflux we observed could only have been passive if the electrochemical equilibrium concentration for cadmium was exceeded inside the cell. From the basolateral membrane potential difference (V_{bl}) the ratio of intracellular to extracellular $[Cd^{2+}]$ can be calculated. Under control conditions V_{bl} was -63.8 mV (see part I for details). At this potential the ratio of $[Cd^{2+}]_o$ over $[Cd^{2+}]_i$ in equilibrium was calculated with the Nernst equation from

$$-63.8\text{mV} = -29.4\text{mV} \cdot \log\frac{[Cd^{2+}]_i}{[Cd^{2+}]_o},$$

where -29.4 mV was the Nernstian slope at the average temperature of 23.1°C when V_{bl} was measured. In equilibrium the Cd^{2+} activity inside the cell ($[Cd^{2+}]_i$) would have been 148 times higher than the Cd^{2+} activity outside the cell ($[Cd^{2+}]_o$). The actual free concentration of Cd^{2+} in the saline was approximately 20% of the total cadmium concentration (see 3.2.12 "Composition of Artificial Salines"). The actual free concentration of Cd^{2+} in the bath would have been 0.6 µM for $[CdCl_2]_{bath}$ = 3.16 µM and 2 µM for $[CdCl_2]_{bath}$ = 10 µM. In equilibrium, the actual free concentration of Cd^{2+} inside the cell would have been 148 times these vaules i.e. 88 µM and 292 µM respectively. The total dissolved intracellular cadmium concentration would have been 5 times these values i.e. 444 µM and 1460 µM! Comparing these theoretical values to the total maximum concentrations of cadmium in the midgut epithelium (105 µM, see calculation in the introduction section) shows, that it is nonsensical to assume that these values could ever have been reached. Therefore it seems reasonable to presume an active mechanism responsible for the Cd^{2+} efflux.

4.4.3 Biological Significance of Basolateral Cadmium Efflux

The $CdCl_2$ concentrations we used for the experiments most probably were orders of magnitude higher than in the hemolymph of a living animal from a cadmium-polluted site. Attempts to measure hemolymph [Cd^{2+}] of animals from the polluted site (with the same type of electrode as used for hemolymph pH, see part I) failed. Most likely the [Cd^{2+}] was below the detection limit of the electrode. Returning to the calculation of the total epithelial cadmium concentration, the maximum total cadmium concentration can be estimated for the "body except for midgut" compartment (Fig. 4.1). This results in 488 nM, which is 210 times lower than the calculated intracellular cadmium concentration in the midgut epithelium (105 µM). Taking into account, that proteins and other components in the hemolymph may bind cadmium and that the body tissues most likely capture some of the cadmium, the actual [Cd^{2+}] in the living animal will be even lower. Because of the high experimental cadmium concentrations compared, the influx of cadmium during the experiments would have been much stronger than in the living animal. The intracellular binding sites for cadmium (MT and other proteins and phosphates) might have been saturated. Cadmium that had entered the cell would not be chemically bound anymore, it would instead increase the intracellular concentration of dissolved cadmium. Thereby it would weaken the cell inward gradient for cadmium. As a consequence, an active extrusion mechanism would work easier. The cadmium efflux would become more pronounced. This would explain, why Cd^{2+} efflux prevailed over Cd^{2+} influx during the observation period, which apparently did not cover the first rapid Cd^{2+} influx. As a conclusion, the Cd^{2+} effluxes we measured most likely did not reflect the actual situation in a living animal. But there might be active extrusion mechanisms in the midgut epithelium by which cadmium leaves the cell across the basolateral membrane.

4.4.4 Scanning for Spatial Differences in Cadmium Fluxes

The intensity of the Cd^{2+} fluxes at the basolateral side was almost equally distributed along the midgut. The entire basolateral side of the midgut therefore may serve to extract cadmium from the hemolymph. Nevertheless there was a very weak but statistically significant influence of the site of measurement on the measurement of Cd^{2+} fluxes. The Cd^{2+} influx was slightly stronger at the aboral than at the oral side. In the living animal, the significance of that may be that the direction of hemolymph circulation is from the oral towards the

aboral side. Cadmium, which leaves the midgut, will be carried away by the hemolymph. The cadmium load of the hemolymph increases while it passes the midgut from the oral to the aboral side. Influx mechanisms, which are more active at the aboral than at the oral side, would counteract this. Thereby the cadmium (re-)uptake from the hemolymph would be made more effective.

5 General Conclusions

Springtails play an important role in the ecosystem of the soil. They promote decomposition processes, they increase the bioavailability of heavy metals and other substances in the soil and they are an important prey for many predators. For these reasons springtails are used as experimental animals in ecology and in ecotoxicology. The springtail *Orchesella cincta* is often used in those studies as a representative of the soil ecosystem or of the springtail fauna in the soil. Many studies deal with the effects of toxicants on this animal.

The midgut is the first barrier against the uptake of toxicants from the food into the body. It is therefore important to study the basic functions of this organ to understand the processes involved in the uptake of toxicants. Up to now, however, no basic information about the physiology of the midgut of *O. cincta* -or other springtails- is available. This thesis tries to fill part of the gap in our knowledge.

In **part IA "General Electrophysiological Properties of the Midgut"** the main electrophysiological properties except for the specific transepithelial resistance (R_{te}) are described. The elements and the osmolality of *O. cincta* hemolymph were analyzed. The hemolymph had a high Na over K concentration and was rich in Cl: (in mM ±SEM) 154 ± 2 Na, 7.0 ± 1.2 K, 9.6 ± 3.5 Ca, 3.5 ± 1.1 Mg, 6.7 ± 0.6 P, 114 ± 14 Cl. ($n_{Na, K, Ca, Mg, P}$=3 hemolymph samples pooled from about 190 individuals, n_{Cl}=11 individuals). The ionic composition of the hemolymph resembled that of other hexapods (insects) from ancestral systematic groups.

Some electrophysiological parameters of the midgut were investigated in relation to intermolt stages and at different basolateral and luminal [K^+]. Under control conditions, the basolateral potential (V_{bl}) was -63.8 ± 1.17 mV (n = 51), the transepithelial potential (V_{te}) was -10.6 ± 0.7 mV (n = 59), lumen negative. The apical potential (V_{ap}) was calculated to be -53.2 mV cell negative. V_{bl} showed an almost perfect Nernstian behavior when the bath [K^+] was increased. The fractional resistance of the basolateral membrane was 17 ± 5% (n = 12) of the total cellular resistance. This low relative resistance in the electrical equivalent circuit of the epithelium and the high relative K^+ conductance in the basolateral membrane allowed to estimate the cell [K^+] from V_{bl} using the Nernst equation: under control conditions (23.1°C) it was 85 mM.

The correlations between potentials and other variables were tested with linear multiple regression. The age of the epithelium, i.e. the intermolt stage, had a significant effect on V_{bl}, but not on V_{te}. V_{bl} was positively correlated with the distance of the impalement

site from the oral end of the midgut. The quality of electrical insulation did not significantly influence the measurements of V_{te}.

pH was measured with ion sensitive microelectrodes in the hemolymph (*in vivo*): 7.26 ± 0.1 (n = 9). In the cells and in the lumen it was 6.81 ± 0.08 (n = 8) and 6.73 ± 0.09 (n = 17) respectively. With a bath pH of 6.8, the electrochemical driving forces acting on protons *in vitro* were cell inward from lumen and hemolymph side.

Part IB " Spatial Distribution of the Electrical Transepithelial Resistance (R_{te})" describes how to distinguish between the effects of electrical leakage and a true spatial distribution of R_{te}. In midguts of different lengths, luminally perfused with symmetrical physiological solutions, average specific transepithelial electrical resistance (R_{te}) was determined with cable analysis for terminated cables. R_{te} was 389 ± 35 $\Omega \cdot cm^2$ (SEM, n = 69) when midguts were perfused in the oral to aboral direction. For the aboral to oral direction R_{te} was 399 ± 41 $\Omega \cdot cm^2$ (SEM, n = 51). In both cases, R_{te} was positively correlated to the length of the perfused piece (L) while the perfusion direction significantly influenced the L – R_{te} relationship: spatial differences in R_{te} were masked by electrical leakage. By calculating the input resistance for L = 0, the total leakage resistance was estimated to be 186 ± 23 Ω (SEM, n = 27). Cable analysis was extended with a computer simulation on an equivalent circuit of the midgut including leakage resistances (R_{leak}). The experimental results were explained by increasing R_{te} from the oral towards the aboral end. For midguts perfused in the oral to aboral direction, the simulated R_{te} was 148 $\Omega \cdot cm^2$ at the oral end of the midgut increasing to 6699 $\Omega \cdot cm^2$ at the aboral end. This might be a slight overestimate of the actual R_{te} under control conditions. The precision of the simulation depends on the correctness of the R_{leak} estimate. We discussed this point and from the fact that R_{leak} was in parallel with the transmural resistance of the midgut we concluded that the estimate was rather an underestimate than an overestimate. Underestimation of R_{leak}, however, could not result in a severe overestimate of the highest R_{te} we found at the aboral side. Nor could it result in an overestimate of the steep oral to aboral increase in R_{te} we found, it rather would result in underestimation ot the true increase in R_{te} along the midgut.

We simulated the V_{te} to explain the experimental results taking R_{leak} and R_{te} values of our simulations into account. The V_{te}-values we needed to introduce into the simulation were so high, that the apical potential difference (V_{ap}) must have been positive or about zero in the aboral part of the midgut. In discussing this point we showed that the simula-

tions of V_{te} were sensitive to an underestimate of R_{leak}. Considering that R_{leak} probably is an underestimate and that the results were nevertheless concealed by leakage, we concluded that the true V_{te} is in between the experimental and the simulated values.

The increase in the R_{te} from the oral to the aboral end suggests a difference in transport functions along the midgut. For the first time, spatial differences in R_{te} could be demonstrated within a distance of as short as 1 mm.

Whenever high R_{te} values are expected for short tubules (terminated cables), our approach may be helpful in estimating true R_{te} and R_{leak} or even in correcting the experimental V_{te} values for leakage.

Part II "Cadmium Fluxes at the Basolateral Face of the Midgut: a Preliminary Study" sums up some preliminary observations of the basolateral cadmium transport of *O. cincta* midguts. In preliminary experiments, we examined whether midguts from animals adapted to cadmium pollution, had higher Cd^{2+} influx rates than midguts from not adapted animals. First of all, we tried to find out whether the vibrating ion-selective electrode technique (SERIS) is a suitable means for detecting Cd^{2+} fluxes at the basolateral face of this preparation.

A Cd^{2+}-selective electrode was successfully implemented in a SERIS setup. This electrode repeatedly measured Cd^{2+} activities at two different positions. The efficiency of the SERIS probe to detect an artificial gradient was 84 ± 3.5% (n = 5). Whole mount midgut preparations of *Orchesella cincta* were exposed to 3.16 µM $CdCl_2$. From the differences in $[Cd^{2+}]$ activity between two known positions near the basolateral side of midgut preparations, Cd^{2+} fluxes were calculated with Fick's first law of diffusion. During the observation period, the Cd^{2+} fluxes were found to oscillate and we observed net Cd^{2+} influx as well as net Cd^{2+} efflux. These fluxes ranged between −1000 to +1000 $fmol \cdot cm^{-2} \cdot s^{-1}$. By static measurements of the Cd^{2+} gradient near the midgut, we found that a strong Cd^{2+} influx had taken place before the observation period began. This was confirmed by eliciting a strong rapid influx of Cd^{2+} through increasing the basolateral $[CdCl_2]$ from 3.16 µM to 10 µM. We could not find statistically significant differences in basolateral Cd^{2+} fluxes between midguts from adapted and not adapted animals.

6 Nederlandstalige Samenvatting

Orchesella cincta is een springstaarten-species van het noordelijk halfrond. Springstaarten spelen een belangrijke rol in de ecologie van de bodem. Zij bevorderen onder meer de afbraakprocessen van dood organisch materiaal en kunnen de biobeschikbaarheid van zware metalen en andere polluënten verhogen. Bovendien zijn zij een belangrijke prooi voor tal van andere soorten. Dat maakt dat springstaarten ondanks hun geringe afmetingen interessant zijn voor ecologisch en ecotoxicologisch bodemonderzoek. Bij dit soort onderzoek worden zij aanzien als vertegenwoordigers van de hele bodemfauna. Er zijn er tal van studies gepubliceerd over de effecten van zware metalen en andere chemische stoffen op springstaarten, onder meer op *Orchesella cincta*.

Het darmstelsel van een dier vormt de eerste barrière tegen de opname van toxische stoffen uit het voedsel. Het is dus een belangrijk om de transporteigenschappen van dat weefsel te bestuderen. Op die manier wordt het mogelijk na te gaan hoe een dier met een eventuele belasting met schadelijke stoffen in het voedsel omgaat. Totnogtoe zijn er geen basisgegevens gekend over de transporteigenschappen van de middendarm van *O. cincta* of andere springstaarten. Dit werk moet helpen deze leemte te vullen. Het geeft een eerste beschrijving van de (elektro-)fysiologie van de middendarm.

De middendarm van springstaarten is het functionele equivalent van de dunne darm van gewervelde dieren. Hier vinden de vertering en de opname van voedingsbestanddelen plaats. Bovendien heeft de middendarm van springstaarten een belangrijke excretiefunctie. In de cellen van het middendarm epitheel worden ongewenste stoffen zoals b.v. urinezuur of metalen in een moeilijk oplosbare vorm opgeslagen. Bij elke vervelling wordt het epitheel in zijn geheel afgestoten en uitgescheiden samen met de erin opgeslagen afvalstoffen, zo als niet-essentiële metalen.

De middendarm is dus onder meer een transportepitheel. Voor de elektrofysiologische karakterisatie van een transportepitheel zoals de middendarm wordt vaak de specifieke elektrische transepitheliale weerstand (R_{te}) gebruikt. De R_{te} wordt algemeen als een goede indicator voor de transporteigenschappen van een epitheel beschouwd voor zover er elektrisch geladen stoffen (ionen, zouten) een rol spelen. In epithelen met een lage R_{te} kunnen de transportsnelheden hoog zijn. Maar, omdat ze ook zeer doorlaatbaar voor water zijn, kunnen epithelen met een lage R_{te} geen noemenswaardige osmotische gradiënten opbouwen. Het water volgt het zout-transport doorheen het epitheel. In epithelen met een hoge R_{te} zijn de transportsnelheden langzamer en hun waterdoorlaatbaarheid is geringer dan die van

de epithelen met een lage R_{te}. De hoge-weerstand epithelen kunnen daarom veel steilere concentratie gradiënten genereren dan de lage-weerstand epithelen.

Voor dit werk werd gebruik gemaakt van een paar basistechnieken van de elektrofysiologie. Potentiaalverschillen over celmembranen werden met behulp van intracellulaire microelectrodes gemeten. Met protonen-selectieve micro-elektroden werden pH-metingen uitgevoerd. Met behulp van de luminale microperfusie techniek werden middendarm-preparaten van *O. cincta* geperfuseerd en transepitheliale potentiaalverschillen gemeten. Deze techniek werd ook gebruikt om de specifieke transepitheliale elektrische weerstand (R_{te}) te bepalen. Door aan één kant -de perfusiekant- stroompulsen in het lumen van de darmen te sturen en aan weerszijden de potentiaaldeflecties ten gevolge van deze stroompulsen te meten, kon de R_{te} berekend worden. De experimenteel verkregen waarden werden met behulp van computersimulaties op elektrische equivalent circuits verklaard.

In **deel 1A "General Electrophysiological Properties of the Midgut"** worden de voornaamste elektrofysiologische eigenschappen van het middentermepitheel beschreven. Met behulp van elementanalysen werden de anorganische bestanddelen, de osmolaliteit en de pH van de hemolymfe van *O. cincta* bepaald. Aan de hand van deze gegevens werd een fysiologische zoutoplossing samengesteld, waarmee de verdere experimenten op de middendarm van dit dier uitgevoerd werden. Met behulp van de luminale perfusie techniek en met intracellulaire microelektroden werden de belangrijkste elektrofysiologische parameters onder controle-omstandigheden gemeten. Het verband tussen deze parameters en de verschillende vervellings-stadia werd onderzocht. Daarnaast werd ook het elektrofysiologisch gedrag van het middentermepitheel bij verschillende kalium (K^+) concentraties bepaald aan de basolaterale (hemolymfe) en aan de luminale kant.

De ionensamenstelling van de hemolymfe kwam overeen met hetgeen bekend was van fylogenetisch oorspronkelijke hexapoden (insecten). De hemolymfe had een hoge natrium over kalium concentratie en was rijk aan chloor. De totale concentraties waren (telkens mM ±SEM): 154 ± 2 Na, 7.0 ± 1.2 K, 9.6 ± 3.5 Ca, 3.5 ± 1.1 Mg, 6.7 ± 0.6 P, 114 ± 14 Cl. ($n_{Na, K, Ca, Mg, P}$ =3 hemolymfe stalen verzameld van telkens circa 190 individuele dieren, n_{Cl}=11 individuele dieren).

In controle-omstandigheden bedroeg het potentiaal verschil over de basolaterale celmembraan (V_{bl}) -63.8 ± 1.17 mV (n = 51). Het potentiaalverschil over het epitheel (V_{te}) was -10.6 ± 0.7 mV (n = 59), lumen negatief. Het potentiaalverschil over de apicale mem-

braan (V_{ap}) kon met $V_{ap} = V_{bl} - V_{te}$ = -53.2 mV, cel negatief, berekend worden. De V_{bl} vertoonde een bijna perfecte Nernst-respons op een verhoging van de basolaterale K^+ concentratie. De fractionele elektrische weerstand van de basolaterale membraan bedroeg 17 ± 5% (n = 12) van de totale cellulaire elektrische weerstand. Het Nernst-gedrag en de lage fractionele weerstand van de basolaterale membraan maakten het mogelijk om de K^+ concentratie in de cel te berekenen met behulp van de Nernst-vergelijking. In controle-omstandigheden, bij een temperatuur van 23.1°C, was dat 85 mM.

De invloed van enkele variabelen op de potentiaalverschillen (V_{bl}, V_{ap} en V_{te}) werd met de multiple regressie procedure getest. Zo had het vervellings-stadium -waarin een dier zich bevond als de metingen uitgevoerd werden- een significante invloed op V_{bl}, maar niet op V_{te}. Bovendien was de V_{bl} aan de orale kant van de middendarm negatiever dan aan de aborale kant. Omdat de elektrische isolatie van het lumen ten opzichte van het geaarde bad cruciaal is voor de qualiteit van de V_{te}-metingen werd ook de invloed van deze parameter op V_{te} getest. De elektrische isolatie van de middendarm preparaten had geen statistisch significante invloed op de metingen van de V_{te}.

De pH van de hemolymfe (*in vivo*), de cellen en het lumen werd met H^+-selectieve microelektroden gemeten. Hij bedroeg respectievelijk 7.26 ± 0.1 (n = 9), 6.81 ± 0.08 (n = 8) en 6.73 ± 0.09 (n = 17). Met behulp van de pH en met de kennis van de potentiaalverschillen konden de elektrochemische drijfkrachten berekend worden, welke op de protonen inwerken. Zowel aan de luminale als aan de basolaterale zijde zijn zij cel-inwaarts gericht.

De meetresultaten van de specifieke transepitheliale elektrische weerstand (R_{te}) waren uiterst variabel. In **deel IB "Spatial Distribution of the Electrical Transepithelial Resistance (R_{te})"** van deze thesis wordt dit feit verder onderzocht. Er waren aanwijzingen, dat er regionale verschillen in de fysiologische eigenschappen van de middendarm zouden kunnen bestaan al was deze morfologisch uniform.

Middendarm stukken van verschillende lengten werden luminaal met dezelfde fysiologische oplossing geperfuseerd als het bad. De houder-pipetten aan de perfusiekant werden op maat van de verschillede uiteinden van de middendarm gemaakt. Daardoor konden de respectievelijke uiteinden (orale of aborale kant) reproduceerbaar in de pipetten gefixeerd worden. De gemiddelde specifieke transepitheliale weerstand (R_{te}) werd berekend met behulp van kabelanalyse voor eindige, door een hoge elektrische weerstand afgesloten kabels (terminated cable). De gemiddelde R_{te} van de middendarm bedroeg 389 ± 35 Ω cm^2

(n = 69) indien de middendarm van de orale naar de aborale zijde geperfuseerd werd. Werd de middendarm in de andere richting, van de aborale naar de orale zijde geperfuseerd, bedroeg de gemiddelde R_{te} 399 ± 41 Ω cm^2 (n = 51). In beide gevallen was er een positieve correlatie tussen de R_{te} en de lengte van het geperfuseerde stuk middendarm (L). De perfusie-richting beïnvloedde op haar beurt en op statistisch significante wijze de correlatie tussen L en R_{te}. Er waren dus verschillen in de R_{te} langsheen de middendarm, maar ze werden door elektrische lekken gecamoufleerd. Door gebruik te maken van het verband tussen L en de ingangsweerstand (R_{input}) werd de waarde van de lek-weerstand (R_{leak}) door extrapolatie voor L = 0 geschat op 186 ± 23 Ω (n = 27). De kabelanalyse werd uitgebreidmet een computer gesteunde simulatie van een elektrische equivalent circuit, dat ook de lekweerstanden aan weerszijden van de middendarm bevatte, . De experimentele waarden werden verklaard met een van oraal naar aboraal stijgende R_{te}. Wanneer de middendarmen van de orale naar de aborale kant toe geperfuseerd werden, bedroeg de gesimuleerde R_{te} aan de orale kant 148 Ω cm^2 en aan de aborale kant 6699 Ω cm^2. Dit is mogelijks een lichte overschatting van de daadwerkelijke R_{te} onder controle-omstandigheden. De precisie van de simulatie hangt af van de betrouwbaarheid van de R_{leak}-berekening. Doordat de R_{leak} en de transmurale weerstand van de middendarm-wand parallelle weerstanden zijn, werd besloten, dat de R_{leak} eerder een onder- dan wel overschat werd. Berekeningen wezen uit dat een onderschatting van de R_{leak} hoe dan ook niet zou resulteren in een grove overschatting van de hoogste R_{te} aan de aborale kant. De steile toename van de R_{te} van de orale naar de aborale kant, die we vonden, zou dan zelfs een onderschatting van de daadwerkelijke toename van de R_{te} geven.

Het transepitheliale potentiaalverschil (V_{te}) werd eveneens gesimuleerd om de experimentele resultaten te verklaren. Bij de simulatie werd rekening gehouden met R_{leak} en de R_{te} waarden, die met de voorafgaande simulaties gevonden werden. Om de experimentele V_{te} waarden te bekomen moesten zeer hoge V_{te} waarde in het model worden ingevoerd. Dit betekende, dat het apicale potentiaalverschil (V_{ap}) in de aborale middendarm positief of ongeveer gelijk aan nul had moeten zijn. Wat aantoont dat de simulaties van V_{te} zeer gevoelig waren voor een onderschatting van R_{leak}. Enerzijds is het niet onwaarschijnlijk, dat de raming van R_{leak} een onderschatting was en anderzijds waren de meetresultaten door elektrische lekken gecamoufleerd. Beide feiten in acht genomen was het erg waarschijnlijk dat de daadwerkelijke V_{te} tussen de gesimuleerde en de gemeten waarden lag.

De toename van R_{te} van de orale naar de aborale kant doet vermoedden, dat er verschillen in de transport-functies langsheen de middendarm aanwezig zijn. Voor de eerste

keer konden regionale verschillen in de R_{te} op een afstand van ongeveer 1 mm aangetoond worden. Wanneer hoge R_{te} waarden verwacht kunnen worden bij korte buisvormige weefsels (terminated cables), zou onze benadering erbij kunnen helpen de daadwerkelijke R_{te} en R_{leak} in te schatten of zelfs de experimentele V_{te} -waarden voor elektrische lekken te corrigeren.

In **deel II "Cadmium Fluxes at the Basolateral Face of the Midgut: a Preliminary Study"** worden preliminaire experimenten met een vibrerende cadmium-selectieve elektrode beschreven. Er werd onderzocht of middendarmen van aan cadmium-vervuiling aangepaste dieren een hogere Cd^{2+}-influx vertoonden dan middendarmen van niet aangepaste dieren. Eerst werd uitgezocht of de techniek van de vibrerende elektrode (SERIS) geschikt is om Cd^{2+}-fluxen aan de basolaterale kant van de middendarm te detecteren. Een Cd^{2+} selectieve elektrode werd met succes in een eenvoudige SERIS-opstelling geïmplementeerd. Deze elektrode mat herhaaldelijk de Cd^{2+} activiteit op twee verschillende posities. De SERIS-elektrode had een efficiëntie van 84 ± 3.5% (n = 5) voor de detectie van een artificiële Cd^{2+}-gradiënt.

Volledige middendarmen werden aan 3.16 µM CdCl2 blootgesteld. Met de verschilmetingen van Cd^{2+}-activiteiten op twee verschillende plaatsen aan de basolaterale zijde van de preparaten, konden de Cd^{2+}-fluxen met behulp van de wet van Fick berekend worden. Gedurende de metingen werden oscillaties in de Cd^{2+}-fluxen waargenomen. Zowel Cd^{2+}-influx als Cd^{2+}-efflux werden vastgesteld. Deze fluxen variëerden tussen -1000 en +1000 $fmol \cdot cm^{-2} \cdot s^{-1}$.

Er werden statische metingen van de Cd^{2+} activiteit in de buurt van de middendarm uitgevoerd. Uit deze metingen werd geconcludeerd dat een sterke Cd^{2+}-influx moest hebben plaatsgevonden vooraleer de metingen begonnen waren. Dit vermoeden werd bevestigd door een sterke, kortstondige Cd^{2+} influx uit te lokken door de basolaterale $CdCl^2$ concentratie te verhogen.

Wij konden geen statistisch significante verschillen vaststellentussen middendarmen van cadmium- aangepaste en niet aangepaste dieren.

7 References

Azuma, M., Harvey, W., Wieczorek, H., 1995. Stoichiometry of K^+/H^+ antiports helps to explain extracellular pH11 in a model epithelium. FEBS Letters 361, 153-156.

Bååth, E., 1991. Tolerance of copper by entomogenous fungi and the use of copper-amended media for isolation of entomogenous fungi from soil. Mycological Research 95, 1140- 1142.

Barrow, G.M., 1973. Physical Chemistry, 3rd ed. McGraw-Hill, New York, St. Luis,.. . p. 693, tab 23-4.

Boudko, D.Y., Moroz, L.L., Linser P.J., Trimarchi, J.R., Smith, P.J.S., Harvey, W.R. 2001. In situ analysis of pH gradients in mosquito larvae using non-invasive, self-referencing, pH-sensitive microelectrodes. Journal of Experimental Biology 204, 691-699.

Boulpaep, E.L., Sackin, H., 1979. Equivalent electrical circuit analysis and rheogenic pumps in epithelia. Federation Proceedings 38, 2030-2036.

Burg, M.B., Grantham, J., Abramow, M., Orloff, J., 1966. Preparation and study of fragments of single rabbit nephrons. American Journal of Physiology 210, 1293-1298.

Chamberlin, M.E., 1990. Ion transport across the midgut of the tobacco hornworm (*Manduca sexta*). Journal of Experimental Biology 150, 425-442.

Cioffi,M., 1979. The morphology and fine structure of the larval midgut of a moth (*Manduca sexta*) in relation to active ion transport. Tissue & Cell 11, 467-479.

Clark, T.M., Koch, A., Moffet, D.F. 1999. The anterior and posterior 'stomach' regions of larval *Aedes aegypti* midgut: regional specialization of ion transport and stimulation by 5-hydroxytryptamine. Journal of Experimental Biology 202, 247-252.

Coleman, J.E., 1967. Metal ion dependent binding of sulphonamide to carbonic anhydrase. Nature 214, 193-194.

Crailsheim, K. 1988b. Intestinal transport of sugars in the honeybee (Apis mellifera L.). Journal of Insect Physiology 34, 839-845.

Dadd, R.H., 1975. Loss of midgut alkalinity in chilled or narcotized mosquito larvae. Annals of the Entomological Society of America 69 (2), 248-254.

Dallai, R. 1966. L'ultrastruttura dell'intestino di *Orchesella villosa* (Geoffroy) (Insecta, Collembola). Annuario dell'instituto e museo di zoologia della universita' di Napoli 17 (5), 1-18.

Dallai, R., Trastullo, E., Lupetti, P., Mencarelli, C., 1993. Unusual cytosceletal association with the intercellular septate junction in the midgut of Collembola (Insecta: Apterygota). International Journal of Insect Morphology and Embryology 22, 473-486.

De With, N.D., Joose, E.N.G., 1971. The ecological effects of molting in Collembola. Revue d'Écologie et de Biologie du Sol 8 (1), 111-117.

Dijkstra, S. 1993. Cl^- transport and H^+ pumping in the primary urine formation in the ant. PhD thesis, dpt. of Physiology, Limburgs Universitair Centrum, Diepenbeek Belgium.

Doughty, J.M., Langton, P.D., 2001. Measurement of chloride flux associated with the myogenic response in rat cerebral arteries. Journal of Physiology 534 (3), 753-761.

Dow, J.A. and Harvey, W.R., 1988. Role of midgut electrogenic K^+ pump potential difference in regulating lumen K^+ and pH in larval Lepidoptera. Journal of Experimental Biology 140, 455-463.

Dow, J.A.T. 1986. Insect midgut function. Advances in Insect Physiology 19, 187-328.

Drasch, G.A., 1983. An increase of cadmium body burden for this century – an investigation on human tissues. The Science of the Total Environment 26, 111-119.

Eisenbeis, G., Meyer, E., 1986. Some ultrastructural features of glacier Collembola *Isotoma 'sp. g.'* and *Isotomurus palliceps* (Uzel, 1891) from the Tyrolean Central Alps. In: Second International Seminar on Apterygota (ed. R. Dallai) pp. 257-272. University of Siena, Siena.

Eisenbeis, G., Wichard, W. 1975a. Histochemischer Chloridnachweis im Transportepithel am Ventraltubus arthropleoner Collembolen. Journal of Insect Physiology 21, 231-236.

Eisenbeis, G., Wichard, W. 1975b. Feinstruktureller und histochemischer Nachweis des Transportepithels am Ventraltubus symphypleoner Collembolen (Insecta, Collembola). Zeitschrift für Morphologie der Tiere 81, 103-110.

Faber, J.H., Verhoef, H.A., 1991. Functional differences between closely-related soil arthropods with respect to decomposition processes in the presence or absence of pine tree roots. Soil Biology and Biochemistry 23, 15-23.

Ferard, M., Poinsot-Balaguer, N., 1998. Influence du type de nourriture sur les spectres esterasiques du Collemboles *Folsomia candida* W. In: Third International Seminar on Apterygota (ed. R. Dallai) pp. 457-466. University of Siena, Siena.

Florkin, M., Jeuniaux, C., 1974. Hemolymph: Composition. The Physiology of Insects (Ed. Morris Rockstein) 255-307. Academic Press, New York.

Friedrich, M., Trautz, D., 1995. Ribosomal DNA phylogeny of the major extant arthropod classes and the evolution of myriapods. Nature 376, 165-167.

Frömter, E., Diamond, J.M., 1972. Route of passive ion permeation in epithelia. Nature New Biology 245, 9-11.

Good, N.E., Winget, G.D., Winter, W., Conolly, T.N., Izawa, S., M.M. Singh Raizada, 1966. Hydrogen ion buffer for biological research. Biochemistry 5(2), 467-477.

Greger, R. Hampel, W. 1981. A modified system for in vitro perfusion of isolated renal tubules. Pflügers Archiv 389, 175-176.

Hågvar, S., 1988. Decomposition studies in an easily-constructed microcosm: effects of microarthropods and varying soil pH. Pedobiologia 31, 293-303.

Harrison, J.F., Phillips, J.E., Gleeson, T.T., 1991. Activity physiology of the two-striped grasshopper, *Melanoplus bivittatus*: gas exchange, hemolymph acid-base status, lactate production and the effect of temperature. Physiological Zoology 64(2), 451-472.

Harvey, W.R., Nedergaard, S., 1964. Sodium-independent active transport of potassium in the isolated midgut of *Hyalophora cecropia*. Proceedings of the National Academy of Sciences of the USA 51, 757-765.

Hensbergen, P.J., van Velzen, M.J.M., Nugroho, R.A., Donker M.H., van Straalen, N.M., 2000. Metallothionein-bound cadmium in the gut of the insect *Orchesella cincta* (Collembola) in relation to dietary cadmium exposure. Comparative Biochemistry and Physiology Part C 125, 17-24.

Hodgkin, A.L., Horowicz, P., 1959. The influence of potassium and chloride ions on the membrane potential of single muscle fibers. Journal of Physiology 148, 127-160.

Hopkin, S.P., 1997. Biology of the Springtails (Insecta: Collembola). Oxford University Press, Oxford.

Hoppe, W., Lohmann, W., Markl, H., Ziegler, H. (Ed.) mit Beiträgen von Bauer, R.D., ... , 1982. Biophysik (2nd ed.). Springer-Verlag, Berlin, Heidelbrg, New York, 479.

Humbert, W. 1978. Cytochemistry and X-ray microprobe analysis of the midgut of *Tomocerus minor* (Lubbock) (Insecta, Collembola) with special reference to the physiological significance of the mineral concretions. Cell and Tissue Research 187, 397-416.

Humbert, W., 1974. Étude du pH intestinal d'un Collembole (Insecte, Apterygote). Revue d'Ecologie et de Biologie du Sol 11, 89-97.

Humbert, W., 1977. The mineral concentrations in the midgut of *Tomocerus minor* (Collembola): microprobe analysis and physiological significance. Revue d'Écologie et de Biologie du Sol 14, 71-80.

Humbert, W., 1979. The midgut of *Tomocerus minor* Lubbock (Insecta, Collembola): ultrastructure, cytochemistry, ageing and renewal during a molting cycle. Cell and Tissue Research 196, 39-57.

Jack, J.J.B., Noble, D., Tsien, R.W., 1975. Electric current flow in exitable cells. Clarendon Press, Oxford.

Janssen, G.M., Joose, E.N.G. 1987. Reproduction and growth in Collembola under laboratory conditions. Pedobiologia 30, 1-8.

Järup, L (ed.). Berglund, M., Elinder C.G., Nordberg, G., Vahter, M., 1998. Health effects of cadmium exposure – a review of the literature and a risk estimate. Scandinavian Journal of Work, Environment & Health 24 suppl. 1, 1-51.

Joose, E.N.G., Testerink, G.J. 1977. Control of numbers in Collembola. Ecological Bulletins (Stockholm) 25, 475-478.

Joosse, E.N.G., 1981. Ecological strategies and population regulation of Collembola in heterogeneous environments. Pedobiologia 21, 346-356.

Joosse, E.N.G., Verhoef, S.C., 1983. Lead tolerance in Collembola. Pedobiologia 25, 11-18.

Jumarie, C., 2002. Cadmium transport through type II alveolar cell monolayers: contribution of transcellular and paracellular pathways in the rat ATII and the human A549 cells.

Jura, C. 1958. The alimentary canal of the *Tetrodontophora bielanensis* Waga (Collembola) and the regeneration of the mid-gut epithelium. Bulletin Entomologique de la Pologne 27 (7), 85-89.

Kaestner, A., 1973. Lehrbuch der Speziellen Zoologie Band I: Wirbellose 3. Teil Insecta: B. Spezieller Teil pp. 296-304. Gustav Fischer Verlag, Stuttgart.

Klaassen, C.D., Liu, J., Choudhuri, S., 1999. Metallothionein: an intracellular protein to protect against cadmium toxicity. Annual Review of Pharmacology and Toxicology 39, 267-294.

Knöpfel, M., Schulthess, G., Funk, F., Hauser, H., 2000. Characterization of an integral protein of the brush border membrane mediating the transport of divalent ions. Biophysical Journal 79(2), 874-884

Kristensen, N.P., 1991. Phylogeny of extant hexapods. In: The Insects of Australia Volume 1 (2nd edn) (ed. CISRO) pp. 125-140. Carlton: Melbourne University Press.

Kubiena, W.L., 1953. The soils of Europe. Thomas Murby, London

Kühtreiber, W.M., Jaffe, L.F., 1990. Detection of extracellular Calcium gradients with a calcium-specific vibrating electrode. The Journal of Cell Biology 110, 1565-1573.

Kukalová-Peck, J., 1987. New Carboniferous Diplura, Monura, and Thysanura, the hexapod ground plan, and the role of thoracic side lobes in the origin of wings (Insecta). Canadian Journal of Zoology 65, 2327-2345.

Kukalová-Peck, J., 1991. Fossil history and the evolution of hexapod structures. In: The Insects of Australia Volume 1 (2nd edn) (ed. CISRO) pp. 141-179. Carlton: Melbourne University Press.

Kumar, S.M., Porterfield, D.M., Muller, K.M., Smith, P.J.S., Sahley, C.L., 2001. Nerve injury induces a rapid efflux of nitric oxide (NO) detected with a novel NO microsensor. Journal of Neuroscience 21 (1), 215-220.

Lane, N.J., 1981. Tight junctions in arthropod tissues. International Review of Cytology 73, 243-318.

Leyssens, A., Steels, P., Lohrmann, E., Weltens, R., Van Kerkhove, E., 1992. Intrinsic regulation of K^+ transport in Malpighian tubules (*Formica*): electrophysiological evidence. Journal of Insect Physiology 38 (6), 431-446.

Lubbock, J. 1873. Monograph of the Collembola and Thysanura. Ray Society, London.

Lupetti, P., Roest, G., Dallai, R. 1992. The midgut ultrastructure of *Orchesella cincta* L. (Insecta, Collembola) after contamination with cadmium nitrate. Atti 54° congresso Unione Zoologica Italiana 1992

Malchow, R.P., Verzi, M.P., Smith, P.J.S., 1998. Extracellular pH gradients measured from isolated retinal cells. Biological Bulletin. 195, 203-204.

Mertens, J., Blancquaert, J-P., 1980. Population dynamics of *Orchesella cincta* (Collembola) in experimental conditions. Pedobiologia 20, 301-308.

Mertens, J., Coessens, R., Blancquaert, J-P., 1982. Population structure *of Orchesella cincta* (Collembola) in the field based on instar-determination. Pedobiologia 23, 9-20.

Nardi, F., Spinsanti, G., Boore, J.L., Carapelli, A., Dallai, R., Frati, F., 2003. Hexapod origins: monophyletic or paraphyletic? Science 299, 1887-1889.

Nation, J.L., 2001. Insect physiology and biochemistry. Boca Raton, CRC Press

Pannabecker, T. 1995. Physiology of the Malpighian tubule. Annual Review of Entomology 40, 493-510.

Parsons, R., 1959. Handbook of chemical constants. Buttersworth Scientific Publications, London, 78-79.

Pawert, M., Triebskorn, R., Gräff, S., Berkus, M., Schulz, J., Köhler, H.-R., 1996. Cellular alterations in collembolan midgut cells as a marker of heavy metal exposure: ultrastruc-

ture and intracellular metal distribution. The Science of the Total Environment 181, 187-200.

Pelc, R., Smith, P.J.S., Ashley, C.C., 1996. In vivo recording of calcium fluxes accompanying 'catch' contraction of molluscan smooth muscle. Journal of Physiology (London) 497P, 41

Petersen, H., 1994. A review of collembolan ecology in ecosystem context. Acta Zoologica Fennica 195, 111-118.

Petersen, H., Luxton, M., 1982. A comparative analysis of soil fauna populations and their role in decomposition processes. Oikos 39, 287-388.

Piñeros, M.A., Shaff, J.E., Kochian, L.V., 1998. Development, characterization, and application of a cadmium-selective microelectrode for the measurement of cadmium fluxes in roots of *Thlaspi* species and wheat. Plant Physiology 116, 1393-1401.

Porterfield, D.M., Laskin, J.D., Jung, S.-K., Malchow, R.P., Billack, B., Smith, P.J.S., Heck, D.E., 2001. Proteins and lipids define the diffusional field of nitric oxide. American Journal of Physiology 281, L904-912.

Posthuma, L, 1990. Genetic differentiation between populations of *Orchesella cincta* (Collembola) from heavy metal contaminated sites. Journal of Applied Ecology 27, 609-622.

Posthuma, L., Hogervorst, R.F., Joosse, E.N.G., Van Straalen, N.M., 1993. Genetic variation and covariation for characteristics associated with cadmium tolerance in natural populations of the springtail *Orchesella cincta* (L.). Evolution 47(2), 619-631.

Posthuma, L., Hogervorst, R.F., Van Straalen, N.M., 1992. Adaptation to soil pollution by cadmium excretion in natural populations of *Orchesella cincta* (L.) (Collembola). Archives of Environmental Contamination and Toxicology 22, 146-156.

Ramsey, J.A., Brown, R.H, Croghan P.C. 1955. Electrometric titration of chloride in small volumes. Journal of Experimental Biology 32, 822-829.

Redman, S.J., McLachlan, E.M., Hirst, G.D.S., 1987. Nonuniform passive membrane properties of rat lumbar sympathetic ganglion cells. Journal of Neurophysiology 57 (3), 633-644.

Rheault, M.R., O'Donnell, M.J., 2001. Analysis of epithelial K^+ transport in Malpighian tubules of *Drosophila melanogaster:* evidence for spatial and temporal heterogeneity. Journal of Experimental Biology 204, 2289-2299.

Sackin, H., 1978. Electrophysiology and transport in the isolated perfused salamander proximal tubule. PhD thesis, Yale University, USA.

Schneider, J.K., Hofstetter, P., Pretsch, E., Amman, D., Simon, W., 1980. N,N,N',N'-Tetrabutyl-3,6-dioxaoctan-dithioamid, Ionophor mit Selektivität für Cd^{2+}. Helvetica Chimica Acta 63, 217-224.

Sedlag, U., 1952. Untersuchungen über den Ventraltubus der Collembolen. Wissenschaftliche Zeitschrift der Martin-Luther-Universität Halle-Wittenberg 1 (1/2), 93-127.

Shirihai, O., Smith P.J.S., Hammar, K., Dagan, D., 1998. H^+ and K^+ gradient generated by microglia H/K-ATPase. Glia 23, 339-348.

Smith, P.J.S., 1995. Non-invasive ion probes – tools for measuring transmembrane ion flux. Nature 378, 645-646.

Smith, P.J.S., Hammar, K., Porterfield, D.M., Sanger, R.H., Trimarchi, J.R., 1999. Self-referencing, non-invasive, ion-selective electrode for single cell detection of trans-plasma membrane calcium flux. Microscopy Research and Technique 46, 398-417.

Smith, P.J.S., Haydon, P.G., Hengstenberg, A., Jung, S.-K., 2001. Analysis of cellular boundary layers: application of electrochemical microsensors. Electrochimica Acta 47, 283-292.

Smith, P.J.S., Trimarchi, J., 2001. Noninvasive measurement of hydrogen and potassium ion flux from single cells and epithelial structures. American Journal of Physiology 280, C1-C11.

Sözen, M.A., Armstrong, J.D., Yang, M., Kaiser, K., Dow, J.A.T., 1997. Functional domains are specified to single-cell resolution in a *Drosophila* epithelium. Proceedings of the National Academy of Sciences of the USA 94, 5207-5212.

Stebaeva, S.K. 1989. Role of Collembola in organic matter decomposition in technogenic Siberian landscapes. In: Third International Seminar on Apterygota (ed. R. Dallai) pp. 299-306. University of Siena, Siena.

Stork, N.E., 1988. Insect diversity: facts, fiction and speculation. Biological Journal of the Linnean Society 35, 321-337.

Stork, N.E., Blackburn, T.M., 1993. Abundance, body size and biomass of arthropods in tropical forest. Oikos 67, 483-489.

Teuben, A., Verhoef, H.A., 1992a. Relevance of micro- and mesocosm experiments for studying soil ecosystem processes. Soil Biology and Biochemistry 24, 1179-1183.

Teuben, A., Verhoef, H.A., 1992b. Direct contribution by soil arthropods to nutrient availability through body and faecal nutrient content. Biology and Fertility of Soils 14, 71-75.

Thibaud, J-M., 1976. Relations chronologiques entre les cycles du tube digestif et de l'appareil génital lors de l'intermue des Insectes Collemboles Revue d'Écologie et de Biologie du Sol 13 (1), 191-204

Tompson, W. (Kelvin, Lord), 1855. On the theory of the electric telegraph. Proceedings of the Royal Society of London 7, 382-399.

Trimarchi, J.R., Liu, L., Smith, P.J.S., Keefe, D.L., 2000. Noninvasive measurement of potassium efflux as an early indicator of cell death in mouse embryos. Biology of Reproduction 63, 851-857.

Trudeau, M.C., Warmke, J.W., Ganetzky, B., Robertson, G.A., 1995. HERG, a Human inward rectifier in the voltage-gated potassium channel family. Science 269, 92-95.

Turunen, S. 1985. Absorption. In: Kerkut, G. A., Gilbert, L. I. (Eds.), Comprehensive Insect Physiology, Biochemistry and Pharmacology, Vol. 3, Pergamon Press, Oxford, 241-253

Van Straalen, N.M. 1987. Turnover of accumulating substances in populations with weight-structure. Ecological Modelling 36, 195-209.

Van Straalen, N.M. and van Meerendonk, J.H., 1987. Biological half-lives of lead in *Orchesella cincta* (L.) (Collembola). Bulletin of Environmental Contamination and Toxicology 38, 213-219.

Van Straalen, N.M., De Goede R.G.M, 1987. Productivity as a population performance index in lifecycle toxicity tests. Water Science and Technology 19, 13-20.

Verhoef, H.A., 1981. Water balance in Collembola and its relation to habitat selection: water content, haemolymph osmotic pressure and transpiration during an instar. Journal of Insect Physiology 27 (11), 755-766.

Verhoef, H.A., Li, K.W., 1983. Physiological adaptations to the effects of dry summer periods in Collembola. New Trends in Soil Biology (ed. by Ph. Lebrun, H.M. André, A. de Medts, C. Grégoire-Wibo and G. Wauthy), 345-356, Dieu-Brichart, Louvain-la-Neuve, Belgium.

Verhoef, H.A., Prast, J.E., Verweij, R.A., 1988. Relative importance of fungi and algae in the diet and nitrogen nutrition of *Orchesella cincta* (L.) and *Tomocerus minor* (Lubbock)(Collembola). Functional Ecology 2, 195-201.

Verhoef, H.A., Witteveen, J., 1980. Water balance in Collembola and its relation to habitat selection; cuticular water loss and water uptake. Journal of Insect Physiology 26, 201-208.

Walker, C.H., Hopkin, S.P., Sibly, R.M., Peakall, D.B., 2001. Principles of ecotoxicology, 2nd ed. Taylor & Francis, London.

Walker, W.A., 1976. Host defense mechanisms in the gastrointestinal tract. Pediatrics 57 (6), 901-916.

Wang, W., Sackin H., Giebisch G., 1992. Renal Potassium Channels and Their Regulation. Annual Review of Physiology 54, 81-96.

Weltens, R., Leyssens A. Z.S.L., Lohrmann E., Steels P., Van Kerkhove E., 1992. Unmasking of the apical electrogenic H-pump in isolated Malpighian tubules (*Formica polyctena*) by the use of barium. Cellular Physiology and Biochemistry 2, 101-116.

Weltens, R., Pirotte P., 1987. KCl-transport in Malphigian tubules: a fast method to prepare double-barreled K^+-sensitive microelectrodes. Archives Internationales de Physiologie et de Biochimie 95, P72-P73.

Wieczorek, H., Grüber, G., Harvey, W.R., Huss, M., Merzendorfer, H., Zeiske, W., 2000. Structure and regulation of insect plasma membrane H^+-V-ATPase. Journal of Experimental Biology 203, 127-135.

Wieczorek, H., Putzenlechner, M., Zeiske, W., Klein, U. 1991. A vacuolar-type proton pump energizes K+/H+ antiport in an animal plasma membrane. Journal of Biological Chemistry 266, 15340-15347.

Wills, N.K., Reuss, L., Lewis, S.A. (Ed.), 1996. Epithelial Transport. A guide to methods and experimental analysis. Chapman & Hall, London.

Zeiske W., Meyer H., Wieczorek H., 2002. Insect midgut K^+ secretion: concerted run-down of apical/basolateral transporters with extra-/intracellular acidity. Journal of Experimental Biology 205, 463-474.

Zeiske, W., 1992. Insect ion homeostasis. Journal of Experimental Biology 172, 323-334.

Zhang, S-L., Leyssens, A., Van Kerkhove, E., Weltens, R., Van Driessche, W., Steels, P., 1994. Electrophysiological evidence for the presence of an apical H+-ATPase in Malphigian tubules of *Formica polyctena*: intracellular and luminal pH measurements. Pflügers Archiv – European Journal of Physiology 426, 288-295.

Zinkler, D, 1969. Vergleichende Untersuchungen zum Wirkungsspektrum der Carbohydrasen von Collembolen (Apterygota). Verhandlungen der Deutschen Zoologische Gesellschaft, 640-644.

Zinkler, D., Schroff, G., 1989. The energetics of of a jumping springtail *Tomocerus flavescens* (Collembola). Third International Seminar on Apterygota (ed. R. Dallai) 443-448. University of Siena, Siena.

8 Appendices

Appendix 1: Derivation of Cable Equations

The derivation of the cable equations for terminated cables as presented in this text is combined from the work of different authors: (Jack, Noble, & Tsien, 1975; Sackin, 1978 and Dijkstra, 1993). These equations are used to calculate the specific transepithelial resistance of the midgut preparations.

Historically, these equations were used to describe the decay of an electrical current in submarine telegraph cables. (Tompson (Lord Kelvin), 1855). These cables are very well insulated wires surrounded by salt water. The insulation separates the core conductor (wire) and the surrounding conductor (salt water). These elements basically make up a capacitor. The capacitance -or the ability of the capacitor to retain and store electric charge- increases with increasing capacitor surface. Along with length therefore the cable surface increases and so does the cable's capacitance. Once a current pulse has entered the cable, it will die away with distance. Because the longer the current travels, the more charges are retained by the capacitor. Moreover, no electrical insulation is perfect meaning that any technical insulation has a finite electrical resistance. Therefore the current will gradually leak across the insulation into the salt water. The resistance of the core conductor may be given for a unit length, as it's specific resistance (R_{core} [$\Omega \cdot cm^{-1}$]). For a unit length the resistance of the insulation may be given as the specific transmural resistance (R_m [$\Omega \cdot cm$]). The electrical resistance of the core conductor will increase with distance: $R_{core} \cdot x$. While on the other hand the resistance of the insulation will decrease with increasing distance $\frac{R_m}{x}$. (The increasing cable surface offers the current an increasing possibility to cross the insulation sheath.) From that it follows, that at a particular distance $R_{core} \cdot x$ will equal $\frac{R_m}{x}$:

$$R_{core} \cdot x = \frac{R_m}{x} \qquad \text{(A1.1)}$$

$$\Rightarrow x^2 = \frac{R_m}{R_{core}} \qquad \text{(A1.2)}$$

$$\Rightarrow x = \sqrt{\frac{R_m}{R_{core}}} = \lambda \qquad \textbf{(A1.3)}$$

The value of x is used to describe the extent of current spread along a cable. It is known as the length constant .

Although these equations were initially developed for technical purposes, they were later applied to biological cable-like structures. They were used e.g. to describe the electrotonic passive current spread in nerve axons and as a means to calculate the transepithelial resistance of a tubular epithelium. The latter application was used in the present study.

The midgut of *Orchesella cincta* is a straight tubule of unfolded epithelium surrounding the luminal fluid. Because this fluid contains ions it is an electrical conductor resembling the conductive core of an electric cable. As a submarine cable this conductor is separated from the surrounding conductive environment by an insulating sheath. The midgut epithelium is considered as the electrical insulation between the conductive luminal fluid and the conductive bathing fluid the midgut is submerged in. For the sake of simplicity, the midgut under study is assumed to have a constant diameter throughout its length. The resistances of the basolateral cell membrane, the apical cell membrane, the smooth junction between the cells, and the cytoplasm are collapsed into one transmural resistance. Furthermore, the axial current injected at one end (perfusion side) is assumed to spread linearly along the tubular lumen without any radial component. The only radial current flow is due to leakage across the tubule wall. Another assumption is that the transmural resistance is a constant or ohmic resistance. This implies that the current crossing the transmural resistance is a linear function of the voltage across the transmural resistance. (Hence the term "linear cable theory" often used in literature.) The physical model the equations are based upon is assumed to be an unbranched cylinder. The current flow in this cylinder is therefore one-dimensional. The model is therefore called the "one-dimensional linear cable model". A sketch of this model is shown in Fig. A1. In this particular model all capacitors were omitted. This is appropriate because the calculation of the transepithelial resistance (R_{te}) is based on steady state measurements of voltage deflections due to current injections (ΔI_0). This implies that the deflection of the transepithelial voltage difference (ΔV_{te}) is measured, when the plateau is reached (Fig. A4B). Only resistors are left in the model. The resistors representing the resistance of the luminal fluid are denoted as R_{core}. Those resistors representing the transmural resistance are denoted as R_m. The equivalent circuit of that model may be drawn as in Fig. A2, showing the relationship between the different voltages within one loop of the circuit.

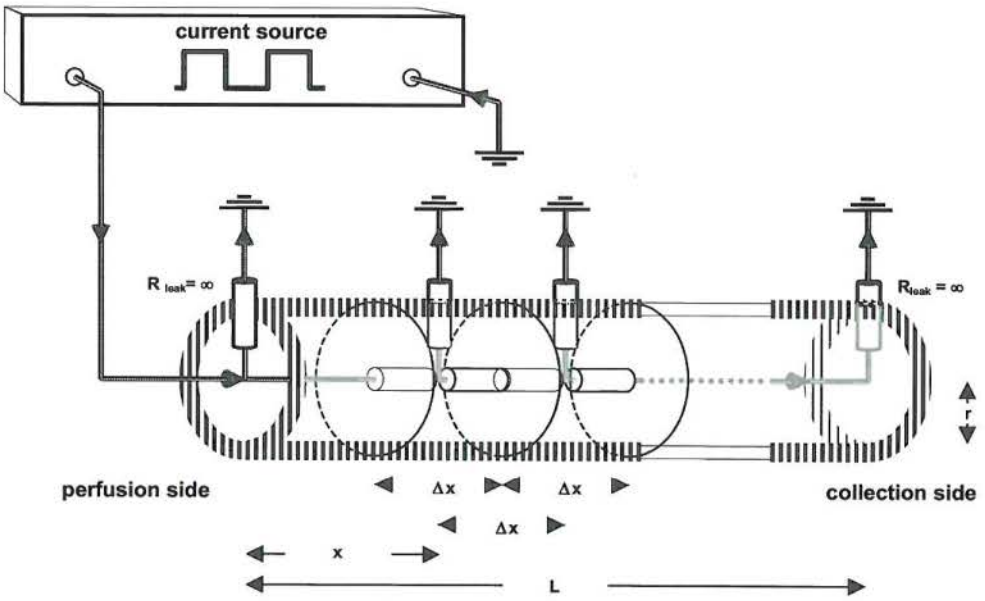

Fig. A1 The discrete one-dimensional linear cable model

This model is only valid for steady state currents, because the capacitors are omitted (see Fig.A4, for explanation see text). The current source supplies step current pulses to the tubular lumen. The tubule is divided into sections of finite length (Δx). In each section, the horizontal resistors represent the ohmic resistances the axial current encounters. The vertical resistors visualize the resistance the current encounters, when it leaks through the tubule wall. The vertical resistors at both ends represent the infinite resistance of an ideal insulation of the tubule against the bathing fluid.

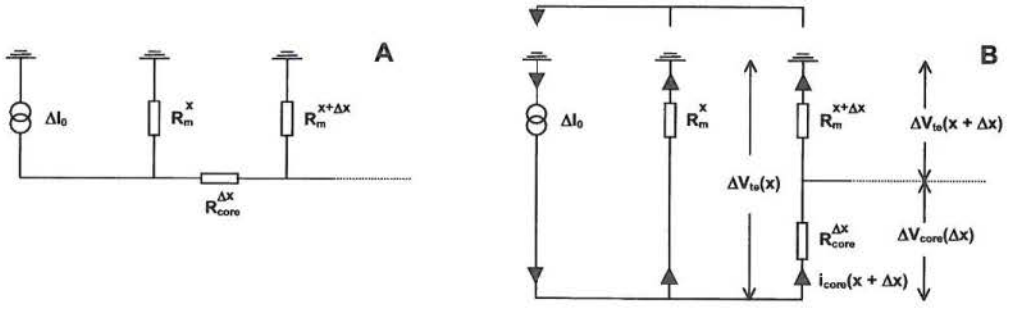

Fig. A2 equivalent circuit of the one-dimensional cable model shown in Fig. A1. A: one section of a cable, notification of resistances; B: circuit A redrawn to demonstrate the voltage relationships

The algebraic sum of all voltages in any closed loop of a circuit must equal zero (Kirchhoff's voltage law). In this case (Fig. A2) it can be written as:

$$\Delta V_{te}(x) = \Delta V_{core}(\Delta x) + \Delta V_{te}(x+\Delta x) \tag{A1.4}$$

$$\Rightarrow \Delta V_{te}(x) = i_{core}(x+\Delta x)\cdot R_{core}^{\Delta x}\cdot \Delta x \; + \; \Delta V_{te}(x+\Delta x) \tag{A1.5}$$

$$\Rightarrow \Delta V_{te}(x) - \Delta V_{te}(x+\Delta x) = i_{core}(x+\Delta x)\cdot R_{core}^{\Delta x}\cdot \Delta x \tag{A1.6}$$

$$\Rightarrow \Delta V_{te}(x+\Delta x) - \Delta V_{te}(x) = -i_{core}(x+\Delta x)\cdot R_{core}^{\Delta x}\cdot \Delta x \tag{A1.7}$$

$$\Rightarrow \frac{\Delta V_{te}(x+\Delta x) - \Delta V_{te}(x)}{\Delta x} = -i_{core}(x+\Delta x)\cdot R_{core}^{\Delta x} \tag{A1.8}$$

$$\Rightarrow \frac{d}{dx}\Delta V_{te}(x) = -i_{core}\cdot R_{core}\,, \tag{A1.9}$$

meaning that Ohm's law applies for pieces of infinitesimal length. Rearrangement of this equation yields an expression for i_{core}:

$$\Rightarrow \frac{d}{dx}\Delta V_{te}(x)\cdot\frac{1}{R_{core}} = -i_{core} \tag{A1.10}$$

$$\Rightarrow \frac{d}{dx}\Delta V_{te}(x)\cdot\frac{-1}{R_{core}} = i_{core}\,, \tag{**A1.11**}$$

which is the axial current flowing through the core conductor (the tubule luminal fluid).

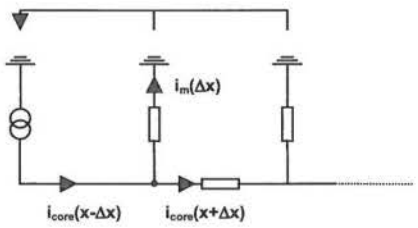

Fig. A3 equivalent circuit of the one-dimensional cable model shown in Fig. A1: notification of currents

In this model, i_{core} divides itself into the transversal and the axial branches of the equivalent circuit (Fig. A3). At any node of the circuit a transmural current i_m branches off, while i_{core} is reduced exactly by that amount of i_m, which leaks through R_m. At any node the sum of all currents entering the node eaquals the sum of all currents leaving the node:

$$i_{core}(x-\Delta x) = i_{core}(x+\Delta x) + i_m \cdot \Delta x \tag{A1.12}$$

$$\Rightarrow i_{core}(x-\Delta x) - i_{core}(x+\Delta x) = i_m \cdot \Delta x \tag{A1.13}$$

$$\Rightarrow i_{core}(x+\Delta x) - i_{core}(x-\Delta x) = -i_m \cdot \Delta x \tag{A1.14}$$

$$\Rightarrow \frac{i_{core}(x+\Delta x) - i_{core}(x-\Delta x)}{\Delta x} = -i_m \tag{A1.15}$$

$$\Rightarrow \frac{d}{dx} i_{core} = -i_m \tag{A1.16}$$

Substitution of i_{core} by the expression described in eq. A1.11 yields:

$$\Rightarrow \frac{d}{dx}\left(\frac{d}{dx}(\Delta V_{te}(x)) \cdot \frac{-1}{R_{core}}\right) = -i_m \tag{A1.17}$$

$$\Rightarrow \frac{-1}{R_{core}} \cdot \frac{d}{dx}\left(\frac{d}{dx}\Delta V_{te}(x)\right) = -i_m \tag{A1.18}$$

$$\Rightarrow \frac{1}{R_{core}} \cdot \frac{d^2}{dx^2}\Delta V_{te}(x) = i_m \tag{A1.19}$$

The current loss through the tubular wall (i_m) is proportional to the inverse of the core resistance times the second derivative of the voltage change as a function of distance.

Amongst other elements, the epithelium consists of cell membranes. Cell membranes are capacitors as well as resistors. Therefore both elements are in parallel (Fig. A4).

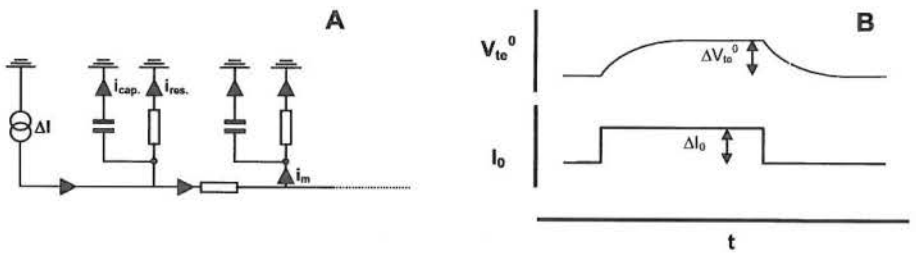

Fig. A4 equivalent circuit of the one-dimensional cable model shown in Fig. A1. A: each section of the epithelium is represented by one RC element; B: application of a step current pulse: voltage and current

Hence, the transepithelial current (i_m) has a capacitive component ($i_{cap.}$) as well as a resistive component ($i_{res.}$):

$$i_m = i_{cap.} + i_{res.} \tag{A1.20}$$

When the injected current pulse (I) is long enough, the capacitor will be fully charged and no current will flow through this branch anymore: $i_{cap} = 0$ (Fig. A4). If this requirement is met, $i_{cap.}$ can be omitted from the equation[1]:

$$i_m = i_{res.} \tag{A1.21}$$

$$\Rightarrow i_m = \frac{\Delta V_{te}(x)}{R_m} \tag{A1.22}$$

$$\Rightarrow \frac{1}{R_{core}} \cdot \frac{d^2}{dx^2} \Delta V_{te}(x) = \frac{\Delta V_{te}(x)}{R_m} \tag{A1.23}$$

This is the basic differential equation of linear cable theory for steady state conditions, when any transient current change has become zero. It is this equation on which the expression defining R_{te} will be based. From multiplying with R_{core}

$$\Rightarrow \frac{d^2}{dx^2} \Delta V_{te}(x) = \frac{R_{core}}{R_m} \cdot \Delta V_{te}(x). \tag{A1.24}$$

This equation describes, that the rate of change in the amplitude of the voltage deflection along with distance $\left(\frac{d^2}{dx^2} \Delta V_{te}(x)\right)$ depends on the ratio of the resistive properties of the core conductor over the resistive properties of the transmural insulation $\left(\frac{R_{core}}{R_m}\right)$. The latter is contained in eq. A1.3, which is an expression for λ.

$$\Rightarrow \frac{d^2}{dx^2} \Delta V_{te}(x) = \frac{1}{\lambda^2} \cdot \Delta V_{te}(x) \tag{A1.25}$$

$$\Rightarrow \frac{d^2}{dx^2} \Delta V_{te}(x) - \frac{1}{\lambda^2} \cdot \Delta V_{te}(x) = 0 \tag{A1.26}$$

---

[1] This eliminates the need of partial differentiation, when two different variables are involved. If the capacitive current is also taken into account, ΔV_{te} would be a function of distance as well as of time: ΔV_{te} (x, t).

$$\Rightarrow \frac{d^2}{dx^2}\Delta V_{te}(x) = \frac{1}{\lambda^2}\cdot \Delta V_{te}(x) \qquad \text{(A1.27)}$$

$$\Rightarrow \lambda^2 \cdot \frac{d^2}{dx^2}\Delta V_{te}(x) = \Delta V_{te}(x) \qquad \text{(A1.28)}$$

defining $\frac{\lambda^2}{x^2} = X^2$, this gives:

$$\Rightarrow \frac{d^2}{dX^2}\Delta V_{te}(x) = \Delta V_{te}(x) \qquad \text{(A1.29)}$$

This equation states, that the function term on the right hand side ($\Delta V_{te}(x)$) equals the second derivative of the same function! The only type of function, which satisfies that requirement, is the exponential function (e^x): the derivative of e^x is e^x itself. Therefore equations of the type

$$\Delta V_{te}(x) = A \cdot e^{(m_1 \cdot X)} + B \cdot e^{(m_2 \cdot X)} \qquad \text{(A1.30)}$$

are valid solutions of the above differential equation. A and B are arbitrary constants. The signs of X in the exponents can be determined by means of the characteristic equation for the above differential equation (eq.A1.29):

$$m_{1,2}^2 - 1 = 0 \qquad \text{(A1.31)}$$

$$m_{1,2}^2 = 1 \qquad \text{(A1.32)}$$

$$m_{1,2} = \sqrt{1} \qquad \text{(A1.33)}$$

$$m_1 = +1; \quad m_2 = -1 \qquad \text{(A1.34)}$$

because $\frac{\lambda^2}{x^2} = X^2 \quad \Rightarrow \quad X = \frac{\lambda}{x}$. Therefore eq. A1.30 becomes:

$$\mathbf{\Delta V_{te}(x) = A \cdot e^{\left(\frac{x}{\lambda}\right)} + B \cdot e^{-\left(\frac{x}{\lambda}\right)}} \qquad \textbf{(A1.35)}$$

By specifying boundary conditions, particular expressions will replace the arbitrary constants A and B. These mathematical operations are tabulated below; finally resulting in the expression for and the expression for R_{te} used in this thesis.

equation		operation giving next equation, comment
		recalling eq. A1.35)
$\Delta V_{te}(x) = A \cdot e^{\left(\frac{x}{\lambda}\right)} + B \cdot e^{-\left(\frac{x}{\lambda}\right)}$	(A1.35)	**boundary condition: x = 0 ,no leak at x = 0** $\Rightarrow e^0 = 1$
$\Rightarrow \Delta V_{te}(0) = A + B$	(A1.36)	
$i_{core} = \frac{-1}{R_{core}} \cdot \frac{d}{dx}(\Delta V_{te}(x))$	(A1.11)	recalling eq. A1.11)
		$\frac{d}{dx}(\Delta V_{te}(x))$ $= \frac{d}{dx}\left(A \cdot e^{\left(\frac{x}{\lambda}\right)} + B \cdot e^{-\left(\frac{x}{\lambda}\right)}\right)$ $= A \cdot \frac{1}{\lambda} \cdot \frac{d}{dx} e^{\left(\frac{x}{\lambda}\right)} + B \cdot \frac{-1}{\lambda} \cdot \frac{d}{dx} e^{-\left(\frac{x}{\lambda}\right)}$ $= A \cdot \frac{1}{\lambda} \cdot e^{\left(\frac{x}{\lambda}\right)} + B \cdot \frac{-1}{\lambda} \cdot e^{-\left(\frac{x}{\lambda}\right)}$ $= \frac{A}{\lambda} \cdot e^{\left(\frac{x}{\lambda}\right)} \frac{B}{\lambda} \cdot e^{-\left(\frac{x}{\lambda}\right)}$
		substituting
$\Rightarrow i_{core} = \frac{-1}{R_{core}} \cdot \left[\frac{A}{\lambda} \cdot e^{\left(\frac{x}{\lambda}\right)} - \frac{B}{\lambda} \cdot e^{-\left(\frac{x}{\lambda}\right)}\right]$	(A1.37)	
$\Rightarrow i_{core} = \frac{-1}{R_{core}} \cdot \frac{A}{\lambda} \cdot e^{\left(\frac{x}{\lambda}\right)} - \frac{-1}{R_{core}} \cdot \frac{B}{\lambda} \cdot e^{-\left(\frac{x}{\lambda}\right)}$	(A1.38)	**boundary condition: at x = L (collection side) no axial current leaves the tubule i.e.** $\mathbf{I_{core} = 0}$
$\Rightarrow 0 = \frac{-1}{R_{core}} \cdot \frac{A}{\lambda} \cdot e^{\left(\frac{L}{\lambda}\right)} - \frac{-1}{R_{core}} \cdot \frac{B}{\lambda} \cdot e^{-\left(\frac{L}{\lambda}\right)}$	(A1.39)	$+\frac{-1}{R_{core}} \cdot \frac{B}{\lambda} \cdot e^{-\left(\frac{L}{\lambda}\right)}$
$\Rightarrow \frac{-1}{R_{core}} \cdot \frac{A}{\lambda} \cdot e^{\left(\frac{L}{\lambda}\right)} = \frac{-1}{R_{core}} \cdot \frac{B}{\lambda} \cdot e^{-\left(\frac{L}{\lambda}\right)}$	(A1.40)	$: \frac{-1}{R_{core}}$

equation		operation giving next equation, comment
$\Rightarrow \frac{A}{\lambda}\cdot e^{\left(\frac{L}{\lambda}\right)} = \frac{B}{\lambda}\cdot e^{-\left(\frac{L}{\lambda}\right)}$	(A1.41)	$\cdot\lambda$
$\Rightarrow A\cdot e^{\left(\frac{x}{\lambda}\right)} = B\cdot e^{-\left(\frac{x}{\lambda}\right)}$	(A1.42)	
$\Rightarrow A = B\cdot\frac{e^{-\left(\frac{L}{\lambda}\right)}}{e^{\left(\frac{L}{\lambda}\right)}}$	(A1.43)	$\frac{e^{-\left(\frac{L}{\lambda}\right)}}{e^{\left(\frac{L}{\lambda}\right)}} = e^{-2\left(\frac{L}{\lambda}\right)}$
$\Rightarrow A = B\cdot e^{-2\left(\frac{L}{\lambda}\right)}$	(A1.44)	eq. A1.44 in eq.A1.36
$\Rightarrow \Delta V_{te}(0) = B\cdot e^{-2\left(\frac{L}{\lambda}\right)} + B$	(A1.45)	:B
$\Rightarrow \frac{\Delta V_{te}(0)}{B} = \frac{B\cdot e^{-2\left(\frac{L}{\lambda}\right)}}{B} + \frac{B}{B}$	A1.46)	reducing
$\Rightarrow \frac{\Delta V_{te}(0)}{B} = e^{-2\left(\frac{L}{\lambda}\right)} + 1$	(A1.47)	$:\Delta V_{te}(0)$
$\Rightarrow \frac{1}{B} = \frac{e^{-2\left(\frac{L}{\lambda}\right)} + 1}{\Delta V_{te}(0)}$	(A1.48)	forming the reciproce
$\Rightarrow B = \frac{\Delta V_{te}(0)}{e^{-2\left(\frac{L}{\lambda}\right)} + 1}$	**(A1.49)**	
$A\cdot e^{\left(\frac{L}{\lambda}\right)} = B\cdot e^{-\left(\frac{L}{\lambda}\right)}$	(A1.42)	recollecting eq. A1.42 $:e^{-\left(\frac{x}{\lambda}\right)}$

equation		operation giving next equation, comment
$\Rightarrow B = A \cdot \frac{e^{\left(\frac{L}{\lambda}\right)}}{e^{-\left(\frac{L}{\lambda}\right)}}$	(A1.50)	eq. A.1.50 in eq. A1.36
$\Rightarrow \Delta V_{te}(0) = A + A \cdot \frac{e^{\left(\frac{L}{\lambda}\right)}}{e^{-\left(\frac{L}{\lambda}\right)}}$	(A1.51)	$\frac{e^{\left(\frac{L}{\lambda}\right)}}{e^{-\left(\frac{L}{\lambda}\right)}} = e^{\left(\frac{L}{\lambda}\right)-\left(-\left(\frac{L}{\lambda}\right)\right)} = e^{2\left(\frac{L}{\lambda}\right)}$
$\Rightarrow \Delta V_{te}(0) = A + A \cdot e^{2\left(\frac{L}{\lambda}\right)}$	(A1.52)	:A
$\Rightarrow \frac{\Delta V_{te}(0)}{A} = \frac{A}{A} + \frac{A \cdot e^{2\left(\frac{L}{\lambda}\right)}}{A}$	(A1.53)	Reducing
$\Rightarrow \frac{\Delta V_{te}(0)}{A} = 1 + e^{2\left(\frac{L}{\lambda}\right)}$	(A1.54)	$:\Delta V_{te}(0)$
$\Rightarrow \frac{1}{A} = \frac{1 + e^{2\left(\frac{L}{\lambda}\right)}}{\Delta V_{te}(0)}$	(A1.55)	Forming the reciprocal
$\Rightarrow A = \frac{\Delta V_{te}(0)}{1 + e^{2\left(\frac{L}{\lambda}\right)}}$	**(A1.56)**	
		recollecting eq. A.1.36 **and** substituting for A and B:
$\Delta V_{te}(x) = A \cdot e^{\left(\frac{x}{\lambda}\right)} + B \cdot e^{-\left(\frac{x}{\lambda}\right)}$	(A1.57)	$A = \frac{\Delta V_{te}(0)}{1 + e^{2\left(\frac{L}{\lambda}\right)}}$ eq. A1.56 $B = \frac{\Delta V_{te}(0) \cdot e^{2\left(\frac{L}{\lambda}\right)}}{e^{2\left(\frac{L}{\lambda}\right)} + 1}$ eq.A1.49

equation		operation giving next equation, comment
$\Rightarrow \Delta V_{te}(x) = \frac{\Delta V_{te}(0)}{1+e^{2\left(\frac{L}{\lambda}\right)}} \cdot e^{\left(\frac{x}{\lambda}\right)} + \frac{\Delta V_{te}(0) \cdot e^{2\left(\frac{L}{\lambda}\right)}}{e^{2\left(\frac{L}{\lambda}\right)}+1} \cdot e^{-\left(\frac{x}{\lambda}\right)}$	(A1.58)	$\cdot e^{-\left(\frac{L}{\lambda}\right)}$
$\Rightarrow \Delta V_{te}(x) = \frac{\Delta V_{te}(0) \cdot e^{-\left(\frac{L}{\lambda}\right)}}{\left[\ 1+e^{2\left(\frac{L}{\lambda}\right)}\ \right] \cdot e^{-\left(\frac{L}{\lambda}\right)}} \cdot e^{\left(\frac{x}{\lambda}\right)} + \frac{\Delta V_{te}(0) \cdot e^{2\left(\frac{L}{\lambda}\right)} \cdot e^{-\left(\frac{L}{\lambda}\right)}}{\left[\ e^{2\left(\frac{L}{\lambda}\right)}+1\ \right] \cdot e^{-\left(\frac{L}{\lambda}\right)}} \cdot e^{-\left(\frac{x}{\lambda}\right)}$	(A1.59)	$\left[\ 1+e^{2\left(\frac{L}{\lambda}\right)}\ \right] \cdot e^{-\left(\frac{L}{\lambda}\right)} = e^{-\left(\frac{L}{\lambda}\right)} + e^{2\left(\frac{L}{\lambda}\right)} \cdot e^{-\left(\frac{L}{\lambda}\right)}$
$\Rightarrow \Delta V_{te}(x) = \frac{\Delta V_{te}(0) \cdot e^{-\left(\frac{L}{\lambda}\right)}}{e^{-\left(\frac{L}{\lambda}\right)} + e^{2\left(\frac{L}{\lambda}\right)} \cdot e^{-\left(\frac{L}{\lambda}\right)}} \cdot e^{\left(\frac{x}{\lambda}\right)} + \frac{\Delta V_{te}(0) \cdot e^{2\left(\frac{L}{\lambda}\right)} \cdot e^{-\left(\frac{L}{\lambda}\right)}}{e^{-\left(\frac{L}{\lambda}\right)} + e^{2\left(\frac{L}{\lambda}\right)} \cdot e^{-\left(\frac{L}{\lambda}\right)}} \cdot e^{-\left(\frac{x}{\lambda}\right)}$	(A1.60)	$e^{2\left(\frac{L}{\lambda}\right)} \cdot e^{-\left(\frac{L}{\lambda}\right)} = e^{\left(\frac{L}{\lambda}\right)}$
$\Rightarrow \Delta V_{te}(x) = \frac{\Delta V_{te}(0)}{e^{-\left(\frac{L}{\lambda}\right)} + e^{\left(\frac{L}{\lambda}\right)}} \cdot e^{-\left(\frac{L}{\lambda}\right)} \cdot e^{\left(\frac{x}{\lambda}\right)} + \frac{\Delta V_{te}(0)}{e^{-\left(\frac{L}{\lambda}\right)} + e^{\left(\frac{L}{\lambda}\right)}} \cdot e^{\left(\frac{L}{\lambda}\right)} \cdot e^{-\left(\frac{x}{\lambda}\right)}$	(A1.61)	factorizing out
$\Rightarrow \Delta V_{te}(x) = \frac{\Delta V_{te}(0)}{e^{-\left(\frac{L}{\lambda}\right)} + e^{\left(\frac{L}{\lambda}\right)}} \cdot \left[e^{-\left(\frac{L}{\lambda}\right)} \cdot e^{\left(\frac{x}{\lambda}\right)} + e^{\left(\frac{L}{\lambda}\right)} \cdot e^{-\left(\frac{x}{\lambda}\right)} \right]$	(A1.62)	$e^{-\left(\frac{L}{\lambda}\right)} \cdot e^{\left(\frac{x}{\lambda}\right)} = e^{\left(\frac{x-L}{\lambda}\right)}$ $e^{\left(\frac{L}{\lambda}\right)} \cdot e^{-\left(\frac{x}{\lambda}\right)} = e^{-\left(\frac{x-L}{\lambda}\right)}$
$\Rightarrow \Delta V_{te}(x) = \frac{\Delta V_{te}(0)}{e^{-\left(\frac{L}{\lambda}\right)} + e^{\left(\frac{L}{\lambda}\right)}} \cdot \left[e^{\left(\frac{x-L}{\lambda}\right)} + e^{-\left(\frac{x-L}{\lambda}\right)} \right]$	(A1.63)	$\cdot 2$
$\Rightarrow \Delta V_{te}(x) \cdot 2 = \Delta V_{te}(0) \cdot \frac{e^{\left(\frac{x-L}{\lambda}\right)} + e^{-\left(\frac{x-L}{\lambda}\right)} \cdot 2}{e^{-\left(\frac{L}{\lambda}\right)} + e^{\left(\frac{L}{\lambda}\right)}}$	(A1.64)	$:2$
$\Rightarrow \Delta V_{te}(x) = \Delta V_{te}(0) \cdot \frac{e^{\left(\frac{x-L}{\lambda}\right)} + e^{-\left(\frac{x-L}{\lambda}\right)}}{2} \cdot \frac{2}{e^{-\left(\frac{L}{\lambda}\right)} + e^{\left(\frac{L}{\lambda}\right)}}$	(A1.65)	$\frac{e^{\left(\frac{x-L}{\lambda}\right)} + e^{-\left(\frac{x-L}{\lambda}\right)}}{2} = \cosh\left(\frac{x-L}{\lambda}\right)$ $\frac{e^{-\left(\frac{L}{\lambda}\right)} + e^{\left(\frac{L}{\lambda}\right)}}{2} = \cosh\left(\frac{L}{\lambda}\right)$ substituting

equation		operation giving next equation, comment
$\Rightarrow \Delta V_{te}(x) = \Delta V_{te}(0) \cdot \frac{\cosh\left(\frac{x-L}{\lambda}\right)}{\cosh\left(\frac{L}{\lambda}\right)}$	(A1.66)	**boundary condition: $\Delta V_{te}(x = L)$ & $x = L$ (can be measured)**
$\Rightarrow \Delta V_{te}(L) = \Delta V_{te}(0) \cdot \frac{\cosh\left(\frac{L-L}{\lambda}\right)}{\cosh\left(\frac{L}{\lambda}\right)}$	(A1.67)	$\cosh\left(\frac{L-L}{\lambda}\right) = \cosh\left(\frac{0}{\lambda}\right)$ $\cosh\left(\frac{0}{\lambda}\right) = \cosh 0$ $\cosh 0 = 1$
$\Rightarrow \Delta V_{te}(L) = \Delta V_{te}(0) \cdot \frac{1}{\cosh\left(\frac{L}{\lambda}\right)}$	(A1.68)	$:\Delta V_{te}(0)$
$\Rightarrow \frac{\Delta V_{te}(L)}{\Delta V_{te}(0)} = \cdot \frac{1}{\cosh\left(\frac{L}{\lambda}\right)}$	(A1.69)	forming the reciprocal
$\Rightarrow \frac{\Delta V_{te}(0)}{\Delta V_{te}(L)} = \cosh\left(\frac{L}{\lambda}\right)$	(A1.70)	forming the arccosh
$\Rightarrow \operatorname{arccosh}\left(\frac{\Delta V_{te}(0)}{\Delta V_{te}(L)}\right) = \operatorname{arccosh} \cosh\left(\frac{L}{\lambda}\right)$	(A1.71)	$\operatorname{arccosh} \cosh\left(\frac{L}{\lambda}\right) = \frac{L}{\lambda}$
$\Rightarrow \operatorname{arccosh}\left(\frac{\Delta V_{te}(0)}{\Delta V_{te}(L)}\right) = \frac{L}{\lambda}$	(A1.72)	$:L$
$\Rightarrow \frac{\operatorname{arccosh}\left(\frac{\Delta V_{te}(0)}{\Delta V_{te}(L)}\right)}{L} = \frac{1}{\lambda}$	(A1.73)	forming the reciprocal

equation		operation giving next equation, comment
		Therefore the space constant (λ) may be calculated with parameters that can be measured: the length of the tubule (L) and the voltage deflections at both ends of the tubule $\Delta V_{te}(0,L)$ where x = 0 & x = L. **eq. A1.74 = eq. 2.3**
$\Rightarrow \lambda = \frac{L}{\operatorname{arccosh}\left(\frac{\Delta V_{te}(0)}{\Delta V_{te}(L)}\right)}$	(A1.74)	
		The purpose of the following steps is to obtain an expression for R_{te}:
$\frac{d}{dx}\Delta V_{te}(x) = -i_{core} \cdot R_{core}$	(A1.75)	
		recollect eq. A1.11 :R_{core}
$\Rightarrow \frac{\frac{d}{dx}\Delta V_{te}(x)}{R_{core}} = -i_{core}$	(A1.76)	$\cdot(-1)$
$\Rightarrow i_{core} = \frac{d}{dx}\Delta V_{te}(x) \cdot \frac{-1}{R_{core}}$	(A1.77)	$i_{core}(x=0) = I_0$
$\Rightarrow I_0 = \left[\frac{d}{dx}\Delta V_{te}(x)\right]_{x=0} \cdot \frac{-1}{R_{core}}$	(A1.78)	$\Delta V_{te}(x) = \Delta V_{te}(0) \cdot \frac{\cosh\left(\frac{x-L}{\lambda}\right)}{\cosh\left(\frac{L}{\lambda}\right)}$
		see eq. A1.66, substituting

equation		operation giving next equation, comment
$\Rightarrow I_0 = \frac{d}{dx}\left[\Delta V_{te}(0)\cdot\frac{\cosh\left(\frac{x-L}{\lambda}\right)}{\cosh\left(\frac{L}{\lambda}\right)}\right]\cdot\frac{-1}{R_{core}}$	(A1.79)	$\frac{d}{dx}[A\cdot f(x)] = A\cdot\frac{d}{dx}f(x)$
$\Rightarrow I_0 = \Delta V_{te}(0)\cdot\frac{d}{dx}\left[\frac{\cosh\left(\frac{x-L}{\lambda}\right)}{\cosh\left(\frac{L}{\lambda}\right)}\right]\cdot\frac{-1}{R_{core}}$	(A1.80)	$\frac{d}{dx}[A\cdot f(x)] = A\cdot\frac{d}{dx}f(x)$
$\Rightarrow I_0 = \Delta V_{te}(0)\cdot\frac{1}{\cosh\left(\frac{L}{\lambda}\right)}\cdot\frac{d}{dx}\cosh\left(\frac{x-L}{\lambda}\right)\cdot\frac{-1}{R_{core}}$	(A1.81)	$\frac{d}{dx}[f(\alpha\cdot x)] = \alpha\cdot\frac{d}{dx}f(\alpha\cdot x)$
$\Rightarrow I_0 = \Delta V_{te}(0)\cdot\frac{1}{\cosh\left(\frac{L}{\lambda}\right)}\cdot\frac{1}{\lambda}\cdot\frac{d}{dx}\cosh\left(\frac{x-L}{\lambda}\right)\cdot\frac{-1}{R_{core}}$	(A1.82)	$\frac{d}{dx}\cosh(\alpha\cdot x) = \sinh(\alpha\cdot x)$
$\Rightarrow I_0 = \Delta V_{te}(0)\cdot\frac{1}{\cosh\left(\frac{L}{\lambda}\right)}\cdot\frac{1}{\lambda}\cdot\sinh\left(\frac{x-L}{\lambda}\right)\cdot\frac{-1}{R_{core}}$	(A1.83)	rearranging
$\Rightarrow I_0 = \frac{\sinh\left(\frac{x-L}{\lambda}\right)}{\cosh\left(\frac{L}{\lambda}\right)}\cdot\frac{\Delta V_{te}(0)}{\lambda}\cdot\frac{-1}{R_{core}}$	(A1.84)	$x = 0 \Rightarrow \frac{x-L}{\lambda} = -\frac{L}{\lambda}$

equation		operation giving next equation, comment
$\Rightarrow I_0 = \frac{\sinh - \left(\frac{L}{\lambda}\right)}{\cosh\left(\frac{L}{\lambda}\right)} \cdot \frac{\Delta V_{te}(0)}{\lambda} \cdot \frac{-1}{R_{core}}$	(A1.85)	$\sinh - \left(\frac{L}{\lambda}\right) = -\sinh\left(\frac{L}{\lambda}\right)$
$\Rightarrow I_0 = \frac{-\sinh\left(\frac{L}{\lambda}\right)}{\cosh\left(\frac{L}{\lambda}\right)} \cdot \frac{\Delta V_{te}(0)}{\lambda} \cdot \frac{-1}{R_{core}}$	(A1.86)	$\frac{-\sinh\left(\frac{L}{\lambda}\right)}{\cosh\left(\frac{L}{\lambda}\right)} = -\tanh\left(\frac{L}{\lambda}\right)$
$\Rightarrow I_0 = -\tanh\left(\frac{L}{\lambda}\right) \cdot \frac{\Delta V_{te}(0)}{\lambda} \cdot \frac{-1}{R_{core}}$	(A1.87)	$: I_0$ & $\cdot R_{core}$
$\Rightarrow R_{core} = -\tanh\left(\frac{L}{\lambda}\right) \cdot \frac{\Delta V_{te}(0)}{I_0 \cdot \lambda} \cdot (-1)$	(A1.88)	rearranging
$\Rightarrow R_{core} = \frac{\Delta V_{te}(0)}{I_0 \cdot \lambda} \cdot \tanh\left(\frac{L}{\lambda}\right)$	(A1.89)	$\frac{\Delta V_{te}(0)}{I_0} = R_{input}$ (resistance, that I_0 encounters when it enters the tubule), substituting
$\Rightarrow R_{core} = \frac{R_{input}}{\lambda} \cdot \tanh\left(\frac{L}{\lambda}\right)$	(A1.90)	$R_{core} = \frac{R_m}{\lambda^2}$ see eq. A1.3, substituting

equation		operation giving next equation, comment
$\Rightarrow \frac{R_m}{\lambda^2} = \frac{R_{input}}{\lambda} \cdot \tanh\left(\frac{L}{\lambda}\right)$	(A1.91)	R_{te} is the specific resistance of a tubule: the specific transmural resistance R_m times the circumference of the tubule: $R_{te} = 2 \cdot \pi \cdot r \cdot R_m$ $\Rightarrow R_m = \frac{R_{te}}{2 \cdot \pi \cdot r}$ substituting
$\frac{R_{te}}{2 \cdot \pi \cdot r \cdot \lambda^2} = \frac{R_{input}}{\lambda} \cdot \tanh\left(\frac{L}{\lambda}\right)$	(A1.92)	$: 2 \cdot \pi \cdot r \cdot \lambda^2$
$\Rightarrow R_{te} = 2 \cdot \pi \cdot r \cdot \lambda^2 \cdot \frac{R_{input}}{\lambda} \cdot \tanh\left(\frac{L}{\lambda}\right)$	(A1.93)	reducing
$\Rightarrow \mathbf{R_{te} = 2 \cdot \pi \cdot r \cdot R_{input} \cdot \lambda \cdot \tanh\left(\frac{L}{\lambda}\right)}$	**(A1.94)**	**eq. A1.94 = eq. 3.1** This is the expression for R_{te} used throughout this thesis to calculate R_{te}.

By this expression R_{te} is implicitly determined by the tubule dimensions, circumference as well as length. Hence the name "specific transepithelial electrical resistance". It is normalized with respect to the tubule surface. Because r and λ are in cm and R_{input} is in Ω, the dimension of R_{te} is $\Omega \cdot cm^2$. All these parameters can be measured directly (r, L) or calculated exactly from the measurements of other parameters (λ, R_{input}). The length constant (λ) can be calculated from the parameters L, $\Delta V_{te}(0)$ and $\Delta V_{te}(L)$. R_{input} can be calculated from I_0 and $\Delta V_{te}(0)$. An overview of the parameters mentioned in this appendix and in part I of the thesis is given in Table A1.

The above terms for λ and R_{te} are derived from a differential equation. They must be therefore considered as a continuous model of the tubule, although they do not contain differential terms themselves. On the other hand, the above differential equation is deduced from the discrete cable model shown in Figs A.1 – A.4 For that purpose the finite sections of the discrete model were reduced to pieces of infinitesimal length in the continuous model. The difference between both is the number of sections the tubule is divided into.

Any change in the transmural resistance (R_m^x) with length is not included in the derivation of the equations for λ and R_{te}. The continuous model is therefore based on the assumption that R_m^x does not change along the tubule. If it does, the above model would become invalid. If there is evidence, that there are nonuniformities in the transmural resistance, the actual value of R_{te} can not be calculated correctly. But the discrete model provides a way out. Different resistors (R_m) then represent the transmural resistances (R_m^x) of each section of the model (Figs A1, A2). These resistors may be given different values. This approach is described in detail in part I B of this thesis.

Table. A1 definition of parameters.

parameter symbol	definition	units
ρ	volume resistivity of the luminal fluid	$\Omega \cdot cm$
g	conductivity, inverse of resistance	mS
ΔI_0	amplitude of current pulse at the perfusion end of the tubule	nA
i_{core}	axial current	nA
i_m	transmural current	nA
i_{res}, i_{cap}	resistive, capacitive current	nA
L	length of the tubule	cm; µm
r	radius of the tubule	cm; µm
R_{core}	specific core resistance of the luminal fluid (per unit length of a particular tubule)	$\frac{\Omega}{cm}$

parameter symbol	definition	units
R_{input}	input resistance $R_{input} = \frac{\Delta V_{te}(0)}{\Delta I_0}$ total resistance of tubule lumen, tubule wall and el. Insulation at both ends	Ω
R_{leak}	insulation / leakage resistance at both ends of the tubule	Ω
R_m^x	specific transmural resistance of the tubule wall per (unit length of a particular tubule)	Ω·cm
R_{te}	specific transepithelial resistance: $R_{te} = 2 \cdot \pi \cdot r \cdot R_{input} \cdot \lambda \cdot \tanh\left(\frac{L}{\lambda}\right)$	Ω·cm²
$\Delta V_{te}(0)$; ΔV_{te}^0	transepithelial voltage deflection at the perfusion end of the tubule	mV
$\Delta V_{te}(L)$; ΔV_{te}^L	transepithelial voltage deflection at the collection end of the tubule	mV
V_{ap}	apical cell membrane potential difference	mV
V_{bl}	basolateral cell membrane potential difference	mV
V_{te}	spontaneous transepithelial voltage difference	mV
x	distance away from the perfusion end	cm; µm
λ	length constant = space constant $\lambda = \frac{L}{\operatorname{arccosh}\left(\frac{\Delta V_{te}(0)}{\Delta V_{te}(L)}\right)}$; $\lambda = \sqrt{\frac{R_m}{R_{core}}}$	cm; µm

References appendix A1

Dijkstra, S. 1993. Cl^- transport and H^+ pumping in the primary urine formation in the ant. PhD thesis, dpt. of Physiology, Limburgs Universitair Centrum, Diepenbeek Belgium.

Jack, J.J.B., Noble, D., Tsien, R.W., 1975. Electric current flow in exitable cells. Clarendon Press, Oxford.

Sackin, H., 1978. Electrophysiology and transport in the isolated perfused salamander proximal tubule. PhD thesis, Yale University, USA.

Tompson, W. (Kelvin, Lord), 1855. On the theory of the electric telegraph. Proceedings of the Royal Society of London 7, 382-399.

Appendix 2: Derivation of Equation 4.2

The derivation of eq. 4.2 was adopted from Kühtreiber and Jaffe (1990). It was used to determine the theoretical response of the vibrating Cd^{2+}-sensitive electrode to an artificial Cd^{2+} gradient.

equation		**operation giving next equation, comment**
		recalling eq. 4.1
$C = C_b + K \cdot \frac{1}{x}$	(A2.1)	differentiating with respect to x C_b: background concentration at an infinite distance from the point source
$\Rightarrow \frac{dC}{dx} = -K \cdot \frac{1}{x^2}$	(A2.2)	
$\Delta V = S \cdot \log\left(\frac{C_2}{C_1}\right)$	(A2.3)	The Nernst equation: S: Nernst slope $C_{1,2}$: concentrations at both electrode positions Transformation: log ->ln The following steps will eventually eliminate the logarithmic term.
$\Rightarrow \Delta V = \frac{S}{2.303} \cdot \ln\left(\frac{C_2}{C_1}\right)$	(A2.4)	$C_2 = C_1 + \Delta C$, where ΔC is the difference in the actual concentration / activity of the analyte ion.
$\Rightarrow \Delta V = \frac{S}{2.303} \cdot \ln\left(\frac{C_1 + \Delta C}{C_1}\right)$	(A2.5)	$\frac{C_1 + \Delta C}{C_1} = 1 + \frac{\Delta C}{C_1}$

equation		operation giving next equation, comment
		When $\frac{\Delta C}{C_1}$ becomes small,
$\Rightarrow \Delta V = \frac{S}{2.303} \cdot \ln\left(1 + \frac{\Delta C}{C_1}\right)$	(A2.6)	$\ln\left(1 + \frac{\Delta C}{C_1}\right) \approx \frac{\Delta C}{C_{av}}$, where C_{av} is the average of C_1 and C_2.
$\Rightarrow \Delta V = \frac{S}{2.303} \cdot \frac{\Delta C}{C_{av}}$	(A2.7)	recalling eq.A2.1: $C_{av} = C = C_b + K \cdot \frac{1}{x}$ for small signals C_b can be used instead of C_{av} substituting
$\Rightarrow \Delta V = \frac{S}{2.303} \cdot \frac{\Delta C}{C_b + K \cdot \frac{1}{x}}$	(A2.8)	recalling eq. 1.1: $\frac{dC}{dx} = -K \cdot \frac{1}{x^2}$ $\Delta C = -K \cdot \frac{1}{x^2} \cdot \Delta x$ substituting
$\Rightarrow \Delta V = \frac{S}{2.303} \cdot \frac{-K \cdot \frac{1}{x^2} \cdot \Delta x}{C_b + K \cdot \frac{1}{x}}$	(A2.9)	factoring out
$\Rightarrow \mathbf{\Delta V = \frac{S}{2.303} \cdot \frac{-K \cdot \Delta x}{C_b \cdot x^2 + K \cdot x}}$	**(A2.10)**	**eq. A2.10 = eq. 4.2** yields the theoretical value for ΔV

Appendix 3: Procedure to solve equivalent circuits

The procedure followed to derive equation 1.1 was adopted from Wills et al. (1996) pp. 328-329: all voltage sources and resistors are lumped into one single voltage source and one single resistor. The V_{te} in the midgut model (chapter 3.3.10 -3.3.12) can be calculated likewise. Simulations performed with PSpice (ORCAD®, Beaverton, Oregon USA) yielded exactly the same values as this procedure.

Combinations of voltage sources and resistors are Thévenin equivalent circuits. Series voltage sources are added. When parallel voltage sources and resistances in series with them must be summed (e.g. Fig. 1.4, E_p and E_{ap}), they can be converted to Norton equivalent circuits. Norton equivalent circuits are combinations of current sources and resistors. A resistor and a voltage source in series equals a current source of infinite resistance and a resistor in parallel (e.g. E_p/R_p). The parallel current sources are added. After reconversion to the Thévenin equivalent circuit the resulting voltage of the combined parallel voltage sources can be calculated. These calculations are outlined in Fig. A2:

- Step 1: Thévenin equivalent circuit, determine the nodes between which the voltage must be calculated, $V_a - V_b$ in this case.
- Step 2: Convert the parallel voltage sources of the sub-circuit c – b - c to Norton equivalents and sum them up. $E_{ap} \rightarrow E_{ap}/R_{ap}$, $E_p \rightarrow E_p/R_p$.
- Step 3: Reconvert the lumped Norton equivalent to one Thévenin equivalent. That is to say multiply the sum of the current sources (E/R) with the total resistance of the sub-circuit (R_t, see chapter 1.2.4, eq. 1.1).
- Step 4: add all series elements. Sum up the total resistance of the sub-circuit c – b – c and R_{sh}.
- Step 5: repeat step 1 to 3 to lump the whole circuit a – b – a in one single resistor and one single voltage source.
- Step 6: decide in what direction the current flows in the Thévenin circuit and give the appropriate positive or negative signs to the voltage sources. In this case they are negative for E_{ap} and for E_p, if E_{bl} is given a positive sign. After factorizing out, this yields eq. 1.1 (chapter 1.2.4).

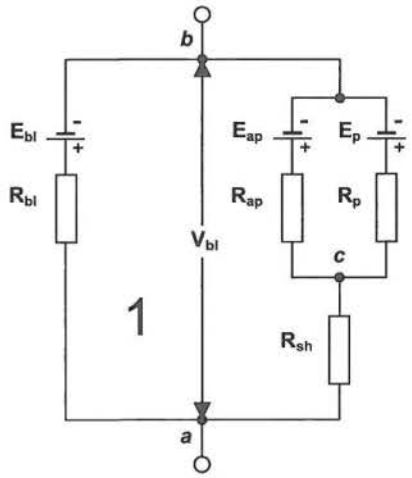

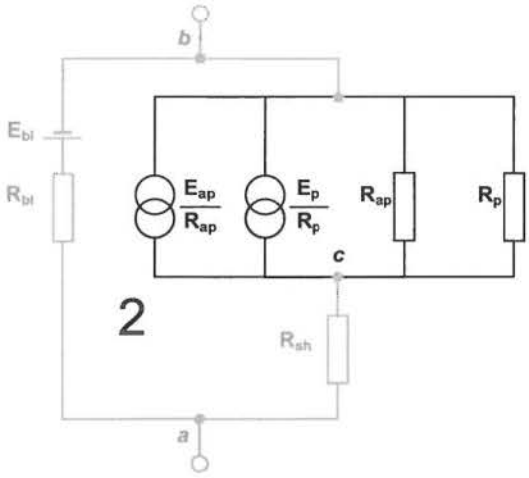

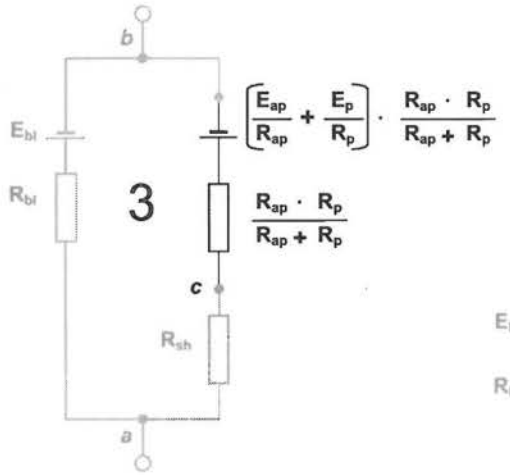

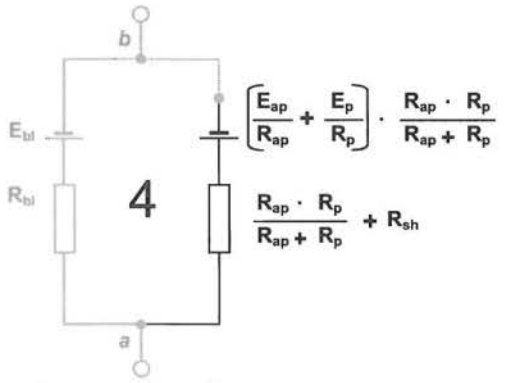

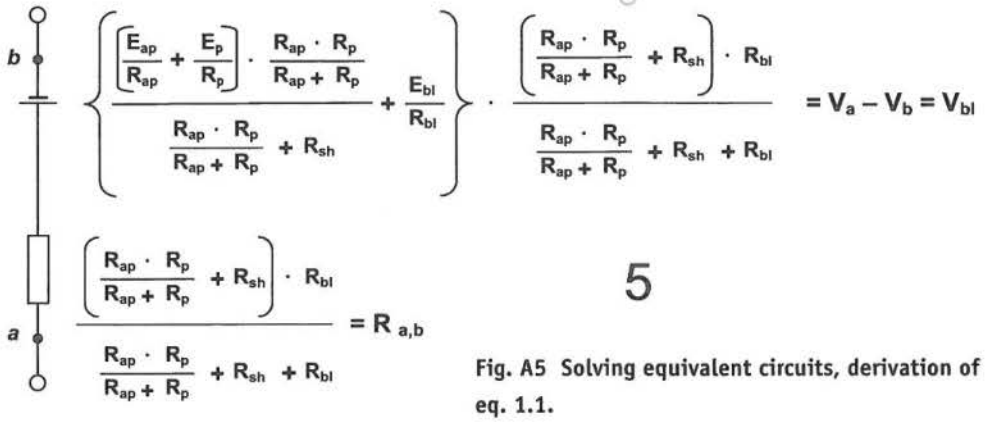

Fig. A5 Solving equivalent circuits, derivation of eq. 1.1.

Dankwoord

Een doctoraat werk je niet zomaar in je eentje af. Ik ben aan veel mensen dank verschuldigd. Daarom wil ik mijn oprechte dank uitdrukken aan alle mensen die dit werk mogelijk gemaakt hebben. In het bijzonder:

Mijn promotor Prof. Emmy Van Kerkhove, zij heeft mij een grote vrijheid gegeven in dit werk en zij was altijd bereid te helpen, te discussiëren en uit te leggen.

Onze technicus Patrick Pirotte, hij heeft mij wegwijs gemaakt in de wereld van de microelectrodes.

De leden van de jury, zij hebben mij met hun commentaren veel ertoe bijgedragen om dit werk tot een goed einde te brengen

Mijn vrouw Gudrun Koppen, zij heeft -vooral tijdens de laatste maanden van het doctoraat- veel geduld met mij gehad.

En verder iedereen van de groep Fysiologie, zowel de bazen als mijn collega's. Zij hebben allen in belangrijke mate ertoe bijgedragen dat de werksfeer prettig bleef. En dat ook in moeilijke momenten. Ik heb hier zo graag gewerkt dat ik het zonder te aarzelen opnieuw zou doen.

Ik draag dit werk op aan mijn vrouw Gudrun en mijn kinderen Judith, Adrian en Norah.

Curriculum vitae

born : Düren (Germany) on 7 May 1959

nationality : German

education : grammar schools Stift. Gymnasium, Düren (1968-74);
Gymnasium Haus Overbach, Jülich (1974-78)

university master of science (Diplom-Biologe) Ruhr-Universität Bochum (Germany)
thesis subject: 'effects of xenobiotics on the development of the Zebrafish', supervisor: Dr. R. Weltens (VITO), reviewers: Prof. Dr H. Mehlhorn (dpt. Zoology and Parsitology , RUB), Prof. Dr. Jens Lehmann, RUB,)
delivery of certificate on 14 June 1996 ('with distinction'

popstgraduate at the Limburgs Universitair Centrum Diepenbeek (Belgium) (1999-2003)

ABSTRACTS

Bierkens, J. Weltens, R. **Klein, G.** et al., 1997. Assessment of the quality of natural surface waters using heat-shock protein 70 synthesis in Selenastrum capricornutum. In: Prospects for the European Environment beyond 2000. Abstract Book of Seventh annual Meting of SETAC-Europe, Amsterdam, The Netherlands, 9-10April 1997, p251.

Bierkens, J., **Klein, G.** et al., 1997. Comparative sensitivity of 20 bioassays for soil quality. Abstract book of International Symposium on Integrated Ecotoxicology, From Molecules/ Organisms to Ecosystems, Italian National Research Council, Milan, 9June-July, p 80.

Bierkens, J. **Klein, G.** et al., 1998. Assessment of soil quality using a multitiered testbattery of bioassays. Abstract in ConSoil '98, Edinburgh May 17-21.

Klein, G., Van Kerkhove, E., 2000. First electrophysiological measurements on the midgut of the springtail Orchesella cincta (L.) Templeton 1835. Abstracts / Comparative Biochemistry and Physiology, Part A 126, S76.

Klein, G. Van Kerkhove, E., 2003. Unequal distribution of transepithelial resistance (R_{te}) within a very short tubule: the midgut of *Orchesella cincta* (Hexapoda, Collembola) Abstract in: Pflügers Archiev - European Journal of Physiology 445, R4.

PEER-REVIEWED

Bierkens, J., **Klein, G.** et al., 1998. Comparative Sensitivity of 20 Bioassays for Soil Quality. In: Chemosphere 37 (14-15), 2935-2947.

Wiehart, U.I.M., **Klein, G.**, Steels, P, Nicolson, S.W., Van Kerkhove, E., 2003. K^+ transport in Malpighian tubules of *Tenebrio molitor*: is a K_{ATP} channel involved? Journal of Experimental Biology 206, 959-965.